Giuseppe Petrone

Characterisation of bio-based structures: models and experiments

"Characterisation of bio-based structures: models and experiments"

Typeset with LaTeX and PGF/TikZ.

This document was typeset using the LaTeX style `classicthesis`, developed by André Miede.

University of Naples FEDERICO II

Department of Industrial Engineering - Aerospace Section
Doctorate School in Industrial Engineering
Ph.D. Course in Aerospace, Naval and Quality Engineering
XXVI cycle

Characterisation of bio-based structures: models and experiments

Candidate:
Giuseppe Petrone

Research Supervisor:
Prof. Sergio De Rosa
Prof. Francesco Franco

The Chairman of the Ph.D. School:
Prof. Luigi de Luca

Thesis submitted in March 2014

I, Giuseppe Petrone, declare that this thesis titled "Characterisation of bio-based structures: models and experiments" and the work presented in it are my own work. I confirm that:

- this work was done wholly or mainly while in candidature for a doctoral degree at this University;

- where any part of this thesis has previously been submitted for a degree or any other qualification at this University or any other institution, this has been clearly stated;

- where I have consulted the published work of others, this is always clearly attributed;

- where I have quoted from the work of others, the source is always given and with the exception of such quotations, this thesis is entirely my own work;

- I have acknowledged all main sources of help;

- where the thesis is based on work done by myself jointly with others, I have made clear exactly what was done by others and what I have contributed myself.

This PhD thesis will be defended in a public dissertation on May 16, 2014 under the judgement of a specialised commission composed by:

- Prof. Annalisa Fregolent, Department of Mechanical and Aerospace Engineering, Universitá di Roma "La Sapienza";

- Dr. Elena Ciappi, INSEAN: Marine Technology Research Institute, Research National Center (CNR), Roma

- Prof. Herve Riou, Department of Mechanical Engineering, Structure and System division, Ecole Normale Supérieure de Cachan;

- Prof. Walter D'Ambrogio, Department of Industrial Engineering, Information and Economy, Universitá degli Studi dell'Aquila.

March 2014
Department of Industrial Engineering
University of Naples Federico II
Naples

Giuseppe Petrone

...to my loving family.

Acknowledgements

Contents

List of Figures

List of Tables

Introduction

Fibre-reinforced plastics (FRP) have until now been largely applied to different engineering applications (automotive, trains, naval, aerospace), especially where high strength and stiffness are required. The great success of this technology (or material) is due to the good specific (i.e. weight-related) properties arising from the low density of the applied matrix systems (unsaturated polyesters, polyurethanes, phenolic or epoxy resins) and from the embedded fibres, that provide the high strength and stiffness (glass, aramid, and carbon fibres). Furthermore, the possibility to tailor the compound material as a function of the desired properties, by changing fibres' orientation, length and materials, made these materials very attractive. Unfortunately, classic fibre-reinforced polymers often pose considerable problems with respect to their re-use or recycling at the end of their usable lifetime. For this reason, in recent years, a significant amount of interest has been shown in the potential of natural fibres, such as abaca, bamboo, flax, hemp, jute, ramie, and sisal to replace wood fibre and glass fibre as the reinforcements. These fibres offer specific benefits such as low density, low pollutant emissions, biodegradability, high specific properties and low cost.

All the natural fibres are lignin-cellulosic and their properties vary with location, origin and age of the plant. The application of natural fibres in the near term are therefore likely to be targeted towards 'low lying fruit', i.e. those applications having limited performance requirements, and where the biocomposites can aim for a relative cost advantage (or at least no cost disadvantage). This has already occurred extensively in the automotive industry. Panels and trims with low mechanical requirements, protected from moisture, are enhancing car makers. Above the automotive industry, natural fibres have been used also in other transport applications: marine, trains, aeronautical and sport. In summary, there are considerable challenges to apply bio-composites to the full range of composite applications, in the range of non-structural and semi-structural applications to replace wood, plastics and similar materials with moderate performance improvement and competitive cost.

This thesis summarises the work done by the author in the frame of the Ph.D. course in Aerospace, Naval and Quality Engineering at the University of Naples Federico II. The author has been involved in the SUPERPANELS project (Strengthening and Upholding the Performances of the new Engineered Research PANELS) funded by European Union (FP7-PEOPLE-2009-IRSES), a People Marie Curie action which aim was to develop innovative panels able to satisfy as much as possible the requirements of different transport engineering applications. Thanks to this project the author, during his first year of PhD course, spent eight months at CACM, the Centre for Advanced Composite Material based at the university

of Auckland (New Zealand). CACM is one of the biggest centre focused research on bio-based composite materials, from manufacturing processes and design to analysis and experimental characterisation. From these experience the author acquired the idea to focus his research on flax fibre as reinforcement in composite panels for using in transport applications.

The thesis is arranged as follows: Chapter 1 provides an overview of the composite materials, a state of the art on natural fibres, including origin, properties and applications and finally general theory on composite. In Chapter 2 an overview of the materials, manufacturing and mechanical testing of the investigated panels is reported. Chapter 3 concerns studies on the dynamic behaviour of flax-PE flat panels. In particular investigation on modal parameters, in terms of natural frequency, mode shapes and damping ratio, was evaluated both experimentally and numerically on a unidirectional panel. Furthermore dispersion curves of this panel were investigated at high frequency range by using ultrasonic waves. The analysis was performed both experimentally, with the pitch-catch technique (usually utilized to detect a damage) and numerically. In Chapter 4, some functional properties such as sound acoustic absorption, vibration damping and energy absorption of flax-PE composites, as honeycomb core and as face sheets, were investigated and reported. Finally the conclusion summarises all the findings of the research work undertaken.

Chapter 1

Literature review

In this chapter a background of composite materials, natural fibres, plastics and their composites is provided to familiarise the reader with the subject. Different natural fibres and some polymers that is commonly used and available for manufacturing natural fibre composites are discussed. Some common manufacturing techniques to produce natural fibre composites have been reviewed and presented.

1.1   Composites

Composites exist almost everywhere, from the human body to spaceships. Many materials existing in nature, such as bones in the human body and wood in the forest, derive their superb mechanical properties by combining two or more macroscopic components or constituents, fibre and matrix, which can be distinguished readily by using a microscope. The matrix gives to composites shape, surface appearance, environmental tolerance and overall durability, while the fibrous reinforcement carries most of the structural loads thus giving to composite stiffness and strength [1, 2]. These two constituents can be any material and the resulting properties of composites are mostly determined by the properties of these individual constituents as well as the compatibility or adhesion between them. For this reason composite materials, usually, exhibit superior mechanical and physical properties than conventional metals and their importance is increasing through the year, as reported in Figure 1.1.

Human bone is a classical example of a naturally occurring fibre reinforced ceramic composites consisting of collagen fibres and a gel-like matrix of calcium phosphate (hydroxyapatite) mineral [3]. The fibres are arranged in a relatively disordered side-to-side packing of collagen molecules but in a regular axial structure and are surrounded by the mineral matrix, in the form of small, poorly-crystalline hydroxyapatite crystals, resulting in the strong structure of human bones. Similarly, most engineering structural materials, like thermoset resin-based composites used in space applications, concrete beams reinforced with steel wire for buildings and metallic alloys for cars, are also combinations of two or more phases designed to give better performance and properties, such as strength,
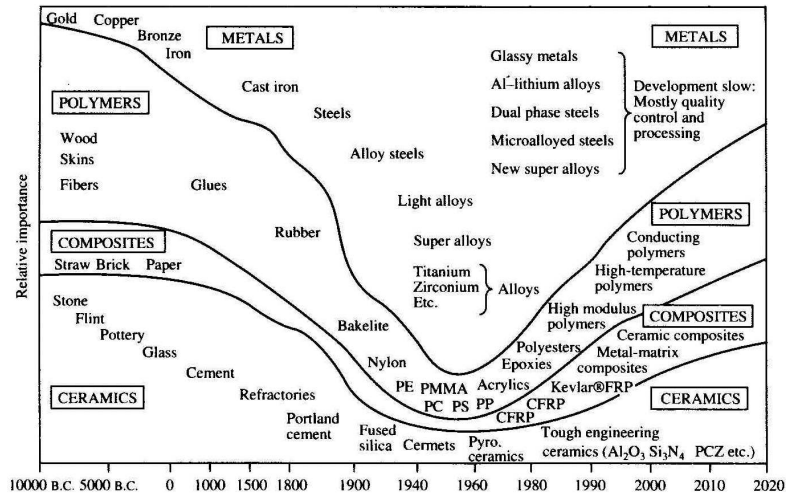
Figure 1.1: Evolution of the relative importance of the materials in the years

stiffness, toughness, thermal resistance, than each single phase material.

Based on the matrix material used composites can be classified into metal, ceramic and polymer composites. Among these, polymer composites possess the advantages to easier processing and fabrication than metal and ceramic composites. Composite materials can take many forms but they can be separated into three categories based on the strengthening mechanism. These categories are dispersion strengthened, particle reinforced and fibre reinforced. Dispersion strengthened composites have a fine distribution of secondary particles in the matrix of the material. These particles impede the mechanisms that allow a material to deform. These mechanisms include dislocation movement and slip. Many metal-matrix composites would fall into the dispersion strengthened composite category. Particle reinforced composites have a large volume fraction of particle dispersed in the matrix and the load is shared by the particles and the matrix. Most commercial ceramics and many filled polymers are particle-reinforced composites. In fibre-reinforced composites, the fibre is the primary load-bearing component. Fibreglass and carbon fibre composites are examples of fibre-reinforced composites. It is common to classify fibre reinforced composites on the basis of the geometry of a representative unit of reinforcement, as presented in Figure 1.2 [4].

Although it is difficult to say with certainty when or where humans first learned about fibrous composites, nature provides us with numerous examples. Fibre reinforced composite materials were widely used as early as 4000 B.C. in Egypt for making laminated writing materials from the papyrus plant [5]. There was a rapid growth in the use of fibre reinforced polymer composites for structural engineering applications in the 1970's [6]. This was because of the composites fabricated using fibres such as graphite and glass which could achieve high strengths. In addition, these composites had significantly lower density compared to metals which they were intended to replace. Many kinds of fibre reinforcement, such as strands, woven and non-woven fabrics, yarns, long and short fibre mats, are commercially available at present. These may be made using synthetic fibres such as carbon,
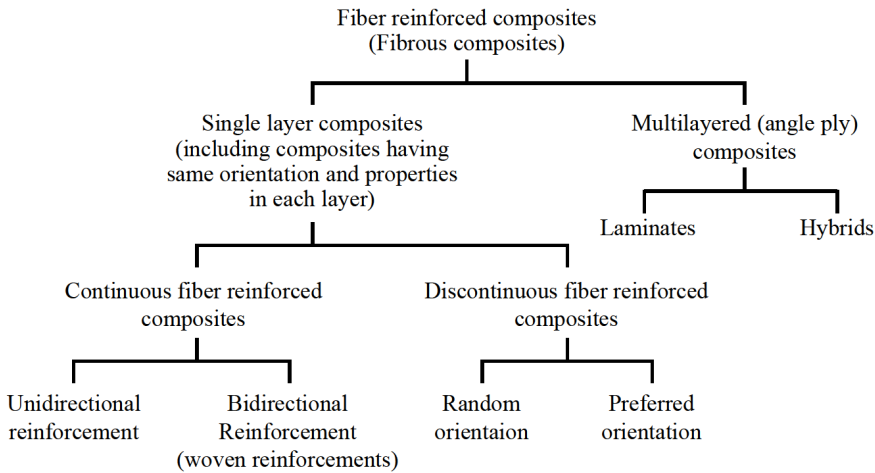
Figure 1.2: Classification of Fibre Reinforced Composites [4]

glass, kevlar, boron or natural fibres such as cotton, ramie, jute and flax. The use of these reinforcements depends on the desired properties of applications of the composites.

1.2 Fibre reinforced composites

Fibre is defined as any single unit of matter characterized by flexibility, fineness and high aspect ratio [7]. Fibres are a class of hair-like material that are continuous filaments or are in discrete elongated pieces, similar to pieces of thread. They can be spun into filaments, thread, or rope. They can be used as a component of composites materials. They can also be matted into sheets to make products such as paper or felt. Fibre reinforced composites consist of fibres of high strength and modulus embedded in a matrix with distinct interfaces between them. Fibre reinforcement improves the stiffness and the strength of the matrix. The fibre reinforced composites exhibit anisotropy in properties. The performance of the composites is controlled by the fibres and depends on factors like aspect ratio, orientation of fibres and fibre-matrix adhesion.

Based on their origin, the fibres may be classified as belonging to one of the following two categories: natural and man-made (Figure1.3).

Man-made fibres can be classified in *regenerated* and *synthetic*. The first are fibres made from cellulose and chemically altered by man, while the second one are made from synthesized polymers or small molecules and usually the compounds that are used to make these fibres come from raw materials such as petroleum based chemicals. Natural fibres can be further classified according to their origin into the following three groups:

- **Vegetable Fibres**: Most of these are cellulose fibres and include cotton, linen, jute, flax, ramie, coir, sisal and hemp. Besides their use as textiles, cellulose fibres are also used in the manufacture of paper and other useful
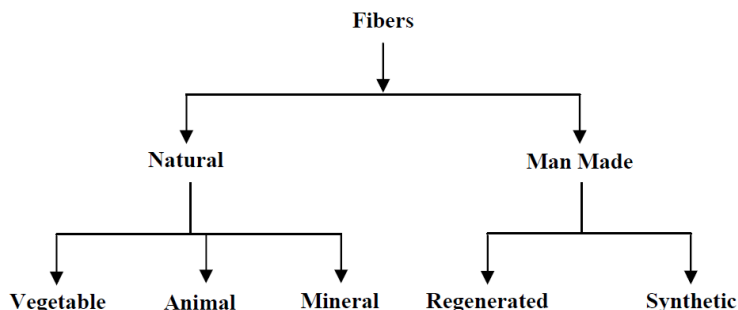
Figure 1.3: Fibre's categories

products like ropes, cords, coir mats, industrial fabrics, etc.

- **Animal Fibres**: They are mostly protein fibres and include wool and silk.

- **Mineral Fibres**: Asbestos is the only naturally occurring mineral fibre that was used extensively for making industrial products but is now being gradually phased out due to its suspected carcinogenic effect.

Though there are major differences in fibre structure between natural and man-made fibres, the long molecules are oriented in both cases and show the presence of both order and disorder in the way molecules are organized. The ordered molecules (which may form crystalline regions) contribute to durability, strength, stability and recovery while the disordered regions (which may form the amorphous phase) make a contribution to elongation, dye and moisture absorption and toughness. There are a number of differences too. The natural fibres show much greater non-uniformity than man-made fibres. Thus testing of natural fibres requires the testing of a very large number of samples before quoting an average value. Another important difference is the complex morphology of natural fibres as opposed to the rather simpler morphology of man-made fibres. A third important difference is that natural fibres absorb a greater amount of moisture because they contain more water absorbing groups than the synthetic fibres. Of course, viscose rayon, a man-made fibre, absorbs a significant amount of moisture because of its cellulosic structure. This makes natural fibres and viscose rayon more comfortable in the form of apparel wear, particularly in tropical and hot climates.

1.2.1 Natural fibres

In recent years a significant amount of interest has been shown in the potential of natural fibres, such as abaca, bamboo, flax, hemp, jute, ramie, and sisal to replace wood fibre and glass fibre as the reinforcements. These fibres offer specific benefits such as low density, low pollutant emissions, biodegradability, high specific properties and low cost [8, 9]. In Table 1.1 the mechanical properties of some representative natural fibres are reported. It can be seen from these data that the density of glass fibre is over 60% higher than that of natural plant based fibres. This provide that the specific stiffness of glass fibre is comparable to that of some natural fibres.

Table 1.1: Mechanical properties of some natural and synthetic fibres [9]

Fibre	Diameter [μm]	Density [g/cm^3]	Elongation at break [%]	Tensile strength [MPa]	Young's modulus [GPa]
Cotton	12 - 13	1.5	7.0 - 8.0	287 - 597	5.5 - 12.6
Jute	10 - 25	1.3	1.5 - 1.8	393 - 773	26.5
Flax	5 - 38	1.5	2.7 - 3.2	345 - 1035	27.6
Hemp	10 - 51	1.4	1.6	690	35
Sisal	8 - 41	1.5	2.0 - 2.5	511 - 635	9.4 - 22.0
Coir		1.2	30.0	175	4 - 6
Bamboo		0.8	-	391 - 1000	48 - 89
Ramie	11 - 80	1.5	3.6 - 3.8	400 - 938	61.4 - 128.0
Glass	10	2.5	2.8	2000 - 3500	70
Carbon	7 - 10	1.4	1.4 - 1.8	4000	230 - 240

Natural cellulosic fibres are generally lignocellulosic consisting of helically wound cellulose microfibrils in an amorphous matrix of lignin and hemicellulose. These fibres consist of several fibrils that run along the length of the fibre.

The properties of these fibres are very difficult to measure with a considerable number of fibres (between 500 and 4000) needing to be tested to obtain statistically significant mean values ($p < 0.05$). These properties are also strongly influenced by many factors, particularly chemical composition and internal fibre structure, which differ between different parts of a plant as well as between different plants [10]. Other factors that may affect the fibre properties are maturity, separating process, microscopic and molecular defects such as pits and nodes, type of soil and weather conditions under which they were grown [11].

Natural cellulosic fibres present many advantages compared to synthetic fibres which make them attractive as reinforcements in composite materials. They come from an abundant and renewable resources [8, 9] at low cost, which ensures a continuous fibre supply and a significant material cost saving to the plastics industry. Cellulose fibres, despite their low strength, can lead to composites with high specific properties because of their low densities (Table 1.1). Unlike brittle fibres, such as glass and carbon fibres, cellulose fibres are flexible and will not fracture when processed over sharp curvatures [12]. This enables the fibres to maintain the desired aspect ratio for good performance. Their non-abrasive nature permits a high volume fraction of filling [12] during processing, and this results in high mechanical properties without the usual machine wear problems associated with synthetic fibres especially glass and ceramic. Natural cellulosic fibres are also non-toxic [13], easy to handle and present no health problems like glass fibres that can cause skin irritations and respiratory diseases when the fibrous dust is inhaled. They offer a high ability for surface modification, are economical, require low amounts of energy for processing and are biodegradable [9]. In terms of socio-economic issues, the use of cellulose fibres as source of raw materials is beneficial because it generates a economic development opportunity for non-food farm products in rural areas. These mentioned advantages are benefits and not likely to be ignored by the plastics industry for use in the automotive, building,

appliance, and other applications [14].

Despite the advantages mentioned above, use of natural cellulosic fibres in thermoplastics has not been extensive. Possible reasons that contribute to unsatisfactory final properties of the composite include:

- Variable quality [15] depending on unpredictable influences, such as weather.

- Limited thermal stability at typical melt processing temperatures of about 200 °C. This excludes some manufacturing processes and limits the type of thermoplastic that can be used to such low-temperature polymers as polypropylene, polystyrene and polyethylene [16]. Higher processing temperatures that reduce melt viscosity and facilitate good mixing, however, are possible, but only for short periods. If degradation occurs, cellulose fibres can be responsible for the formation of tar-like products and pyrolysis acids that may have various damaging effects both on the processing equipment and the composite properties. One simple method that can be used to overcome this problem involves acetylation.

- Poor dispersion characteristics in the non - polar olefinic thermoplastic melt due to strong hydrogen forces between the fibres.

- Limited compatibility with many thermoplastic matrices due to their highly hydrophilic character; this results in poor mechanical properties of the composites produced [17].

- High moisture absorption of the fibres that can affect the dimensional stability of the composite [12] and the interfacial bond strength. The high moisture absorption [16] of the fibres due to hydrogen bonding of water molecules to the hydroxyl groups within the fibre cell wall leads to a moisture build-up in the fibre cell wall (fibre swelling) and also in the fibre-matrix interface. This is responsible for changes in the dimensions of cellulose-based composites, particularly in the thickness and the linear expansion due to reversible and irreversible swelling of the composites. The tendency of cellulose fibres to absorb moisture causes off-gassing (void formation) during compounding and, furthermore, the fibre-matrix adhesion is weak. The amount of moisture absorption in the cellulose fibres can be dramatically reduced through chemical modification, such as acetylation, of some of the hydroxyl groups present in the fibres [12, 16].

The incorporation of cellulose fibres into synthetic polymers is often associated with a lack of fibre dispersion due to the wide differences in polarity and also the strong intermolecular hydrogen bonding between the fibres [18]. This lack of fibre dispersion can result in clumping and agglomeration of cellulose fibres which will act as stress concentration points to initiate cracks during loading. This effect contributes to inferior mechanical properties. This problem can be overcome by pretreatment of the fibres with polymer coating materials. The introduction of polymer coatings on fibre surfaces helps to separate fibres from each other, eliminating the hydrogen bonding that holds them together [19]. This approach also induces bond formation between the fibres and the matrix resulting in improved composite properties.

There are many reports on the potential use and limitation of cellulose fibres as reinforcement in thermoplastics available in the literature. These studies show that the problems mentioned above are common, independent of the type and origin of the fibre employed. Other factors that may hamper increased use of cellulose fibres in plastics are problems and costs associated with the collection and storage which are not yet mechanized and standardized to produce fibres of high and uniform quality.

1.2.2   Natural fibre application

There is growing urgency to develop and commercialize new crops, new biobased products and other innovative technology which do not rely on fossil fuel [8]. There are several advantages of fully green composites over petroleum based composites: low density, low cost of the components, reduced dermal and respiratory irritation, enhanced energy recovery, and biodegradability. Fully green composites (biocomposites) are becoming one of the most important factors in creating a more ecological future. The number of developments in making biocomposites using materials obtained from renewable resources as reinforcements and matrix have been increasing year by year, spurred by the growing seriousness of environmental problems [20]. Reinforcing biofibres, biodegradable polymers and biocomposites have been reviewed by Mohanty et al. [8]. A large number of interesting applications made out of biodegradable materials are appearing commercially all over the world [21]. In the US, Canada and Australia, wood fibre based composites for buildings have been under development for some time. In India and South America, jute and sugar cane bagasse fibres are used in low cost housing, and rice husk based composites have been developed recently to make planking/shelving. In Japan, FUJITSU Corporation introduced biodegradable laptop computer casings made out of poly(lactic acid) (PLA), which is derived from corn starch. NEC Corporation in Japan has presented a cell phone made of kenaf fibre reinforced bio plastics based on PLA resin for the first time in the world [22].

Recently, in Europe, the automotive manufacturers have started using natural fibres such as jute and flax instead of glass fibres [8, 23, 24, 25, 26]. Their use is not a new idea since as long ago as 1941, Henry Ford developed a prototype composite car made from hemp fibres [12]. He, believing that "the most environmentally friendly thing you can do for a car that burns gasoline is to make lighter bodies", had hoped to shift from steel to lower-weight materials [25]. Reducing the total weight of cars should aid in saving fossil resources because, for instance, nearly half of the mineral oil products consumed in Germany are burned as fuel in cars [27]. Nowadays, the automotive field is still the predominant one in NFC (Natural Fibre Composites) applications: uses of natural fibre reinforcement have proven viable in a number of automotive parts. Flax, sisal and hemp are processed into door cladding, seatback linings, and floor panels. Coconut fibre is used to make seat bottoms, back cushions, and head restraints, while cotton is used to provide sound proofing, and wood fibre is used in seatback cushions. Acaba is used in underfloor body panels, and other manufacturers are implementing natural ingredients into their cars as well. For example, the BMW Group incorporates a considerable amount of renewable raw materials into its vehicles, including 10,000 tonnes of natural fibres in 2004. The Mercedes S-class [25] uses 43 kg of natural

(a)	(b)

Figure 1.4: Natural fibre composite parts for automotive interior applications

fibre (hemp fibres) reinforced thermoplastics (polypropylene) in door cards, seat bases, pillar inners, head liner, rear cargo shelf and trunk components and other internal applications (Figure 1.4); the 2005 Ford Mondeo uses polypropylene reinforced with kenaf in its door linings [28]. A recent study (Karus, Kaup, and Lohmeyer) conducted by the nova - Institut (Germany) in cooperation with Asta Edert Composite consulting (Austria/Finland) reports the first comprehensive and detailed picture of the use and amount of wood and natural fibre reinforced composites in the European bio - based economy.

Figure 1.5 shows the total volume of 80,000 tonnes different wood and natural fibres used in 150,000 tonnes of composites in passenger cars and lorries, produced in Europe in 2012 (90,000 tonnes Natural Fibre Composites and 60,000 tonnes WPC). Recycled Cotton Fibre Composites are mainly used for the driver cabins of lorries. The highest market shares are made up for by wood (European origin), recycled cotton (from world market) and flax fibres (European origin). Compared to the last survey for the year 2005, the shares of kenaf (from Asia) and hemp fibres (European origin) show the biggest increase in percentage.
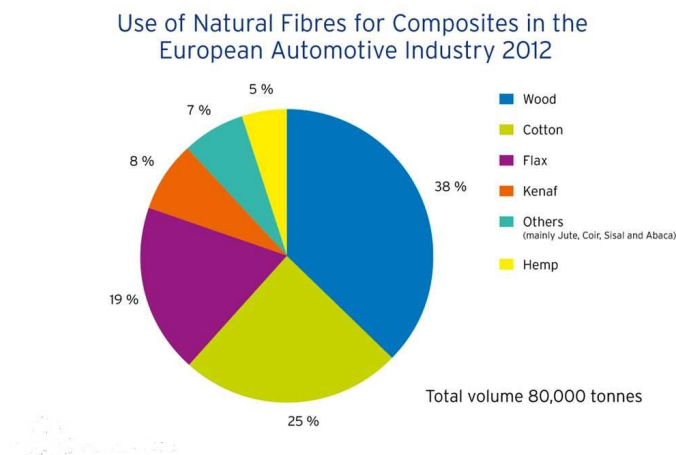
Figure 1.5: Use of Natural Fibres for Composites in the European Automotive Industry 2012

1.3 Plastic matrices

Synthetic large molecules that are made by joining together thousands of small molecular units known as monomers and a relatively long chain of monomers are known as polymers. When additives are coupled with the polymers to improve its inherent property, then the material is termed as plastics. According to molecular chain structure and type of linkage, plastics are classified as thermosetting, elastomeric and thermoplastic materials.

1.3.1 Thermosets

A thermosetting plastic is produced by a chemical reaction that forms long chain-like molecules whose molecular chains are not cross-linked, but on application heat and pressure, the cross-linking reaction takes place resulting in a rigid structure. As during this stage, the long chains are interlinked, the material cannot be softened due to the presence of strong bonds. This feature of single use renders them difficult to recycle hence the name thermoset. They therefore offer high thermal stability, good rigidity and hardness, and resistance to creep.

Thermosetting resins have little use a pure resin, but require addition of other chemicals to render them processable. For reinforced plastics, the compounds usually comprise a resin system (with curing agents, hardeners, inhibitors, plasticisers) and fillers and /or reinforcement. The resin system provides the 'binder,' to a large extent dictating the cost, dimensional stability, heat and chemical resistance, and basic flammability. The reinforcement can influence these (particularly heat and dimensional stability) but the main effect is on tensile strength and toughness. High performance fibres, of course, have a fundamental influence on cost. Special fillers and additives can influence mechanical properties, especially for improvement in dimensional stability, but they are mainly used to confer specific properties, such as flame retardancy, ultraviolet (UV) stability or electrical conductivity.

Typical thermosetting materials are polyester (UP) resin, epoxy (EP) resin, phenol-formaldehyde (PF) resins, urea-formaldehyde (UF) resins and melamine formaldehyde (MF) resins.

1.3.2 Thermoplastics

The use of biodegradable polymers has become more popular recently due to growing environmental awareness of the environmental impact of petroleum-based plastics. It is also regarded as one of the alternatives to minimize the dependency on petroleum-based plastics, especially in the packaging applications since this sector is the largest consumer of petroleum-based polymers worldwide [8]. Since the inception of this new class of materials nearly 50 years ago, the market for polymers and polymer blends has grown at a phenomenal rate. Commodity resins including polyethylene (PE), polypropylene (PP), polystyrene (PS), acrylonitrilebutadiene-styrene (ABS) and polyvinyl chloride (PVC) now account for 79% of all plastics consumption (Figure 1.6). Plastics have displaced conventional materials in a wide variety of both technical and consumer applications and in 2002 Utracki [30] reported that the worldwide market for polymer blends was in the vicinity of US$200 billion annually. In the same year over 80% (by
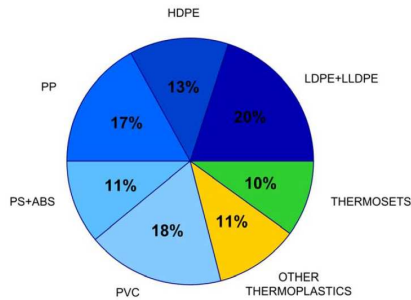
Figure 1.6: World market share of major polymer resins (1995-2000)[30].

weight) of all plastics were consumed in producing polymer blends, alloys and composites.

Thermoplastic materials are manufactured by the process of polymerisation, during which a large numbers of small molecules (monomer units) combine to form a uni-dimensional, long chain macromolecule which are not cross-linked. Due to this characteristic property, they can be converted to different shapes by increasing the temperature to its softening state, which on cooling revert to its rigid state retaining its shape. As this is temperature dependent, these plastics provide the advantage of re-processing. In theory this process may be repeated indefinitely, but repetition is in fact limited by the processing stability of the material used. Over the re-processing other advantages in thermoplastic matrix compared with thermosetting matrix composites are: the absence of chemical reactions during processing and fabrication, the fact that no special storage conditions are required, the rapid fabrication and the reduction in initial and in-service costs [31]. The Greenpeace reported a 'pyramid of plastics' (Figure 1.7) illustrating which plastics are harmful to the environment: PVC is the worst option, polyolefins (PE and PP) the best.
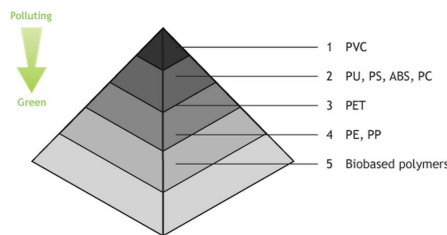
Figure 1.7: Piramid of plastics

Polyolefins are simpler polymer structures that do not need plasticizers, although they do use additives such as UV and heat stabilizers, antioxidants and in some applications flame retardants. Both PE and PP are versatile and cheap, and can be designed to replace almost all PVC applications. PE can be made either hard, or very flexible, without the use of plasticizers. PP is easy to mold and can also be used in a wide range of applications. In comparison with PVC, PE and PP use fewer problematic additives, have reduced leaching potential in landfills, reduced potential for dioxin formation during burning (provided that

brominated/chlorinated flame retardants are not used), and reduced technical problems and costs during recycling. The mechanical properties of some thermoplastics are shown in Table 1.2.

Table 1.2: Mechanical properties of some thermoplastcs [32]

Matrix polymer	Density $[kg/m^3]$	Tensile Strength $[MPa]$	Tensile Modulus $[GPa]$	Flexural Strength $[MPa]$	Impact Strength $[J/cm^3]$
PVC	1.4 - 1.54	24 - 62	2.4 - 4.1	69 - 110	0.2 - 10.6
PS	1.04 - 1.11	35 - 84	2.8 - 3.5	83 - 118	0.13 - 0.34
PET	1.34	41.5	2.46	61.5	-
LDPE	0.918 - 0.940	0.4 - 16	0.12 - 0.24	-	no break
HDPE	0.95 - 0.965	21 - 38	0.42 - 1.4	35 - 50	0.6
PP	0.9 - 0.91	27 - 40	0.5 - 1.9	45 - 50	0.2 - 1.2

1.4 Biocomposites

Broadly defined, biocomposites (Figure 1.8) are composite materials made from natural fibre and petroleum-derived non-biodegradable polymers like PP, PE, and epoxies or biopolymers like PLA and PHAs. Composite materials derived from biopolymer and synthetic fibres such as glass and carbon also come under biocomposites. Biocomposites derived from plant-derived fibre (natural/biofibre) and crop/bioderived plastic (biopolymer/bioplastic) are likely more ecofriendly, and such biocomposites are sometimes termed "green composites" [8].
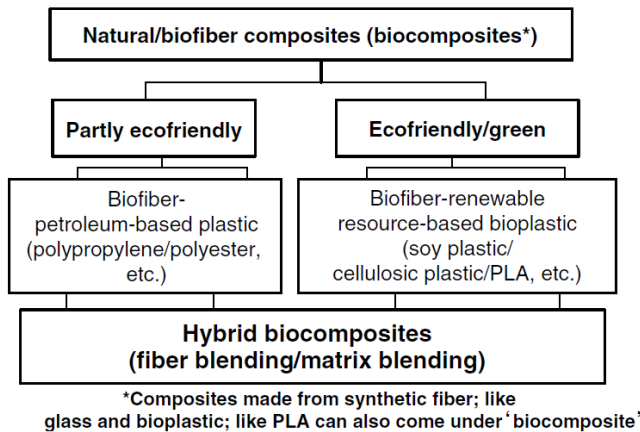
Figure 1.8: Classification of biobased composites

1.5 Manufacturing

Numerous composite manufacturing processes have been invented to process different matrices (thermoset or thermoplastic) and reinforcements (continuous or discontinuous). Each process has advantages that make it the most suitable for a particular application. Depending on the type of matrix and reinforcement used, these manufacturing processes can be broadly categorised into three main groups [33]. For short or discountinuous fibre reinforcements, Compression Moulding, Extrusion and Injection Moulding are the main processes. In these processes, either a thermoset or a thermoplastic matrix can be used. For a thermoplastic matrix and long fibre reinforcements, Composite Sheet Forming and Pultrusion are the main processes. Hand Lay-up, Autoclave Moulding, Liquid Composite Moulding (LCM), and Filament Winding are the main processes for long fibre reinforcements using a thermoset matrix. In addition, based on the moulding arrangement, the last category of processes can also be categorised as either open (e.g. Hand Lay-up) or closed (e.g. LCM) mould processes. A good review of manufacturing and forming composites has been compiled by [34]. Most common methods of natural fibre thermoplastic composites manufacturing include compression moulding, injection moulding, continuous extrusion, pultrusion and rotational moulding.

1.5.1 Thermoplastics forming

Thermoplastics (TPC) forming involves a number of simultaneous and/or sequential operations including heating, forming, consolidation and cooling of the material. There are specific properties of a TPC which require careful control of the process cycle during forming to achieve all of the above operations and produce a quality part. In particular, the thermoplastic matrix, at melt processing temperatures, has a high viscosity ($\sim 10^3 Pas$) by comparison with a thermoset ($\sim 1 Pas$). For forming, the material must firstly be heated above the matrix melting temperature where it will be sufficiently flexible to partially conform to a shaped mould. Sufficient pressure and time, at the melt temperature, is then needed to achieve full mould conformation, impregnation of the fibre reinforcement by the matrix and consequent full consolidation of the TPC. The required time at pressure depends on the matrix viscosity, the heating regime and the TPC material form. For the latter a number of forms have been developed specifically to reduce the impregnation/consolidation times. Fully pre-consolidated, commingled and powder impregnated forms all reduce the flow distance for the matrix allowing lower pressure processing and/or shorter cycle times [35].

Two processes are available: 'isothermal' and 'non-isothermal'. In the isothermal process, shown in Figure 1.9 (a), the preform (and tool) are heated to above the matrix melt temperature, i.e. the forming/consolidation temperature, and pressure is applied whilst the temperature is held constant at this level. Pressure is then maintained during cooling to below the recrystallisation temperature to ensure the consolidation achieved during the isothermal part of the cycle is maintained and the resulting part has low void content ($< 1\%$). Quenching (rapid cooling) can take place beyond this time to speed up the process. Whereas isothermal moulding like this can achieve high quality parts with excellent consolidation, as required by the aerospace industry, for instance, the cycle time is

(a)

(b)
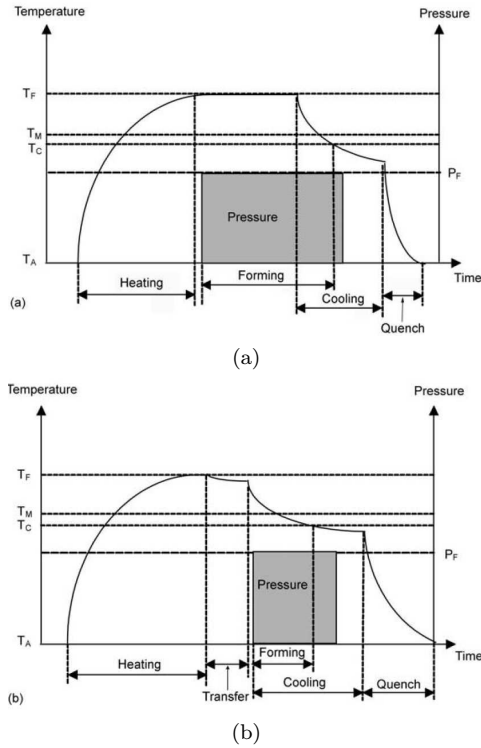
Figure 1.9: Temperature and pressure *vs.* time profile for (a) isothermal and (b) non-isothermal forming of thermoplastic composites

compromised by having to cycle the tool temperature during the process.

By contrast, a shorter cycle time can be achieved using the non-isothermal process shown in Figure 1.9 (b). Here, the preform is preheated to the forming/consolidation temperature usually separately in an oven. The preheated charge is then rapidly transferred to a forming tool located in a pressing station (e.g., press or vacuum, etc.). Pressure is then applied quickly at the same time the charge is cooling on contact with the tool, i.e. non-isothermal forming. Pressure can then be removed when the temperature has reduced to below the matrix recrystallisation temperature and quenching can follow if required. The non-isothermal process requires no temperature cycling of the tool and consequently heating and cooling times can be significantly shorter than the isothermal process. Process cycle times are therefore shorter. However, there is a limited time and temperature window during which forming and consolidation can take place. Consequently, the method is often applied to materials with lower reinforcement volume fraction and/or with forms requiring lower consolidation pressures and times, e.g. commingled and powder impregnated materials. The non-isothermal process is also attractive where medium to high production volumes, i.e. short cycle times, are required, and higher void content levels are acceptable, such as in the automotive industry.

1.5.2   Compression Moulding

Compression moulding is one of the most common methods used to produce articles from thermosetting plastics. The process can also be used for thermoplastics but this is less common. Compression moulding was first developed to manufacture composite parts for metal replacement applications, typically for parts of a flat or moderately curved geometry. In compression moulding technique, a composite prepreg is laid in a mould and pressed for a certain time at elevated temperature and pressure, which is subsequently cooled. Mould temperatures are usually in the range of 130-200 °C. Hydraulic presses with heating and cooling options are usually used to accomplish this. The main advantage of compression moulding is that the process does not impose restrictions on the reinforcing fibre length, as opposed to injection moulding and extrusion processes. However incorporation of long fibres in the form of tows or mats and restraining them from movement during consolidation process may prove to be a tedious task. Another advantage of compression moulding is that the cost of tooling involved in this process is relatively lower compared to that of extrusion and injection moulding processes [36]. Matched-die forming is most widely used to manufacture natural fibre thermoplastics. Many researchers have applied compression moulding to manufacture variety of materials such as, mats comprising of long natural-polymer commingled fibres, layers of extruded wood flour-thermoplastic pellets, fibre mats interleaved between thermoplastic sheets. They found that the properties of the composites manufactured from compression moulding depend on the processing parameters such as the platen temperature, pressure applied and the consolidation time. Bowis ([37]) has determined the process parameters experimentally by varying them at different levels and comparing the mechanical properties of the woodfibre-PP composites with respect to the processing parameters. He has obtained maximum mechanical properties at pressures of 1.4 MPa, temperature of 185°C and consolidation time of 10 min. Though compression moulding offers several advantages such as low tooling, minimum wastage of material and the use of long fibres, it is limited to a semi-continuous process. Therefore, in cases where continuous production is required, continuous extrusion or injection moulding is preferred to compression moulding.
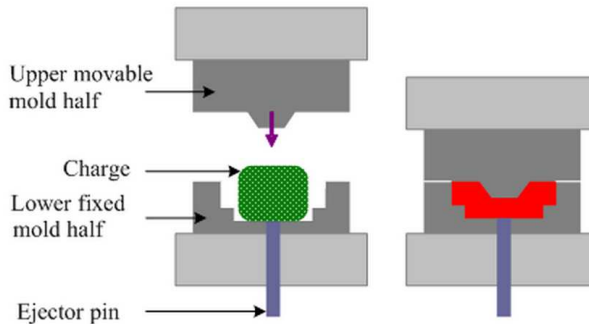
Figure 1.10: Compression Moulding

1.5.3 Vacuum forming

Vacuum forming is a common technique for forming TPCs similar to the method used for thermosets. Figure 1.11 shows the basic isothermal process. The TPC laminate is laid up on a single-sided mould (metal, metal shell or composite) and covered with a release film (i.e. peel ply) and breather cloth. The former prevents the breather cloth bonding to the laminate and the latter ensures all air is extracted under vacuum, and even distribution of pressure. A vacuum bag is then positioned over the arrangement and sealed around its edges against the mould. Typical bag materials include disposable nylon film or reusable silicon rubber. The air is pumped out until vacuum pressure up to 0.9 ± 0.95 bar is achieved. The whole arrangement is then placed in a circulating air oven and the temperature raised to above the matrix melting temperature for forming and consolidation to take place. Consolidation time depends on part size, material thickness and degree of void content allowable in the final part. Generally 10 $\pm$ 15 minutes consolidation time will result in void content below 2%. Longer times are necessary for better quality. It is also important that sufficient heating time has been allowed to ensure the tool reaches the processing temperature and the laminate is heated through its full thickness. Large tools (for large parts) can result in significant heating times (hours) making the technique, in most cases, a low volume process. To speed up the process, shell tools with lower thermal inertia can be used but this will depend on the economics of the process. Following consolidation, the tool, etc., is removed from the oven and allowed to cool before the part can be removed. Vacuum is maintained during cooling. Again, depending on the size and construction of the tool, cooling can be a slow process. An alternative to oven heating, is to heat the tool directly using oil or electrical methods. This can, in some cases, speed up the process, but its viability depends very much on the part size and shape. More complex shaped parts prohibit uniform heating by this method.
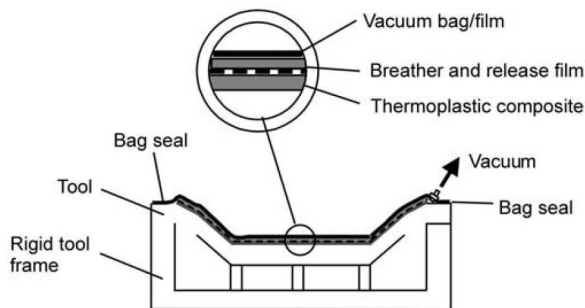
Figure 1.11: Schematic diagram of the isothermal vacuum forming process

Chapter 2

Flax-PE composites: Manufacturing and testing

In this chapter a background of the investigated materials, with an accurate and sinthetic description concerning origin, mechanical properties, cost and using of flax fibres and polyethylene, has been reported. Than the manufacturing method and the mechanical performance of these panels have been investigated.

2.1 Flax fibres

The flax family, Linaceae, contains about 230 species from all over the world. One of the species, Linum angustifolium, is a wild flax plant that still exists in some European regions (e.g. the Caucasus, the Alps and Corsica), and which is considered to be the parent of the flax plant as known today: Linumusitatissimum, a cultivated species mostly used as a fibre-producing plant.

Flax (*Linum usitatissimum L.*) is probably the oldest textile fibre known to mankind. It has been used since ancient times for the production of linen cloth. The first well documented application is the use of the linen fabric by the Egyptians to wrap their mummies. Linen fabric was found in graves in Egypt dating from before 5000 B.C.. At that time the Egyptians were able to produce yarns and fabrics of a fineness that is nowadays unobtainable [38]. However, the theory that the Phoenician merchants brought the plant and the knowledge from Egypt to the European continent around 2200 B.C. is vitiated by the discoveries done in Switzerland during the 19th century: several remainders of linen fabrics, flax yarns and tools (flax seeds, twines and fishing net) were found near the Lake Constance, which date back from the Neolithic Ages (5000 B.C. - 1900 B.C.). This proves the simultaneous existence of the flax culture in both Europe and Egypt. Over the millennia flax has always been used as the basis for fabric, not only for clothing but also for sails and tents [39], and it was the all important fibre used for war outfit until 1950, after which synthetic fibres took over [38]. The flax industry has been declining ever since 1955, after which the competition of synthetic fibres became stronger and stronger in different application areas. Only quite recently flax is blended with synthetic fibres to combine the advan-

tages of both different materials, and the apparel market has once more become a large buyer for the flax industry. However, flax and especially the production of long fibres, has in this way become very dependent on the fashion industry. Consequently the flax industry has become a very cyclical business, and the industry is searching for new, preferably high value, steady markets. Although the waste streams of the flax production, like the woody shives, have since long been used in for instance chipboards for building applications, only in the last decade a renewed interest to use also the bast fibres as reinforcement in plastic matrix composites has risen. The low elasticity of the flax fibres compared to other fibres like wool and cotton, which is a disadvantage during the spinning process, is for the use in composites a prerequisite. One of the first uses in this field was linen fabric as reinforcement for phenol resin for the construction of a Spitfire aircraft during World War II. More recent applications are found in modern cars like for instance several Mercedes models and other European cars, where non-woven fibre mats are used commercially for interior panels [25], sometimes in combination with other agrofibres. Presently two types of flax are grown, fibre flax and seed flax. Fibre flax is optimised for the production of thin strong fibres. Seed flax gives coarser fibres, but far more linseed, since this plant does not have one straight stem, but the stem divides towards various flower heads. Flax grows in moderate climates and is presently cultivated among others in large parts of Western and Eastern Europe, in Canada and the USA and in Russia. World-wide approximately 5 million hectare flax is grown. Circa 3.8 million hectare is used for the production of linseed only, 0.2 hectare for fibres only, and approximately 1 million hectare for both linseed and fibres [40]. In the traditional flax countries like the Netherlands, Belgium and France, the main focus of the flax production lies still on the apparel and home textile market. The main output from this production chain are the long fibres for spinning yarn. For this purpose flax fibres are isolated from the plant via processes known as retting, breaking, scutching and hackling. Short fibres are produced as an inevitable by-product. In the new flax (and hemp) countries processing of the fibres is almost entirely done by the 'lin-total' concept, in which long and short fibres are not separated. The output of this process are short fibres. In 1999 in the EU approximately 60 to 70 kton of short fibres was produced, these found their application in specialty pulps (45%) in the apparel and home textiles (20%) in composites for the automotive industry (6%, 4 kton) and in various other applications, of which especially the thermal insulation materials were expected to grow significantly. The expectation was in 1999 that the application of European flax in composites for automotive would grow quickly to 5.5 kton, in 2000 (Karus, Kaup, and Lohmeyer). Vegetable fibres (e.g., cotton, flax, hemp,jute) are composed of cellulose,and they can be generally classified as bast, leaf, or seed-hair fibres, depending on their origin. In plants, bast and leaf fibres provide mechanical support to the stem or leaf, respectively, as is the case in flax, hemp, jute, or ramie. A schematic representation of a flax fibre from stam to microfibril is shown in Figure 2.1.

 Many natural fibres, as flax, have a hollow space (the lumen), as well as nodes at irregular distances that divide the fibre into individual cells. The surface of natural fibres is rough and uneven and provides good adhesion to the matrix in a composite structure. The morphology of the fibres shows similarities and composites produced using them show similar properties. The industrially important flax fibres are placed as fibre bundles in the outer surface of the plant stem as
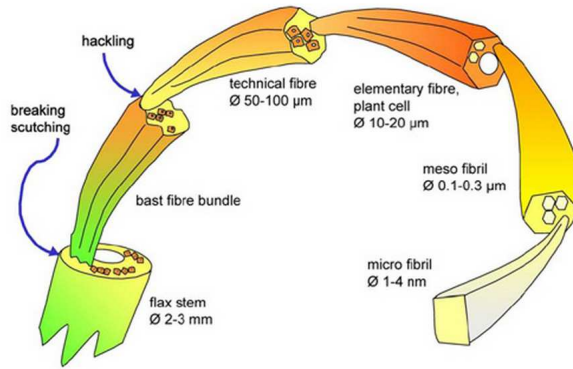
Figure 2.1: Schematic representation of a flax fibre from stam to microfibril

shown in Figure 2.2. The bundles (technical fibres) are between 60 and 140 cm long and their diameter ranges from 40 to 80 μm. The flax stem contains 20-50 bundles in their cross section. Each bundle consists of 10-40 spindle shaped single (elementary) fibres of 1-12 cm length and 15-30 μm diameter [41]. The single fibres have been shown to possess different cross sectional shapes along the fibre axis. Some researchers have approximated fibres possessing hexagonal or pentagonal cross-sections [42]. However, the fibres vary in their non-uniform geometrical shapes along the fibre axis. Owing to these irregularities in the thickness of the cell walls, the fibres vary greatly in strength (i.e. failure load, N). A single fibre across the cross section consists of a primary cell wall and secondary cell walls, and a lumen in the centre of the fibre [43]. Charlet et al. [44] showed that the fibre diameter can vary two to threefold within a few millimetres of fibre length. They studied the diameter of the elementary fibres isolated from the bottom, the middle and the top part of the flax stems. The mean fibre diameter was found to decrease from the bottom to the top of the stems. The cross sectional area of fibres from each zone was analysed to measure the fibre cell wall area. They also found that the mechanical properties of the fibres are strongly influenced by their location in the stem.
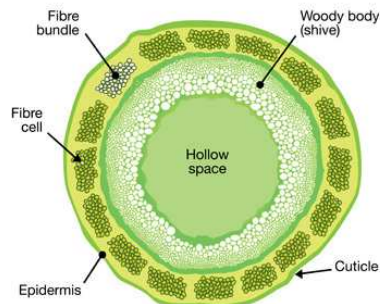
Figure 2.2: Flax fibre section

2.2 Polyethylene (PE)

Fibres are embedded in a matrix, the task of which is to hold the fibres together. This provides and stabilizes the shape of the composite structure, transmits the shear forces between the mechanically high-quality fibres, and protects them against radiation and other aggressive media. Polymers (except elastomers) are usually subdivided into thermosets and thermoplastics, both of which are suitable as matrix systems for construction materials made from biocomposites. Thermoset, thermoplastic starch, and polyolefines (polyethylene and polypropylene) are all matrix materials for natural-fibre reinforced composites. Polypropylene is the most common matrix studied in biocomposites because of its low cost, unproblematic ecological recycling, and good heat resistance [45]. Although polyethylene has suitable characteristics as a matrix in natural fibre-reinforced composites [46] compared with polypropylene, studies on polyethylene being used as a matrix still need to be developed. Polyethylene has a very low glass transition temperature (T_g= -110°C) associated with a good retention of mechanical properties, including flexibility and impact resistance at low temperatures, which makes it a competitive material as a matrix.

(a) (b)

Figure 2.3: Polyethylene as film (a) and as granules (b)

2.3 Polyethylene composites

Natural fibre reinforced high density poly ethylene (HDPE), low density poly ethylene (LDPE) and lineasr low density poly ethylene (LLDPE) composites were studied in detail by researchers. The mechanical and viscoelastical behaviour of jute fibre reinforced high density polyethylene (HDPE) vere studied by Mohanty [9]. Variations in mechanical strength, storage modulus (E'), loss modulus (E") and damping parameter (tan δ) with the addition of fibres and coupling agents were investigated. The deformation and fracture of a natural fibre (flax fibre) / recycled polymer (HDPE) composite was done by Singleton [47]. Improvements in strength and stiffness combined with high thoughness were achieved by varying in the fibre volume fraction and controlling the bonding between layers of the composite. Natural fibres are generally incompatible with polyolefins, because of their hydrophilic character compared to the hydrophobic character of polyolefins. Most of the studies were therefore aimed at investigating the influence of different

fibre treatments on the properties of the composites. Lu et al. [48] investigated coupling efficiency of seven coupling agents in wood-polymer composites (WPC). The improvement on the interfacial bonding strength, flexural modulus, and other mechanical properties of the resultant wood fibre/high-density polyethylene composites was mainly related to the coupling agent type, function groups, molecular weight and chain structure. Coconut fibre has been used as reinforcement in low density polyethylene [49]. It was found that fibre/matrix interfacial bonding was higher in the as received fibre compared to the wax free fibre. George et al. [50] analysed the improved interfacial interactions in the pineapple leaf fibre reinforced polyethylene composites. they used various chemical treatments using reagents such as NaOH, silane and peroxide to improve the interfacial bonding and found that the treatment improved the mechanical properties.

2.4 Manufacturing

2.4.1 Flat panel manufacturing

The panel investigated, of thickness 3.6 mm, is made of unidirectional flax fibres mat (UD180-C003) of 180 g/m^2 from Lineo, Belgium (at 0.3 volume fraction) combined with Linear Low Density PolyEthylene (LLDPE) films with a density of 0.91 g/cm^3. The panels herein discussed were manufactured at CACM (Centre for Advanced Composite Material) of the University of Auckland using a vacuum bag technique. The vacuum bagging is a clamping method that uses atmospheric pressure to hold the adhesive or resin-coated components of a lamination in place until the adhesive cures. This technique involves first the positioning of the panel lay-up onto a tool, hence the placing and sealing of a flexible bag over the lay-up. All the air is evacuated from under the bag by using a vacuum pump. The removal of the air forces the bag down onto the lay-up thanks to the atmospheric pressure (1 bar). At the end, the assembly, including the vacuum bag as well, is placed inside an oven. The vacuum bag machine used to manufacture the sandwich panels is shown in Figure 2.4.

Figure 2.4: Panel manufacturing: vacuum bag equipment installed in the oven

2.4.2 Sandwich manufacturing

Several sandwich panels, with different face sheets and cores materials and configurations were manufactured at C.A.C.M. and investigated. Two different configurations of sandwich panels were investigated. The first configuration consists

in face sheets enclosing a recyclable, pre-preg foam core; the second one consists in face sheets enclosing honeycomb core made of PE reinforced with flax fibres. The different face sheets materials were used. The first type of face sheets is made of five plies of Plytron^{TM}, with a lay-up 0/90/0/90/0. The other type of face sheets is made of five plies of flax/PE, with a lay-up 0/90/0/90/0. Both the face sheets were manufactured by means of the vacuum bag technique. The honeycomb cores are manufactured by using a film-stacking process where the dry flax mat and LLDPE films are interleaved and laid between half hexagonal matched-dies with heating and cooling ability. The matched-die is heated to $\sim$165 °C after closing the mould at 500 mm/s, constant forming pressure of $\sim$ 0.5 MPa is maintained during the heating cycle for consolidation and the formed part is cooled within the die to avoid spring-back. The half-hexagonal corrugations are laser cut to 20 mm and 40 mm, which are then assembled and bonded using ultrasonic methods (Figure 2.5). Plytron^{TM} face sheets that are consolidated under vacuum in an oven maintained at 185°C are then bonded to the cores using ultrasonic method to make sandwich panels. All the panels are designed to fail in core shear and more about ultrasonic bonding conditions and sandwich panel design can be found in [51].

Figure 2.6 shows the manufacturing process of the NFC honeycomb core. First, the raw materials were chosen and the fibres were dried. Than the plies of fibres and matrix were assembled according to the desired configuration. The laminate was then thermoformed in a matched die to produce half-hexagonal corrugation that was cut, stacked and ultrasonically bonded to produce the complete hexagonal honeycomb core. Face sheets were manufactured using vacuum bagging technique and bonded to core to make sandwich panels.

Figure 2.5: Sandwich panel manufacturing: (a) matched-die used for forming and (b) ultrasonic bonding

2.5 Mechanical properties

Many researchers have investigated flax fibre properties at the levels of elementary fibres and technical fibres, and it can be concluded from the results that there is a large variability in the reported tensile strength and Young's modulus of flax fibres. Table 2.1 represents the tensile properties of elementary flax fibres measured in various studies. The reason for the scattering has been attributed partly to uncertainties in the measurement of the fibre cross sectional area (i.e. due to the irregularity in the cross sectional fibre shape). The tensile strength
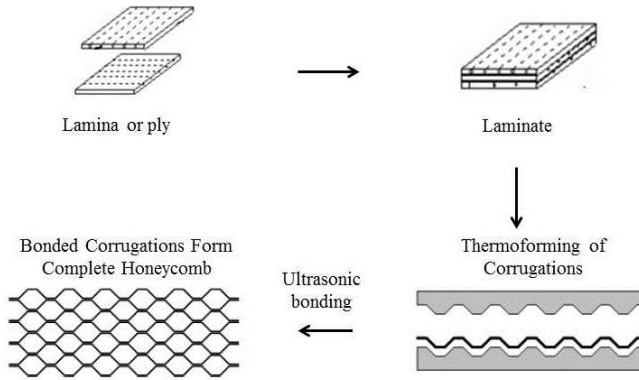
Figure 2.6: Schematic of NFC honeycomb manufacturing process

data has been mostly described using a Weibull distribution function [52]. Bos [43] showed that tensile strength of the fibres depends on the isolation procedure. Hand isolated fibres are stronger than mechanically isolated fibres. Bos found also that the mechanical treatments were found to induce kink bands in the fibres and thereby reducing their tensile strength and that,instead, the fibre strength decreases with increasing fibre gauge length. Baley has determined the tensile strength of elementary flax fibres [42]. He suggested that the fibre kink bands and micro compression defects cause a loss of tensile strength of the fibres, and they act as points of fracture initiation during fibre failure. The tensile strength and Young's modulus of the fibres were found to decrease with increasing fibre diameter.

Table 2.1: Tensile properties of elementary flax fibres

Method	Gauge Length [mm]	Average Strength ± std. dev. [MPa]	Young's Modulus ± std. dev. [GPa]	Failure strain ± std. dev. [%]
Green fibre	5	678 ± 216	-	-
Dew retted	5	906 ± 224	83 - 118	0.13 - 0.34
Enzyme retted	9	591 ± 250	57 ± 22	1.4 ± 0.9
Scutched	5	732 ± 220	-	-
Hackled	3	1522 ± 400	-	-
Hackled	10	945 ± 190	57 ± 35	2.0 ± 0.4

2.5.1 Mechanical testing set-up

It is necessary to outline the testing equipment and set-up used to determine the mechanical properties of flax-PE panels. This section details the different tests and the different grips used for each. The testing standards that were followed, as well as important test parameters such as crosshead speeds, gauge lengths and initial strain rates are also provided. Tensile and flexural tests were performed using Instron universal testing machines. Moulded specimens were tested on a

Instron machine (model 5567), pictured in Figure 2.7. Load cells were used and low value extension was measured using an advanced video extensometer. Extension outside the range of measuring equipment was determined from crosshead displacement. Test specimens underwent conditioning and testing at 23 °C ± 2°C and 50 ± 5 % relative humidity. All tensile, compression and flexural tests were performed on a minimum of five specimens and the mean and standard deviation of each set of results is reported. Experimental designs tested a minimum of ten specimens in each sample.

2.5.2 Method for determining tensile modulus and Poisson's ratio

(a)   (b)
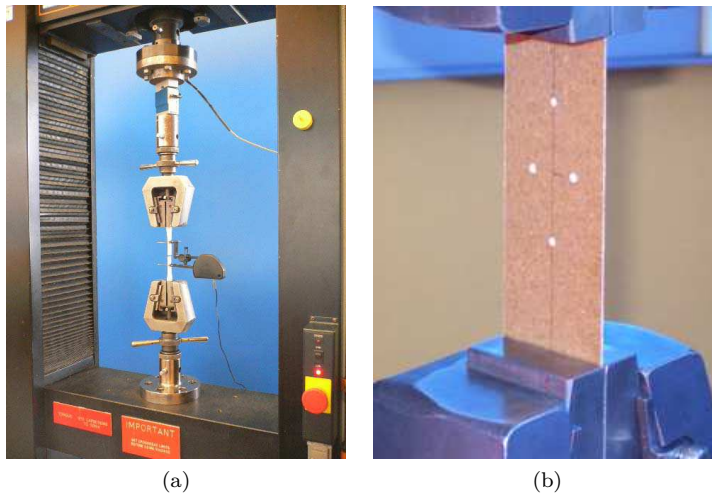
Figure 2.7: Instron universal testing machine (a) and flax-PE specimen (b)

Tensile testing in the longitudinal and transverse directions was conducted according to ASTM D3039 [53] to determine the tensile modulus and strength in both directions. The test was conducted on an Instron 5567 universal testing instrument, as shown in Figure 2.7; the distance between the grips measured 150 mm and a crosshead speed of 2 mm/min was used. Specimen were prepared in accordance with ASTM D3039 with a rectangular shape with an overall length of 220 mm, a width of 30 mm and a thickness of 3 mm and were cut on a CNC milling machine. The width and thickness of each specimen was measured in three places along the narrow section and then used to calculate the average cross-sectional area. The load cell measured the tensile load. The stress was calculated using the measured area and load data. A gauge length of 50 mm was established by marking the specimen with two white dots. A video extensometer measured the displacement of the white dots and thus the strain of the specimen. Using this stress and strain information, the tensile strength and modulus were determined. Furthermore, transverse and longitudinal strain was plotted and the gradient of the linear region, where linear elasticity is present, was used to determine the Poisson's ratio. All test specimens were conditioned from the environmental conditioning of the laboratory (Temperature=23,9 °C and humid-

Material property	Unit	Symbol	Value	Test standard
Tensile modulus	$[GPa]$	E_{11}	9.50	ASTM D 3039
Tensile modulus	$[GPa]$	E_{22}	1.30	ASTM D 3039
Tensile modulus	$[GPa]$	E_{33}	1.30	ASTM D 3039
Shear modulus	$[GPa]$	G_{12}	0.55	ASTM D 4255
Shear modulus	$[GPa]$	G_{13}	0.55	ASTM D 4255
Shear modulus	$[GPa]$	G_{23}	0.40	ASTM D 4255
Poisson ratio		ν_{12}	0.40	ASTM D 3039
Poisson ratio		ν_{13}	0.40	ASTM D 3039
Poisson ratio		ν_{23}	0.60	ASTM D 3039
Sheet density	$[kg/m^3]$	ϱ	1025	Conventional method

Table 2.2: Mechanical properties of flax-PE composites

ity= 54%). In plane shear properties were determined using two-rail shear test as per standard ASTM D 4255 [54]. Constantan alloy strain gauge rosette, EA-06-060RZ-120 of resistance 120 ($\pm 0.4\%$) and a gauge factor 2.06 at 24 °C was used to record strain. All the mechanical properties are reported in Table 2.2.

Chapter 3

Flax-PE as flat panels

In this chapter a unidirectional flax-PE panel is investigated experimentally and numerically. The modal parameters, natural frequencies, mode shapes and modal damping, are carried out from experimental tests. A finite element model is built and validated by comparing the numerical and experimental results. Finally, since the modal analysis is limited to low frequency range where the modes are well separated each other, estimation of the dispersion curves at high frequency range is performed experimentally by using Lamb waves (patch-catch technique) and experimental results are than compared with numerical ones. Both the analysis, modal and the one by means of Lamb waves, permit also to evaluate the material properties (Reverse Engineering process). This trend is particularly noticeable in the design of orthotropic panels, in which, except the parameter types like mass density or shell thickness, the mechanical properties are most uncertain.

3.1 Modal analysis

3.1.1 Introduction

Modal analysis is a method for decomposing the vibrational response of a structure into its component modes. Theory states that all vibrations are composed of individual modes, the frequencies and shapes of which are determined by the geometry, properties and supports of the structure. By exciting the structure and measuring the resulting vibration, it is possible to find the individual modes that are present. This may be achieved either by exciting the structure at a single point and measuring the vibration at many points, or by exciting the structure at many points and measuring the vibration at a single point. Excitation is typically by a shaker or an impedance hammer and it is measured by a force transducer. The resulting vibration may be measured by many methods, but often an accelerometer or laser vibrometer is used. When the output is converted to velocity (for acceleration measurements this is achieved by dividing by iw), the ratio of output velocity to input force is known as the admittance, A = v/F. Another measure in common use is impedance which is the reciprocal of admittance.

3.1.2 Experimental set-up

Frequency response measurements depend on a few major factors such as: type of structure to be tested, level of results desired, support fixture, excitation mechanism. This section investigates some of the current instrumentation and technique available for acquiring frequency response function and investigate their influence on the results. Two different testing set-up were used and are here reported. In the first test the frequency response measurements were determined through modal tests, adopting the so-called roving hammer technique. An impact hammer (ENDEVCO Modal Hammer 2302) was preferred over an electro-dynamic shaker to provide the excitation since the panel is small and light. The panel dimensions are 706x496x3.6 mm^3. Two accelerometers (PCB 352B10) were used to measure the response at the bottom corner and on sideward of the panel. Vibration measurements were taken in the frequency range 0-256 Hz. Because an impact test is not replicable (unless a mechanical device is used to hit the panel with the hammer) and in order to reduce the noise level, each measurement was obtained as the spectrum averaging of the responses of five different impacts, ensuring a coherence as much as possible close to the unity. The mesh consisted of seven points along x-axis and ten along the y-axis, equally spaced. As a rule of thumb, 2nw+1 grid points are required to describe nw half-waves, which means that the used mesh allowed to describe four half-waves along the longest side and three half-waves along the shortest one. The frequency response data was recorded using the acquisition system LMS SCADAS III and then analysed by means of the software LMS Test.Lab 8B. The panel was assumed to be not constrained to overcome any kind of problems arising from the boundary conditions. Thus the panel was suspended with bungee cords in order to simulate a free-free boundary conditions on all sides. A schematic diagram of the experimental set-up is shown in Figure 3.1.
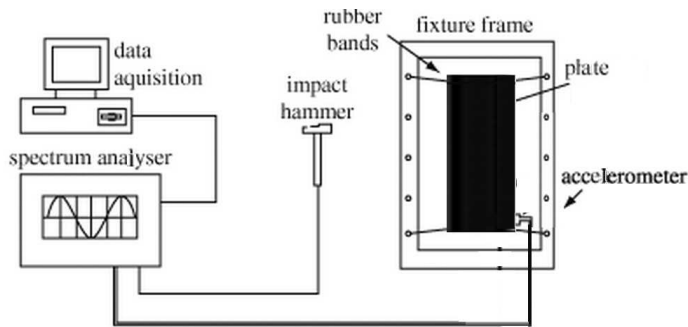
Figure 3.1: Experimental set-up: impact hammer and accelerometer

The second test set-up adopted consists in using a laser vibrometer (Polytec Scanning Vibrometer PSV 300) to evaluate the vibration measurements and a shaker to excite the structure. Laser vibrometers use optical interferometry to measure surface velocities ranging from 0 to 125 $mm/s/V$ and from 0 to 30 MHz depending on equipment arrangements. For the current testing, a Polytec neon-helium laser (OFV-302) and scanning head (OFV-040) were used. The vibrating surface orthogonal to the laser causes the frequency of a laser beam to be shifted due to the Doppler effect. The shift in signal beam frequency is related to the

velocity of the vibrating surface and the wavelength (λ) of the laser ($\lambda = 6.32\text{E-}7$ m for helium-neon lasers) through the equation 4.3.

$$f_s = \frac{2v}{\lambda} \qquad (3.1)$$

where f_s is the frequency shift of the beam and v is the vibrating surface velocity. The signal beam and a known frequency reference beam are then combined to create an interference signal. This signal contains the velocity of the measured system. The primary advantage of using a laser vibrometer is the non-contact nature of the transducer, which eliminates mass loading of the structure due to response measurement transducers. For methods employing piezoelectric transducers, additional steps and mathematical equations have been developed to alleviate mass loading measurement discrepancies [55] and [56]. A shaker was attached to the window on the opposite side of the panel through a stinger-force transducer combination as illustrated in Figure 3.2. The driving point was chosen away from the symmetric axis and the edges to excite as many modes as possible.
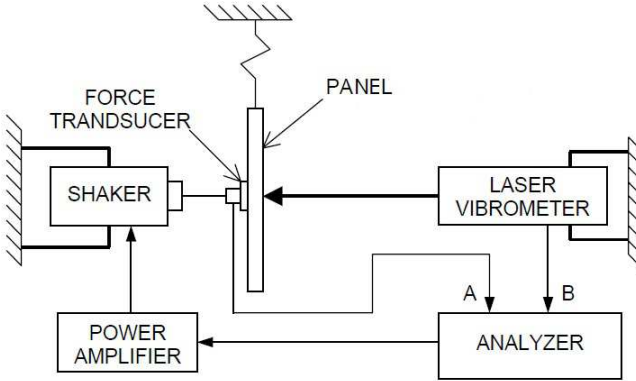
Figure 3.2: Experimental set-up: shaker and vibrometer laser

3.1.3 Numerical model

Numerical simulations were conducted, in terms of modal analysis and frequency response function, using the commercial finite element solver MSC/Nastran 2008, focusing on the low frequency region where panels belonging to the same class have a quite similar behaviour. A 2-D model was realised: the panel was modelled using 4-nodes quadrilateral (CQUAD4) elements. The numerical mesh consisted of 26 x 36 nodes along the in plane-directions. The panel was not constrained along its edges, as assumed in the experimental tests. A unit force is applied on the numerical node corresponding to the corner point as in the experimental test, in order to compare the frequency response functions. Once the model was built, first of all a modal analysis was performed in order to identify the first ten modes parameters; thus, the frequency response function was evaluated based on the modal frequencies. An isometric view of the numerical model is shown in Figure 3.3. The elastic material properties used in the FEM modelling are reported in Table 2.2.
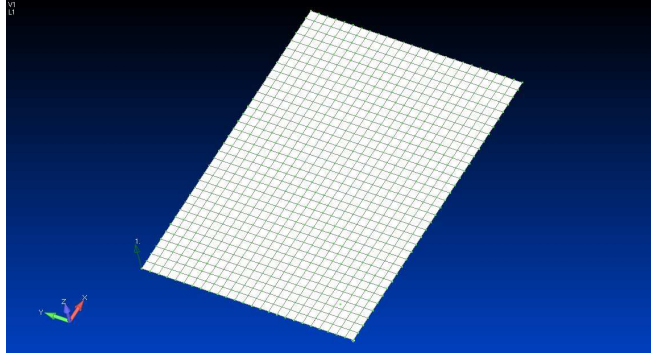
Figure 3.3: Isometric view of the numerical model of the flat panel

3.1.4 Results

The section of the results is organized in subsections in order to lead the reader through the investigated problem. First of all the experimental comparison is presented, where the effect of two different instrumentation set-up on the modal parameters extraction is investigated. Follow a section dedicated to numerical results, carried out by using a FE solver. Finally a comparison between numerical and experimental results is reported in terms of Modal Assurance Criterion. The comparison between the experimental and numerical solutions give to the designer information about the accuracy of the numerical model (geometry, material, boundary condition) and permit to evaluate if the material properties estimated by static test or provided by the supplier are exact or they have to be updated.

3.1.4.1 Experimental comparison

Modal parameters in terms of natural frequency, modal shape and modal damping were extracted by the analysis of the FRFs of the unidirectional flax-PE panel. Table 3.1 shows the natural frequencies and the modal damping values of the original panels according to their modes.

The evaluated modal damping is the critical damping ratio (ζ):

$$\zeta = \frac{c}{c_{cr}} \tag{3.2}$$

which is the ratio between the damping coefficient (c) and the critical damping value ($c_{cr} = 2\sqrt{km}$) [57]. The damping in composite materials is essentially due to the matrix visco-elasticity, to the fibre material and to the sliding of the fibre at the interface with the matrix. Comparing the natural frequencies carried out with two different set-up instrumentation, it is evident that the values are comparable although some slight difference (less 5 %), as reported in the third column of the Table 3.1, is present. This test was done in order to investigate the influence of the instrumentation set-up on the results and to evaluate the repeatability of the results. Once this was validated all the other test were performed with

Mode number	EMA (ham-acc) [Hz]	EMA (shak-las) [Hz]	Δf [Hz]	Damping ratio (%)
1	8.884	8.456	0.23	2.73
2	17.584	18.617	1.03	2.11
3	24.567	24.747	0.18	2.76
4	28.563	29.076	0.51	1.31
5	47.374	49.274	1.90	0.49
6	54.294	54.129	0.16	1.22
7	69.321	74.150	4.83	0.84
8	86.540	82.353	4.18	0.86

Table 3.1: Experimental correlation of the unidirectional panel by means of two different instrumentation set-up

laser and shaker because of their advantage to use a pure tone as excitation and more nodes in which evaluate the output. In table the used instrumentations (hammer, accelerometer, shaker and laser) are reported respectively with the following abbreviations: *ham*, *acc*, *shak* and *las*.

3.1.4.2 Numerical solution

The first numerical results were obtained by using the material properties estimated by static test. From static test only the two in-plane stiffness moduli and the in-plane shear moduli and Poisson ratio were estimated, while the other were obtained by using the classical equations for composites. By analysis of the results, the natural frequencies and the mode shapes were quite good in overall the investigated frequency with slight errors for some frequencies. These errors are expected on the value of E_2 that was successfully identified by increasing its initial value of 30% and minimizing, thus, the difference between measured and estimated resonance frequencies. The Table 2.2 refers to the updated mechanical properties. In order to avoid repetition the numerical results are reported directly in Table 3.5 in comparison with the experimental ones.

3.1.4.3 Experimental-numerical comparison

By the analysis of the FRFs, numerical and experimental ones, the modal parameters were extracted. The first five modal shapes, experimental and numerical, of the unidirectional flax-PE panels are depicted in Table 3.2. As it can be noted the mode shapes carried out by means of an experimental test and of a numerical analysis are the same, with the order of modes respected. However the numerical modes seems to be more clear, i.e. the shapes are more regular, than of the experimental ones because they refer to an ideal numerical model where the geometry and the material orthotropic is perfect and the boundary condition and the applied force are ideal. While these could not be always respected completely in the case of a real panel due to possibility of lack in manufacturing or influence of the instrumentation set-up during test. This is particular evident in the forth mode where only one edge reproduce the same mode shape of the numerical one

while the other edge seems to be more stiff. To be noted that the different colours of the contour plots in Figure 3.2 is only due to a different scale.

The evaluation of the correlation between estimated and measured modal shapes is performed by calculating the Modal Assurance Criterion (MAC). The MAC is a mathematical tool to compare two vectors to each other [58]. It can be used to investigate the validity of estimated modal vectors originating from different sources, for instance modal vectors from a finite element analysis can be compared with those determined experimentally. The MAC between two mode shape vectors $\{\Psi\}_r$ and $\{\Psi\}_s$ is defined as:

$$MAC\left(\{\Psi\}_r, \{\Psi\}_s\right) = \frac{\left|\{\Psi\}_r^{*T}\{\Psi\}_s\right|^2}{\left(\{\Psi\}_r^{*T}\{\Psi\}_r\right)\left(\{\Psi\}_r^{*T}\{\Psi\}_r\right)}. \tag{3.3}$$

A MAC value close to 1 (or 100%) indicates a high degree of correlation between two mode shapes. The MAC matrix calculated between the numerical and experimental mode shapes of the investigated panel is depicted in Fig. 3.5, whereas a complete comparison of the numerical and experimental results is reported in Table 3.3. The correlation, and thus the evaluation of MAC, was done by using FEMtools software. Correlation analysis quantitatively and qualitatively compares two sets of analysis results data. It consists in overlapping the experimental (red grid mesh)and the numerical (blue grid mesh) model associating nodes of the first with those of the second (Figure 3.4); then the MAC is calculated.
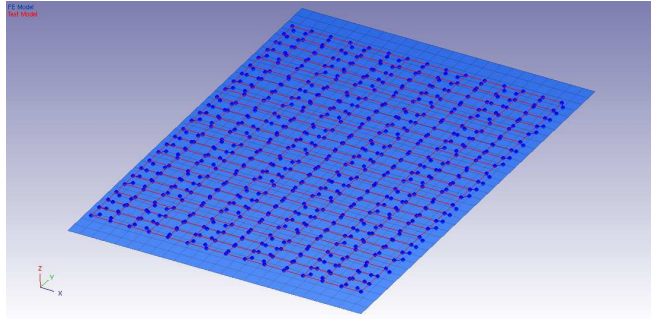
Figure 3.4: Numerical-experimental panel mesh matching

The MAC matrix calculated is diagonal, which means that the order of the eigenvectors is preserved and the diagonal values is high, i.e. the eigenvectors, numerically and experimentally, of the panel are estimates of the same mode shapes. However the not-perfect correlation of the forth mode, already presented in Figure 3.2, numerical and experimental mode shape is confirmed by a value of MAC pairs to 48.9 % and the same is for the seventh mode.

Mode number	Experimental	Numerical
1		
2		
3		
4		
5		
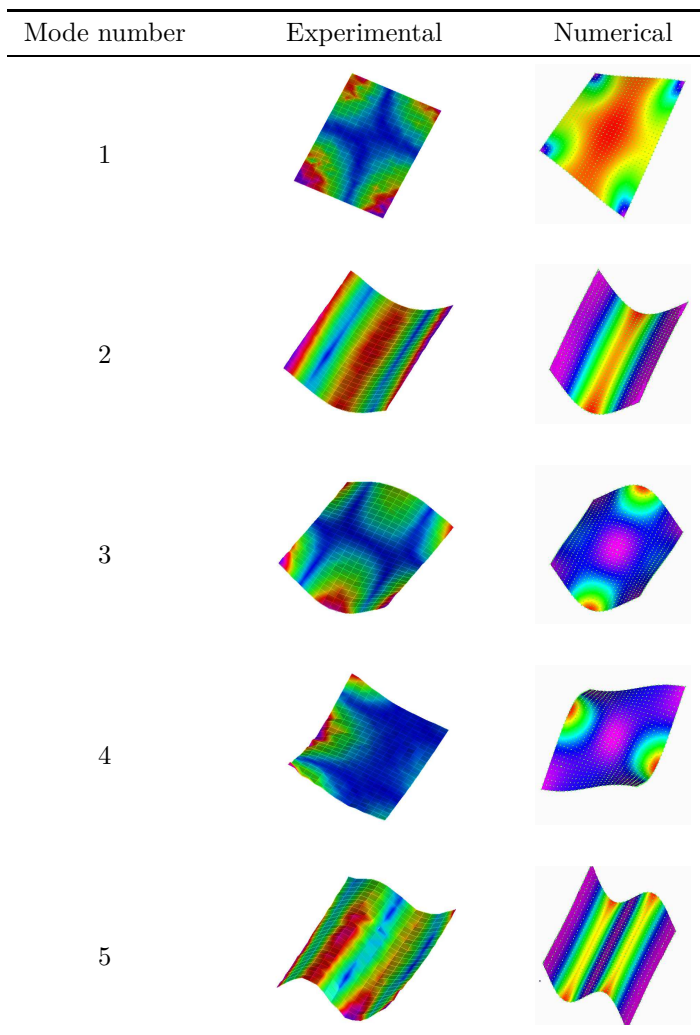
Table 3.2: The first five numerical and experimental modal shapes of flax-PE unidirectional panel

Mode number	FEA [Hz]	EMA [Hz]	Diff. (%)	MAC (%)
1	8.057	8.456	0.39	80.0
2	16.97	18.617	1.64	92.5
3	23.59	24.747	1.15	89.6
4	27.77	29.076	1.3	48.9
5	47.26	49.274	2.01	88.5
6	52.62	54.129	1.5	79.7
7	67.08	74.150	7.07	51.8
8	97.58	104.627	7.04	74.5

Table 3.3: Numerical-Experimental correlation of the unidirectional panel
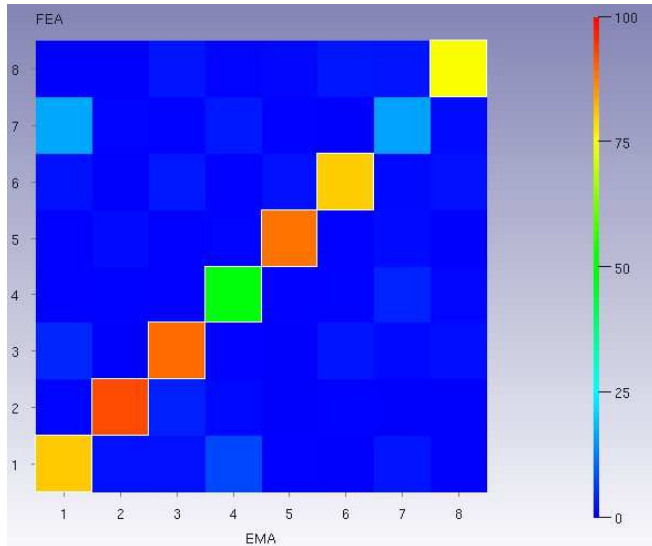
Figure 3.5: Isometric view of the MAC of the unidirectional flax-PE panel

3.2 Dispersion curves of flat panel

3.2.1 Ultrasonic waves: a brief introduction

Sound waves define a sequence of compression and rarefaction and is the means by which acoustic energy propagates in an elastic medium. The number of repeated sequences per unit time is called the frequency which can be used to classify the sound waves. The ability of the human ear to detect sound is used as the threshold limits along the frequency axis, where the sound wave frequency lower and upper limits are called infrasound and ultrasound, respectively. Ultrasonics (from ultrasound) is a term which refers to the application of sound waves in transporting mechanical energy at a frequency greater than the upper threshold limit (typically considered to be 20 kHz).

Ultrasonic waves found a great interest in the last years in the Structural Health Monitoring (SHM) field, especially in composites, for the identification of cracks, delaminations, interfacial debondings, fibre fractures and breakages, matrix cracking [59, 60, 61]. The general concept is that an ultrasonic wave, travelling in thin walled structures, propagates undisturbed as long as no obstacles are present on its path, whereas, if any of the above-mentioned damage appears, it is typically reflected, diffracted, and also mode conversions might occur. The obstacle or discontinuity can also be represented by a structural component that is part of the structure, such as a rivet hole, a stiffener or a change in thickness.

Over structural health monitoring ultrasonic guided waves offer a variety of applications in fields such as non-destructive testing [62, 63] and material characterization [64]. About the last, in fact, the ultrasonic tests allow to characterize materials meticulously and mostly non destructively, providing an accurate determination of the elastic constants. However wave propagation in composite structures is more complex respect to an isotropic structure due to the nature of het-

Wave types in solids	Particle Vibrations
Longitudinal	Parallel to wave direction
Transverse (Shear)	Perpendicular to wave direction
Surface - Rayleigh	Elliptical orbit - symmetric mode
Plate wave - Lamb	Component perpendicular to surface (extensional wave)
Plate wave - Love	Parallel to plane layer, perpendicular to wave direction
Stoneley	Wave guided along interface

Table 3.4: Some wave types in solids

erogeneity of the constituents, inherent material anisotropy and the multi-layered construction, which introduces many interesting wave phenomena: a directional dependence of wave speed, a difference between phase and group velocity of the waves, wave skewing, and so on. Since many parameters influence the wave propagation an understanding of the nature of the waves in composites is required. In this sense, propagation characteristics of Lamb waves in a unidirectional flax fibres reinforced PE laminate, with emphasis on group velocity, were investigated experimentally and numerically in order to characterize the material properties of the structure and validate the one obtained from static test. Before to discuss about numerical and experimental evaluation of the panel under investigation a brief introduction to ultrasonic waves, with a special emphasis to Lamb waves, is needed.

In solids, sound waves can propagate in four principle modes that are based on the way the particles oscillate. Sound can propagate as longitudinal waves, shear waves, surface waves, and in thin materials as plate waves. Some types of waves in solids is reported in Table 3.4. The particle movement responsible for the propagation of longitudinal and shear waves is illustrated below.

In longitudinal waves, the oscillations occur in the longitudinal direction or the direction of wave propagation. Since compressional and dilational forces are active in these waves, they are also called pressure or compressional waves. They are also sometimes called density waves because their particle density fluctuates as they move. Compression waves can be generated in liquids, as well as solids because the energy travels through the atomic structure by a series of compressions and expansion (rarefaction) movements.
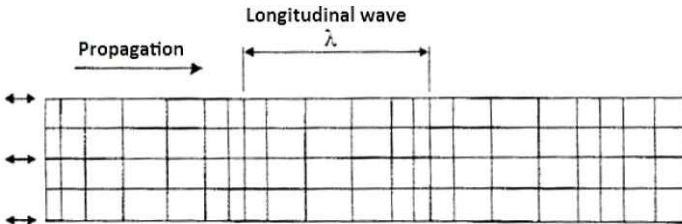
Figure 3.6: Longitudinal wave

In transverse or shear wave, the particles oscillate at a right angle or transverse

to the direction of propagation. Shear waves require an acoustically solid material for effective propagation, and therefore, are not effectively propagated in materials such as liquids or gasses. Shear waves are relatively weak when compared to longitudinal waves. In fact, shear waves are usually generated in materials using some of the energy from longitudinal waves.
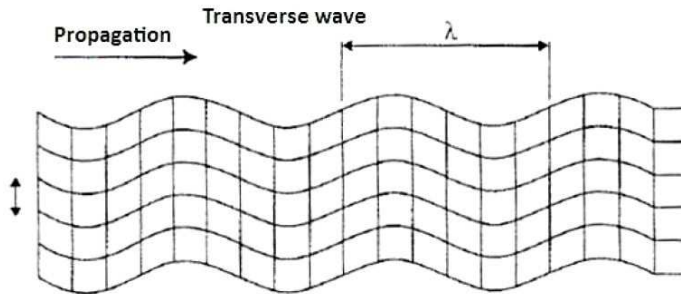
Figure 3.7: Transverse wave

Surface (or Rayleigh) waves travel the surface of a relatively thick solid material penetrating to a depth of one wavelength. Surface waves combine both a longitudinal and transverse motion to create an elliptic orbit motion as shown in the image and animation below. The major axis of the ellipse is perpendicular to the surface of the solid. As the depth of an individual atom from the surface increases the width of its elliptical motion decreases. Surface waves are generated when a longitudinal wave intersects a surface near the second critical angle and they travel at a velocity between .87 and .95 of a shear wave.
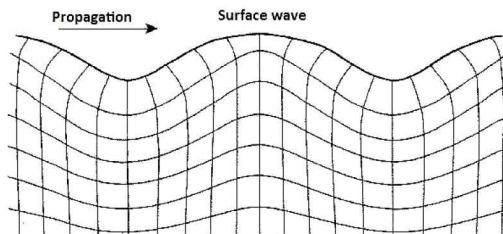
Figure 3.8: Rayleigh wave

Plate waves are similar to surface waves except they can only be generated in materials a few wavelengths thick. Lamb waves are complex vibrational waves, a combination of longitudinal and vertically polarized shear bulk waves propagating in a direction parallel to the plate throughout the thickness of the material. Propagation of Lamb waves depends on the density and the elastic material properties of a component. They are also influenced a great deal by the test frequency and material thickness. Lamb waves are generated at an incident angle in which the parallel component of the velocity of the wave in the source is equal to the velocity of the wave in the test material. Lamb waves will travel several meters in steel and so are useful to scan plate, wire, and tubes. The theory of Lamb waves has been fully documented in a number of textbooks [65],

[66]. Lamb waves are commonly seen in plate like structures. They consist of two basic modes: an extensional or symmetric (S_0) mode that often appears at higher velocity but lower amplitude waves preceding flexural or asymmetric (A_0) mode (Figure 3.10). For instance, the Figure 3.11 reports the aforementioned waves (longitudinal, flexural, Lamb and Rayleigh) for a 1-mm thick aluminium plate. Note that axial and flexural waver are only low-frequency approximations of the Lamb wave S_0 and A_0 modes. The Rayleigh wave is the high-frequency asymptote of the Lamb wave S_0 and A_0 modes [67].
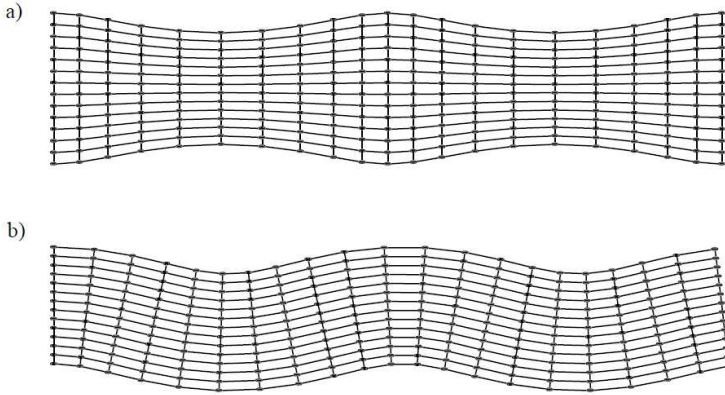
Figure 3.9: Zero-order symmetric (a) and asymmetric (b) Lamb waves in plate
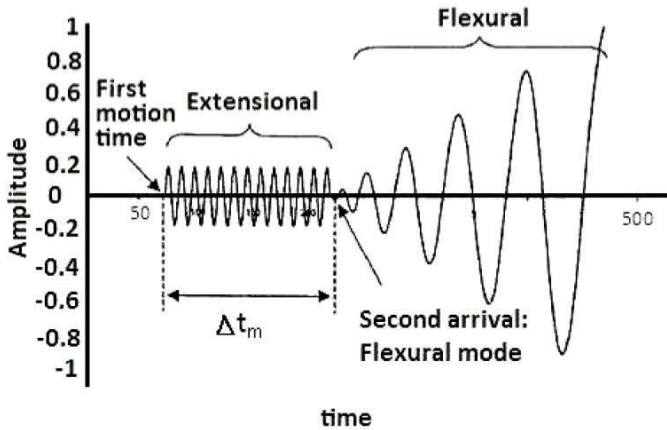
Figure 3.10: Early arriving symmetric mode and later asymmetric one

3.2.2 Derivation of Lamb waves equations

The derivation of the Lamb-wave equations is provided in this section. In this derivation, we will consider straight-crested Lamb waves propagating in a plate of thickness $h = 2d$. The three dimensional wave equation describing the propagation of elastic waves in an isotropic solid media without external force is:
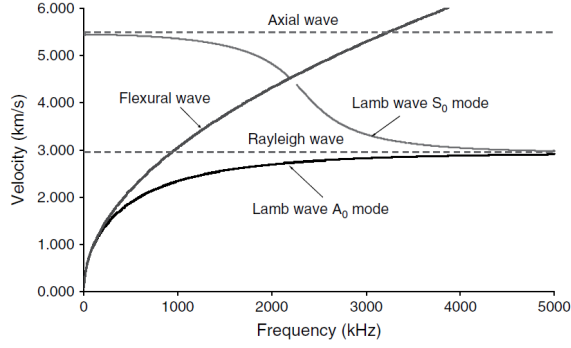
Figure 3.11: Velocity *vs* Frequency of different waves for a 1-mm thick aluminium plate

$$(\lambda + \mu)\underline{\nabla}(\nabla \cdot \underline{u}) + \mu \nabla^2 \underline{u} = \varrho \ddot{u} \tag{3.4}$$

with $\underline{u}$ displacements vector, λ and μ Lame constants and ϱ density of the isotropic material. Through the Helmoltz theorem the vector $\underline{u}$ can be decomposed using two potentials ϕ and ψ:

$$\underline{u} = \underline{\nabla}\phi + \underline{\nabla} \times \underline{\psi} \tag{3.5}$$

By combining the equations (3.4) and (3.5) we obtain:

$$c_p^2 \nabla \phi = \ddot{\phi} \tag{3.6}$$
$$c_s^2 \nabla \psi = \ddot{\psi} \tag{3.7}$$

where $c_p{}^2=(\lambda + 2\mu)/\varrho$ and $c_s{}^2= \mu/\varrho$ are the pressure (longitudinal) and (shear) wave speeds. For harmonic wave propagation in the x direction, $e^{i(\xi x - \omega t)}$, the equations take the form:

$$\frac{d^2\phi}{dy^2} + p^2\phi = 0 \tag{3.8}$$

$$\frac{d^2\psi}{dy^2} + q^2\psi = 0 \tag{3.9}$$

where $p^2=\omega^2/c_p{}^2 - \xi^2$; $q^2=\omega^2/c_s{}^2 - \xi^2$ and $\xi=\omega/c$. The general solution of the equation (3.15) is:

$$\phi = A_1 \sin py + A_2 \cos py \tag{3.10}$$
$$\psi = B_1 \sin qy + B_2 \cos qy \tag{3.11}$$

Hence, the displacements are:

$$u_x = i\xi(A_1 \sin py + A_2 \cos py) + q(B_1 \cos qy - B_2 \sin qy) \tag{3.12}$$
$$u_y = p(A_1 \cos py - A_2 \sin py) - i\xi(B_1 \sin qy + B_2 \cos qy) \tag{3.13}$$

These can be grouped into symmetric and antisymmetric components:

$$u_x = (A_2 i\xi \cos py + B_1 q \cos qy) + (A_1 i\xi \sin py - B_2 q \sin qy) \tag{3.14}$$
$$u_y = -(A_2 p \sin py + B_1 i\xi \sin qy) + (A_1 p \cos py - B_2 i\xi \cos qy) \tag{3.15}$$
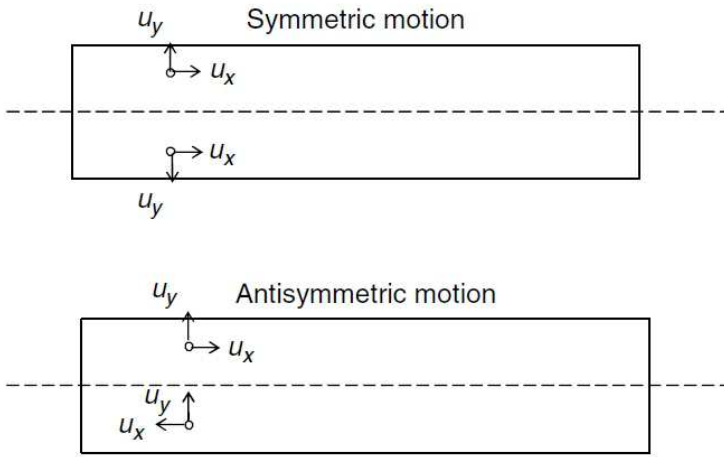
Figure 3.12: Symmetric and antisymmetric particle motion in the plate thickness

The four integration constants are to be found from the boundary conditions. The derivatives of the potentials with respect to y are:

$$\frac{\partial \phi}{\partial y} = A_1 p \cos py - A_2 p \sin py; \quad \frac{\partial^2 \phi}{\partial y^2} = -A_1 p^2 \sin py - A_2 p^2 \cos py = -p^2 \phi \tag{3.16}$$

$$\frac{\partial \psi}{\partial y} = B_1 q \cos qy - B_2 q \sin qy; \quad \frac{\partial^2 \psi}{\partial y^2} = -B_1 q^2 \sin qy - B_2 q^2 \cos qy = -q^2 \psi \tag{3.17}$$

The stresses are given by:

$$\tau_{yx} = \mu \left(2i\xi \frac{d\phi}{dy} + \xi^2 \psi + \frac{d^2 \psi}{dy^2} \right) \tag{3.18}$$

$$\tau_{yy} = \lambda \left(-\xi^2 \psi + \frac{d^2 \phi}{dy^2} \right) + 2\mu \left(\frac{d^2 \phi}{dy^2} - i\xi \frac{d\psi}{dy} \right) \tag{3.19}$$

At this stage, it is advantageous to split the problem into symmetric and antisymmetric behaviour (Figure 3.12). Replacing the derivatives of the potentials (Eq. 3.17) in the equations of the stresses (Eq. 3.19), and applying the boundary conditions for each case, symmetric and antisymmetric modes, the Rayleigh-Lamb equations are obtained.

- **Symmetric solution**

The symmetric solution of the Lamb waves equations assumes symmetry of displacements and stresses about the midplane:

$$u_x(x,-d) = u_x(x,d), \quad \tau_{yx}(x,-d) = -\tau_{yx}(x,d) \tag{3.20}$$
$$u_y(x,-d) = u_y(x,d), \quad \tau_{yy}(x,-d) = \tau_{yy}(x,d) \tag{3.21}$$

Positive shear stresses have opposite directions on the upper and lower surfaces, hence the negative sign on τ_{yx} in (Eq. 3.32). Therefore, the displacements and potentials for symmetric motion are

$$u_x = (A_2 i\xi \cos py + B_1 q \cos qy), \qquad \phi = A_2 \cos py \tag{3.22}$$
$$u_y = -(A_2 p \sin py + B_1 i\xi \sin qy), \qquad \psi = B_1 \sin qy \tag{3.23}$$

The symmetric boundary conditions are:

$$\tau_{yx}(x,-d) = -\tau_{yx}(x,d) = 0 \tag{3.24}$$
$$\tau_{yy}(x,-d) = \tau_{yy}(x,d) = 0 \tag{3.25}$$

Replacing and applying the boundary conditions a linear system is obtained:

$$-A_2 i\xi p \sin pd + B_1(\xi^2 - q^2)\sin qd = 0 \tag{3.26}$$
$$A_2(\xi^2 - q^2)\cos pd - B_1 2i\xi q \cos qd = 0 \tag{3.27}$$

Solution of this homogeneous system of linear equation is only possible if the determinant is zero:

$$D_s = (\xi^2 - q^2)^2 \cos pd \sin qd + 4\xi^2 pq \sin pd \cos qd = 0 \tag{3.28}$$

This is the Rayleigh-Lamb equation for symmetric modes. An often used form of the symmetric Rayleigh-Lamb equation is:

$$\frac{\tanh(pd)}{\tanh(qd)} = -\frac{(\xi^2 - q^2)^2}{4\xi^2 pq} \quad \text{symmetric modes (S)} \tag{3.29}$$

$$\tag{3.30}$$

- **Antisymmetric solution**

The antisymmetric solution of the Lamb waves equations assumes that displacements and stresses are antisymmetric about the midplane:

$$u_x(x, -d) = -u_x(x, d), \qquad \tau_{yx}(x, -h) = \tau_{yx}(x, h) \qquad (3.31)$$
$$u_y(x, -d) = u_y(x, d), \qquad \tau_{yy}(x, -h) = \tau_{yy}(x, h) \qquad (3.32)$$

In this case the positive shear stresses have opposite directions on the upper and lower surfaces. They are inherently antisymmetric. Hence, the displacements and potentials for antisymmetric motion are:

$$u_x = (A_1 i\xi \sin py - B_2 q \sin qy), \qquad \phi = A_1 \sin py \qquad (3.33)$$
$$u_y = (A_1 p \cos py - B_2 i\xi \cos qy), \qquad \psi = B_2 \cos qy \qquad (3.34)$$

The antisymmetric boundary conditions are:

$$\tau_{yx}(x, -d) = \tau_{yx}(x, d) = 0 \qquad (3.35)$$
$$\tau_{yy}(x, -d) = -\tau_{yy}(x, d) = 0 \qquad (3.36)$$

Replacing and applying the boundary conditions a linear system is obtained:

$$A_2 i\xi p \cos pd + B_2 (\xi^2 - q^2) \cos qd = 0 \qquad (3.37)$$
$$A_1 (\xi^2 - q^2) \sin pd + B_2 2i\xi q \sin qd = 0 \qquad (3.38)$$

Solution of this homogeneous system of linear equation is only possible if the determinant is zero:

$$D_s = (\xi^2 - q^2)^2 \sin pd \cos qd + 4\xi^2 pq \cos pd \sin qd = 0 \qquad (3.39)$$

This is the Rayleigh-Lamb equation for antisymmetric modes. An often used form of the symmetric Rayleigh-Lamb equation is:

$$\frac{\tanh(pd)}{\tanh(qd)} = -\frac{4\xi^2 pq}{(\xi^2 - q^2)^2} \quad \text{antisymmetric modes (A)} \qquad (3.40)$$

The solutions of the two equations (3.30, 3.40) represent the phase velocities c_{ph} of the various Lamb waves modes: these curves do not exist in a closed form, so numerical algorithms are needed in this case. Each one of the two Rayleigh-Lamb equations presents a number of solution curves defining more than one relation between wave number and frequency, or even wave velocity and frequency: several orders are present for both symmetric and antisymmetric modes. By considering the velocity of Lamb waves packets travelling in the plate, we introduce the group velocity c_g which is linked to phase velocity through the relation:

$$c_g = \frac{\partial \omega}{\partial c_{ph}} \tag{3.41}$$
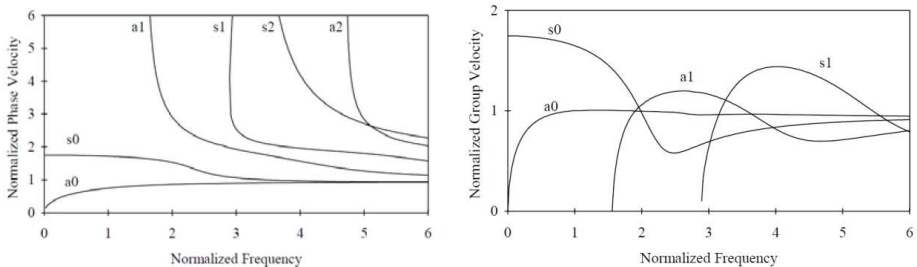
Figure 3.13: Dispersion curves for an aluminium plate, lowest order solutions

In Figure 3.13 the frequency-velocity dispersion curves for an aluminium plate are presented. It is possible to see the strong dependence of the wave speeds with frequency, showing the typical dispersive behaviour. The zero order modes are present at all frequencies, while the higher orders appear at certain cut-off frequencies. Dispersion curves, the graphs that show relationships between wave velocity (or wave number) and frequency in dispersive systems, can be presented in various forms. The form that gives the greatest insight into the underlying physics has ω (angular frequency) on the y-axis and ξ (wave number) on the x-axis. In some textbooks, such as the one by Viktorov [65], dispersion curves graphs are reported with a different form with wave velocity on the y-axis and d/λ, the thickness/wavelength ratio, on the x-axis. The most practical form of all has wave velocity on the y-axis and $f \cdot d$, the frequency-thickness product, on the x-axis. For values of frequency that tends to zero the problem can be simplified and the velocities for the S_0 and A_0 modes have, respectively, the following expression:

$$\lim_{\omega \to 0} c_{ph} = \sqrt{\frac{E}{\varrho(1 - \nu^2)}}; \quad c_g = c_{ph} \tag{3.42}$$

$$\lim_{\omega \to 0} c_{ph} = \sqrt[4]{\frac{E}{3\varrho(1 - \nu^2)}}; \quad c_g = 2c_{ph} \tag{3.43}$$

The phase velocity is the velocity of seismic wave propagation in the direction of the wavefront normal. The group (ray) velocity, on the other hand is the velocity of energy propagation, which is aligned with the source-receiver raypath.

3.2.3 Experimental evaluation

Dispersion curves of the same panel previously tested for modal analysis purpose were evaluated. The investigated panel was a unidirectional flax-PE laminate having dimensions $706 \, \text{mm} \times 496 \, \text{mm} \times 3.6 \, \text{mm}$. Four piezoelectric (PICE-RAMIC PIC 255) with a diameter of 10 mm and a thickness of 0.25 mm were

used and bonded on the plate surface. One piezoelectric, used as actuator, was positioned in the centre of the panel, while the other three (receivers) were placed at a distance of 150 mm from the actuator in the three principal directions (0°, 45° and 90°).

A piezoelectric material is a material whose main feature is the generation of an electric field when a stress/strain field is present: also the opposite occurs. This means that when a piezoelectric material is deformed the potential difference (Volts) between two electrodes soldered onto two of its faces is measured. A piezoelectric disk is characterized by two modes of deformation: an in-plane mode and an out-of-plane mode (Figure 3.14).
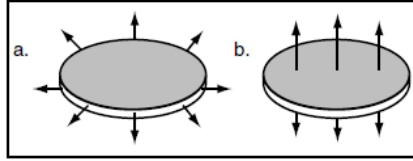
Figure 3.14: Deformation modes of a piezoelectric sensor

As excitation a 4.5 sine cycles curve with a Hanning window was used in order to obtain a narrow-band bell curve in the frequency domain. Narrow-band excitations are needed in order to limit the problem of the dispersiveness of Lamb waves, strongly dependent on frequency. An example of the excitation curve at 25 kHz is shown in Figure 3.15. The aforementioned signal is generated trough a signal generator (HP/Agilent 33120A) connected to the actuator and the acquisitions were performed by using an oscilloscope (Agilent InfiniiVision DSO7014A). The experimental instrumentation of the set-up for the Lamb waves acquisition is reported in Figure 3.16, while a schematic example of set-up is reported in Figure 3.17.
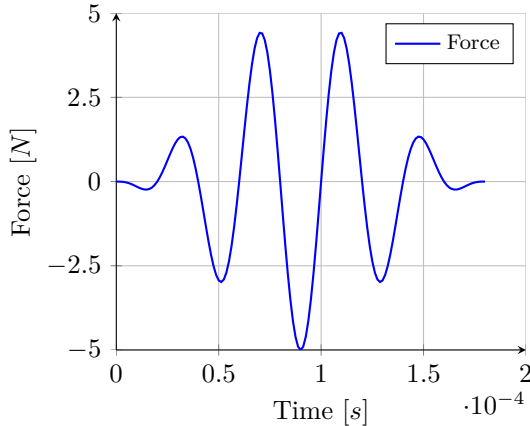
Figure 3.15: Excitation curve: 4.5 sine cycles with Hanning window

The excitation frequency was varied from 10 to 40 kHz with a step of 5 kHz in order to obtain the tuning and the dispersion curves of A_0 modes in the three directions. The upper frequency range was due to the presence of S_0 modes

(a)   (b)   (c)
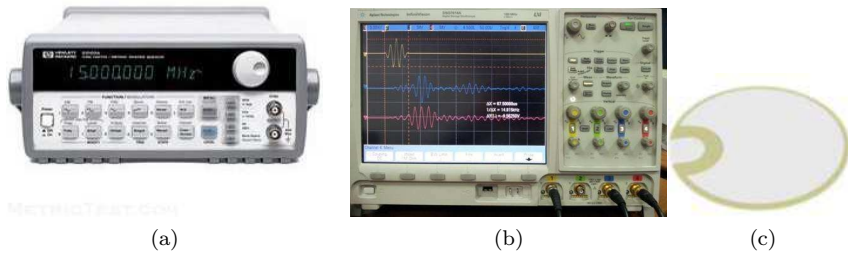
Figure 3.16: Experimental instrumentation set-up: signal generator(a), oscilloscope (b) and piezoelectric (c)
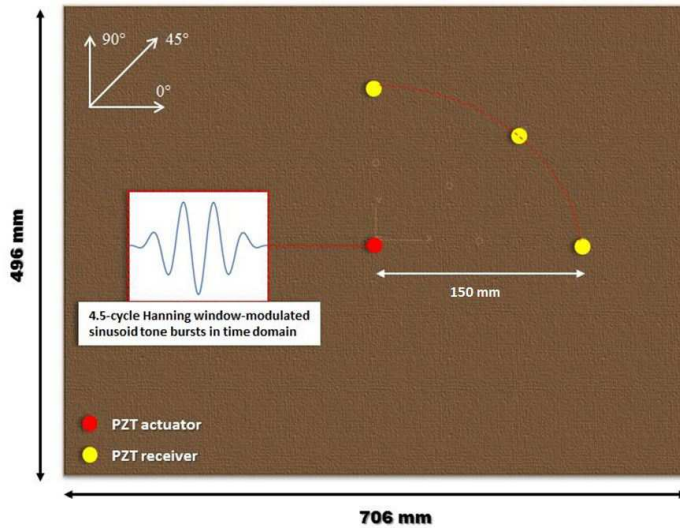
Figure 3.17: Composite panel under investigation

reflections from plate edges overlapping the first incoming A_0 waves packet at sensor's location. Once the signals were recorded and the distance between the piezoelectric sensors and the excitation frequency are known it is possible to calculate the time of flight (TOF), i.e the time interval between the maximum energy of the actuator and of the receiver wavefronts, using a simple Matlab algorithm, able to calculate the Short-Time Fourier Transform (STFT) of the acquired signals (Figure 3.18).

 For instance, in Figure 3.19 the two curves of the signals of the actuator and the receiver at a frequency of 25 kHz in the 0° direction are reported and a black arrow between, more or less, the points of maximum energy of the signals indicates the TOF. Once the TOF and the distance between the two piezoelectric sensors are known it is possible to determine the propagation velocity as the space-time ratio. In the Figure 3.19 it is possible to note also the presence of a second wavefront that represents the acquisition of the piezo of the wavefront reflected. It should be noted also that the TOF is usually calculated as the distance between the maximum peak of the actuator and receiver signals by committing a little error.
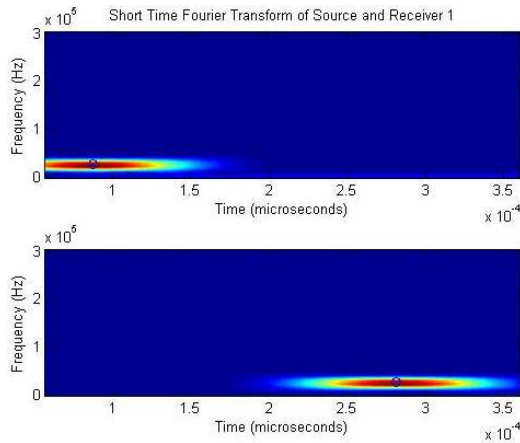
Figure 3.18: Short-Time Fourier Transform of the actuator and receiver in 0° direction at 25 kHz
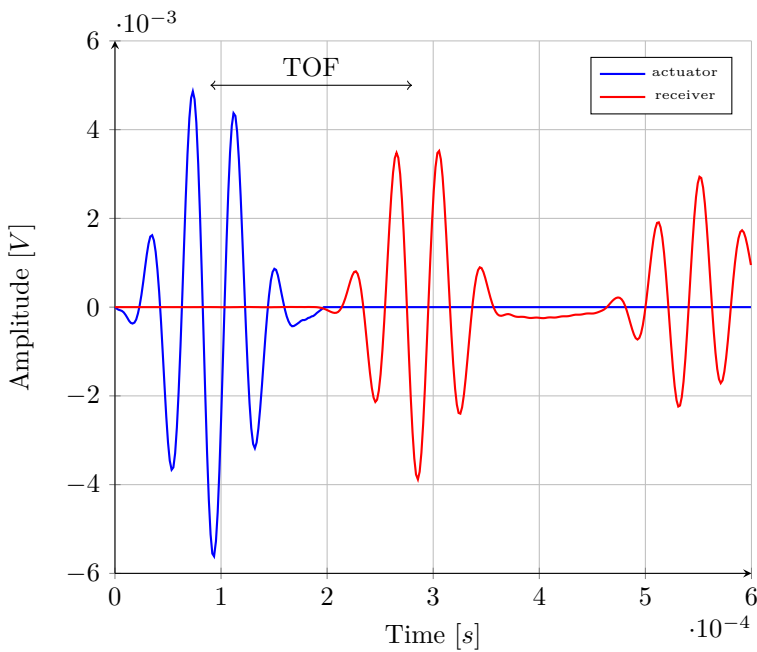
Figure 3.19: TOF of the unidirectional flax-PE panel

There is a strong dependence of Lamb waves amplitudes with frequency, for both symmetric and antisymmetric modes. The function linking waves amplitude with frequency presents some maxima and minima respectively corresponding to the two conditions:

$$l_a = (2n-1)\frac{\lambda(f)}{2} \quad \text{max amplitude}$$

$$l_a = (2n)\frac{\lambda(f)}{2} \quad \text{min amplitude}$$

l_a is the piezoelectric dimension, λ is the wavelength function of frequency, n is a natural number including zero. Since different Lamb wave modes propagate with different speeds, the various conditions of maxima and minima happen at different frequencies for the different modes.
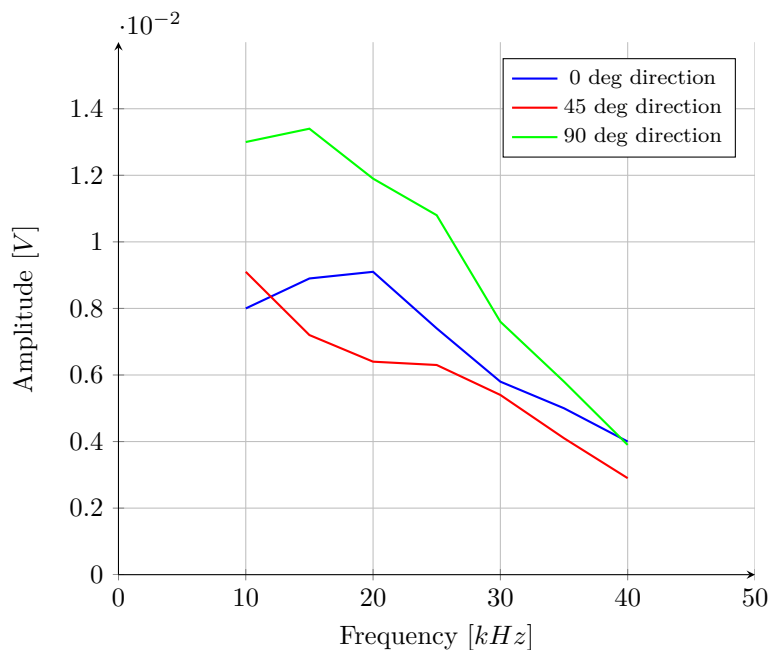
Figure 3.20: Tuning: Amplitude *vs.* Frequency for the unidirectional flax-PE panel

3.2.4   Numerical simulation

In recent years the study of the Lamb wave propagation in thin structures has received increased emphasis. Various numerical codes, using various plate theories, that give the displacements or stress/strains at various locations on both isotropic and composite plates, for a given excitation force curve were developed [68, 69, 70]. Generally these codes assume that the plate is infinite and that there are no obstacles (holes, cracks, rivets) in the propagation path of the guided waves. The last represents a limit of these codes and so, when the structure under investigation has a complex geometry an alternative numerical modelling approach is needed.
The Finite Element Method is the most versatile and powerful method due to its ability to model complex geometries. It constitutes a numerical technique to
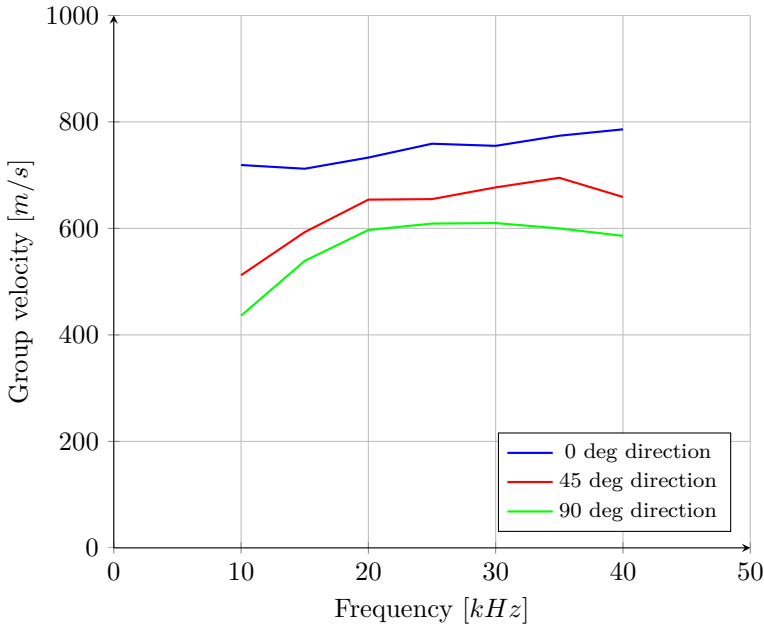
Figure 3.21: Group velocity *vs.* Frequency for the unidirectional Flax-PE panel

solve problems governed by partial differential equations over complex domains. Depending on the strategy used to convert the differential equations into algebraic equations, finite element methods can be divided into explicit and implicit types. In explicit types, the value of a variable such as displacement at a certain time is determined based on its known values at earlier time steps; while, in implicit algorithms, values of variables at future time steps are needed to determine their current values. Implicit methods are more complex to program and require more computational time for each time step. Explicit methods are easier to program. However, they demand smaller time steps compared to implicit ones but for problems involving dynamic phenomenon such as ultrasonic wave propagation, where instantaneous results at each time step are required, explicit methods are preferred.

After the experimental campaign was performed, the wave propagation of the zero order antisymmetric A_0 guided wave modes in a unidirectional laminate plate was simulated using a FE model. A direct transient analysis was carried out by using the explicit FEM code LS-DYNA. Since the A_0 mode Lamb waves are dispersive in nature their velocity depends on the thickness of the plate. An average thickness, pairs to 3.6 mm, was considered for the FE model, although it was not perfectly constant in the real panel because of manufacturing process. Furthermore since the panel was a unidirectional laminate, it was not necessary to discretize the eight layers that make up the laminate and only a layer having the panel thickness and the lamina properties was taken into account. The laminate plate was modelled with 3D brick elements having dimensions $2\,\text{mm} \times 2\,\text{mm} \times 2\,\text{mm}$. The numerical mesh consisted of 150 x 150 elements along the in plane-directions and 8 along the thickness, for a total of 180000 elements. The element size is chosen so that the propagating waves are spatially identified for a wide frequency

range of interest (more than 10 nodes per wavelength) and to adhere to the usual stability criteria (together with the time step). The information obtained from the analysis of the FE model are the displacement time histories of the nodes which are the values that the displacements of the nodes assume during the observation time. Each node can have more time histories, one for each degree of freedom of interest. The degree of freedom used in this work is the out-of-plane displacement U2 because, thanks to the force adopted, the main displacement is in this direction and because the antisymmetric mode has a component in U2. These histories were processed to obtain the Time Of Flight (TOF) needed for the calculation of the group velocity of the A_0 mode of Lamb wave. As described in the previous section the excitation was provided to the structure by means of a piezoelectric sensor which is characterized by two modes of deformation: in-plane mode and out-of-plane mode (Figure 3.14). Since the excitation is not to be considered as nodal source of disturbance, in order to reproduce the characteristic deformation of a circular piezoelectric actuator excited by an electrical impulse, the piezoelectric sensor was modelled employing 8 knots arranged with constant angular pitch of 45° along a circle with a diameter of 10 mm (Figure 3.22) and on each node a pair in plane orthogonal forces were applied. Only the in-plane deformation were considered for the numerical analysis. The excitation pulse, applied in the centre of the panel to coincide with the planned experimental instrumentation, was set as a 4.5 cycle tone burst with a center frequency at 10/15/20/25/30/35/40 kHz similar to the measurements described above.
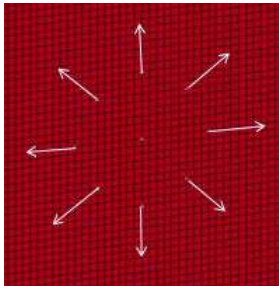
Figure 3.22: Modelling of piezoelectric acting as actuator

The numeric total propagation time of Lamb mode was set at 0.6 ms. A transient excitation pulse used for modelling the piezoelectric mechanism is shown in Figure 3.15. The receivers were discretized with a single node (monitoring point). The transmitter and receiver nodes were placed at a distance of 150 mm.

Contour plots of the von Mises stresses of the unidirectional flax-PE panel at different time step for an excitation with a 4.5 sine Hanning windowed signal with a frequency 25 kHz is reported in Figures 3.24, 3.25, 3.27, 3.28. The von Mises stress field at different times show how the stress wave propagates. A generic consideration is about the wavefront shape non perfectly circular but slightly stretched along the main directions of the panel. This distortion probably can be attributed to material property rather than to numerical effects. The first frame (Figure 3.24) shows the initial stresses after the panel was excited, the wave front started from the centre of the panel and is expanding. In the second frame (Figure 3.25) the wavefront is seen approaching to the node simulating the piezo, i.e. where the response is calculated. In the third frame (Figure 3.27)
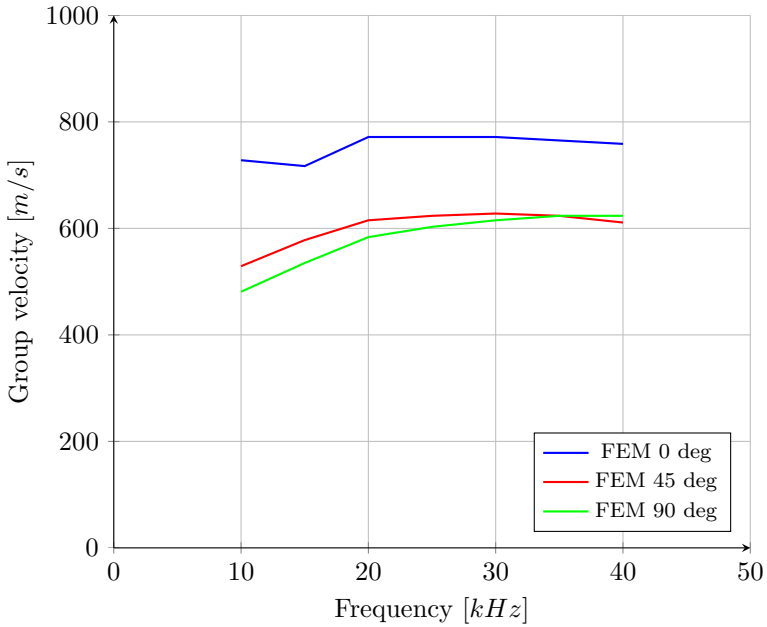
Figure 3.23: Group velocity *vs.* frequency at different directions

the wavefront approached the sideward of the panel and the reflection started. Finally in the fourth frame (Figure 3.28) it is possible to recognize the wave reflection coming back.
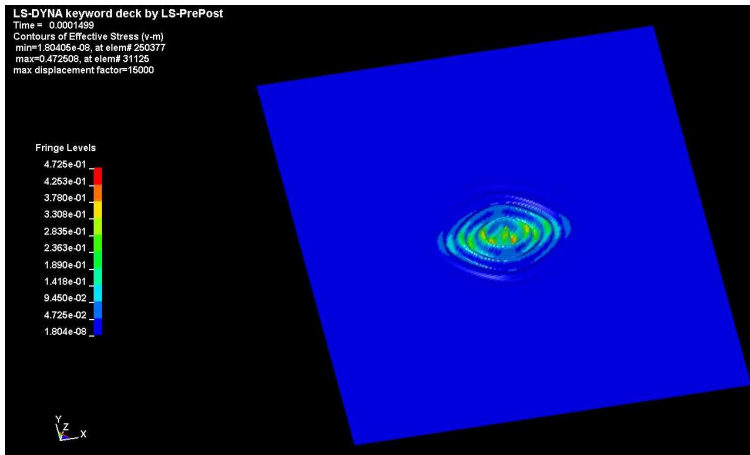
Figure 3.24: von Mises stresses at time 0.000149 s

In Figure 3.26 a zoom of the numerical wavefront is reported.
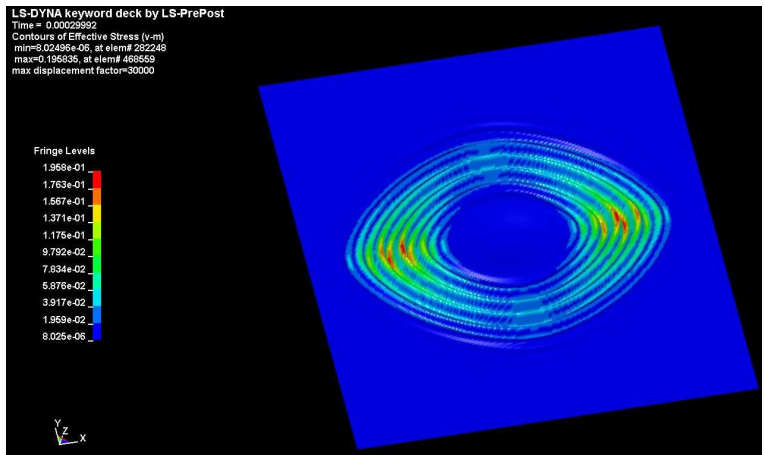
Figure 3.25: von Mises stresses at time 0.000299 s
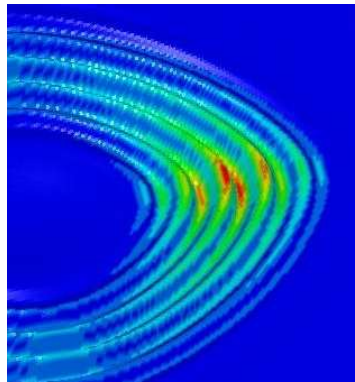
Figure 3.26: Zoom of the wavefront von Mises stresses at time 0.000299 s
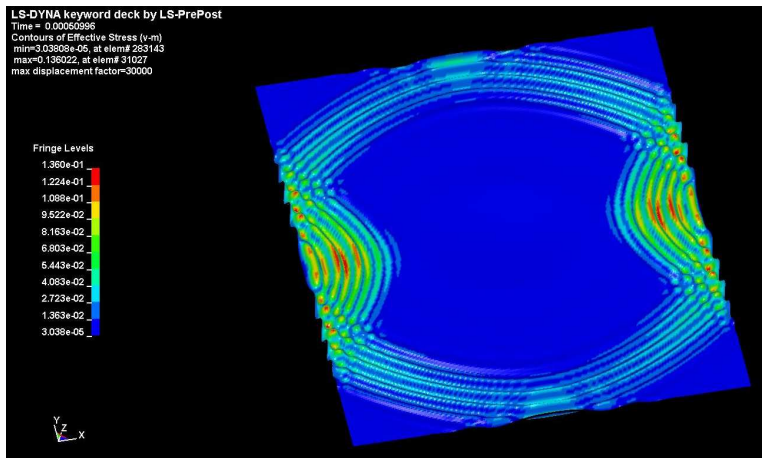
Figure 3.27: von Mises stresses at time 0.000509 s
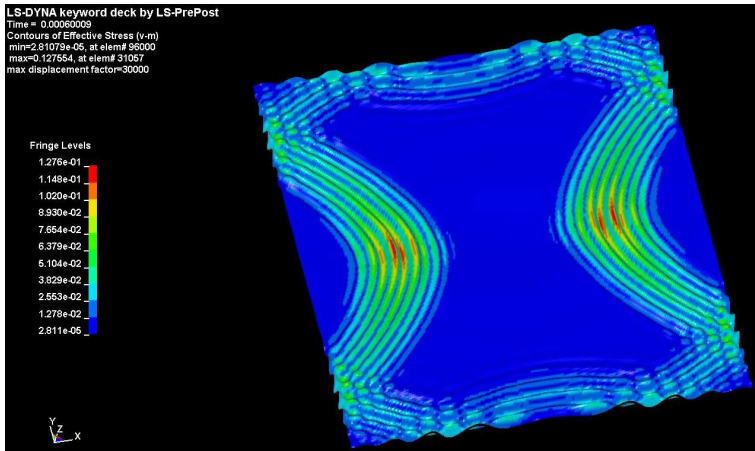
Figure 3.28: von Mises stresses at time 0.0006 s

3.2.5 Experimental-numerical correlation on unidirectional panel

Numerical and experimental results are shown in Figure 3.29 and listed in Tables 3.5, 3.6, 3.7 together with the percentage relative error for the three principal directions. A good correlation is shown with relative percentage error less then 10% for the panel in the three directions at all investigated frequency range. Slight differences (less than 5%) at 0° direction is observed; on the other hand, major differences (less than 11%) are present in the other two investigated directions (45° and 90°). A percentage error less than 11% can be considerable acceptable and this can be due to different behaviour of the composites depending on the manufacturing process, presence of defects, and on the use of the nominal properties in the numerical model. The discrepancy can be attributed also to not-perfect constant thickness between actuator and receiver and initial stress state which could arise as residual stresses in manufacturing process that can significantly affect the mechanical behaviour of the panel [71]. Despite these drawbacks, it is possible to confirm the ability of these experimental technique to represent the characteristics of the propagation of elastic waves in composite panels and to confirm the dependence and the variability of the group velocity with the direction of propagation. Group velocity in the direction of the fibres are faster than the one in the direction orthogonal to fibres, i.e. group velocity is dependent to elastic properties of the laminate. Higher the elastic property, higher the group velocity.

3.2.6 Correlation FEM-WFEM

Several techniques for Lamb wave propagation simulation are available: the Finite Element Method (FEM), the Boundary Element Method and the Finite Difference Method. The FEM is the best method when complex damage, geometry or boundary is involved. However, high Lamb wave frequency requires very small element size thus high computational cost in FEM analysis. By using the
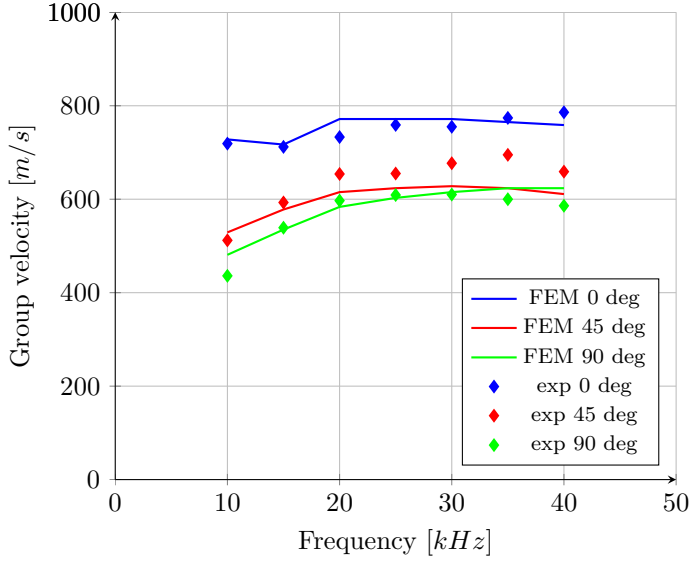
Figure 3.29: Group velocity *vs.* frequency at different directions

Direction [°]	Freq. [kHz]	Numerical [m/s]	Experimental [m/s]	Δv [%]
0	10	719	728	1
0	15	712	717	1
0	20	733	771.6	5
0	25	759	771.6	2
0	30	755	771.6	2
0	35	774	765.1	1
0	40	786	758.7	4

Table 3.5: Numerical-Experimental correlation of the group velocity in the 0° direction of the unidirectional flax-PE panel.

Direction [°]	Freq. [kHz]	Numerical [m/s]	Experimental [m/s]	Δv [%]
45	10	529	512	3
45	15	578	593	3
45	20	615.2	654	6
45	25	623.6	655	5
45	30	627.9	677	8
45	35	623.6	695	11
45	40	611	659	8

Table 3.6: Numerical-Experimental correlation of the group velocity in the 45° direction of the unidirectional flax-PE panel

Direction [°]	Freq. [kHz]	Numerical [m/s]	Experimental [m/s]	Δv [%]
90	10	481	436	9
90	15	535	539	1
90	20	583.6	597	2
90	25	602.9	609	1
90	30	615.2	610	1
90	35	623.6	600	4
90	40	623.6	586	6

Table 3.7: Numerical-Experimental correlation of the group velocity in the 90° direction of the unidirectional flax-PE panel.

existence of periodicity in plates, an attempt to reduce this computational cost is done using Wave FEM. The Wave and Finite Element Method (WFEM) is a numerical technique to investigate the wave motion in structural waveguides and periodic structures, both in one-dimensional (e.g. beams [72, 73, 74, 75, 76]) and two-dimensional (e.g. plates and cylinders [77, 78]) domains. The method is based on the Finite Element model of an elementary cell of the waveguide under investigation, eventually obtained through commercial codes. Starting from the stiffness and mass matrices, an eigenvalue problem is formulated by applying periodicity conditions, continuity of displacements and equilibrium of forces between two adjacent cells. The solutions of the eigenproblem provide the dispersion curves of the structure. Through the WFEM, the experimental results are further validated by D'Alessandro [79], who estimated the group velocity of the unidirectional flax/PE panel along 0° and 90° directions (Figure 3.30). The elementary cell has in-plane dimensions $0.1 \times 0.1 \ mm^2$, ensuring that the length of the sides is shorter than the minimum wavelength. The FE model of the cell was made through ANSYS, using an element SHELL181 (4-noded, 6 DOFs per node). Results reported in Figure 3.30 show a good correlation between the values obtained with two different numerical techniques. On one hand FEM results provide a high computation cost but give more informations, respect to the WFEM ones, with the visualization of the dispersion curves. On the other hand, WFEM results show a potential use of this method to reduce the computational cost in FEM, since only the element matrix from the basis cell is needed, instead of assembling all elements in the model.
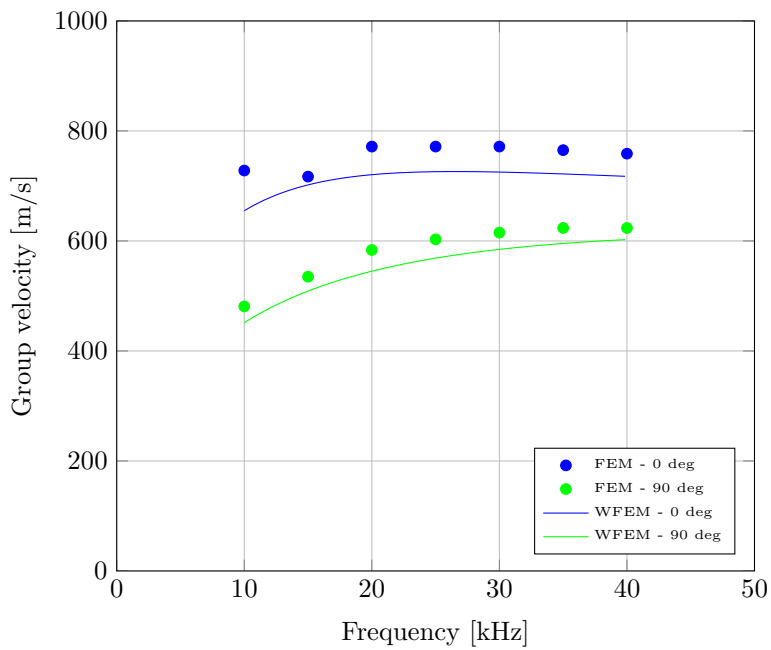
Figure 3.30: FEM-WFEM group velocity *vs.* frequency at 0° and 90° directions

Chapter 4

Flax-PE as sandwich structures

In the previous chapter the manufacturing and the analysis of flax-PE composites has been discussed. Frequency response functions analysis and technique of propagation of ultrasonic waves, in particular Lamb waves, were performed in order to validate, experimentally and numerically, the mechanical properties carried out by the classical static test. Both techniques led to the same results and furthermore the modal parameters: natural frequency, mode shapes and modal damping and the dispersion curves were carried out. In this chapter flax-PE composites were investigated as sandwich materials. Firstly flax-PE honeycomb cores were evaluated both from structural point of view, with low velocity impact test, and from the functional point of view investigating the acoustic performance and the vibration damping. Then the flax-PE composites were manufactured and evaluated also as face sheets materials ans again their performance as vibration damping has been evaluated numerically and experimentally.

4.1 Sandwich structures

Nature discovered and evolved low density cellular materials soon after on earth life began. Today tall trees could not support the bending loads applied by strong winds and our bones would not be able to support our weight were it not for low density (very light) cellular materials configures as the cores of columns and beams with strong (denser) outer surfaces. Figure 4.1 shows examples of the structure of a Hornbill beak and an avian wing bone which demonstrate how well nature exploits these clever design practices to create structures that can support high bending loads at minimal weight.

With far superior synthetic materials now available from which to make cellular material, materials scientists and mechanical engineers are beginning to fabricate cellular solids that rival those of nature.

Sandwich structures were developed as early as the 1820's but not widely accepted commercially until the 1930's after successful production of structural glue. Earlier production of sandwich materials used casein glues, during which
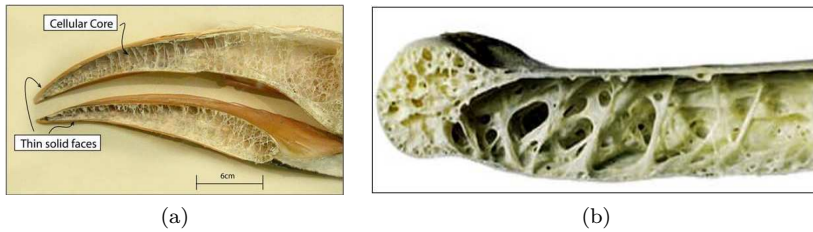
Figure 4.1: Cross section of the beak of a Hornbill (a) and an avian wing bone (b)

the primary materials were mostly wood. As technology advanced, better adhesives such as rubber and vinyl phenolics were developed which made it possible to bond metals and hence use sandwich structures in a wider range of application [80]. Aluminium core sandwich structures are extensively used in military and space vehicles. In recent years, they have also found application in the manufacture of cargo containers, ship interiors, small boats and yachts, cars and recreational sports equipment such as snow skis and surf boards. Sandwich structures provide an advantage of a high strength to weight ratio and are widely accepted and used in the construction industry also. Sandwich construction consists of two thin, stiff and strong sheets of metallic or fibre composite material enclosing a thick, lightweight layer, called core having a lower stiffness and strength compared to the face sheets. The faces carry the tensile and compressive stresses in the sandwich. The local flexural rigidity is so small that it can be often neglected. The core, which can be realised using several materials and/or architectures, has several important functions. In particular, it must be stiff enough

1. along the normal to the faces to keep constant the distance between the faces;

2. in shear to ensure that when the panel is bent the faces do not slides over each other, otherwise the faces merely behave as two independent plates and the main sandwich effect is lost.

Figure 4.2 displays schematically a symmetrical sandwich panel made up of:

- an upper facing of composite having modulus E_f and thickness t.

- a lower facing of the same composite having modulus E_f and thickness t.

- a core of foam having modulus E_c and thickness C.

Figure 4.2: Schematic of a sandwich panel

The principle of the sandwich panel in structural application is similar to that of a conventional I-beam where the flanges carry the flexural load and the web

carries the shear loading; however, in the case of sandwich materials, the shear load is sustained by the core and the flexural load is carried by the facings. In view to demonstrate the main advantage of a sandwich, i.e. the high strength to weight ratio a little example is reported below. For a beam of width b, the formula for flexural rigidity (D) can be expressed as:

$$D = \frac{E_f bt^3}{6} + 0.5E_f bt(C+t)^2 + \frac{E_c bC^3}{12} \qquad (4.1)$$

E_c is negligible compared to E_f and the last term can be omitted to lead to a simpler expression:

$$D = \frac{E_f bt^3}{6} + 0.5E_f bt(C+t)^2 \qquad (4.2)$$

Comparing various sandwich structures of the same materials and same facings with increasing core thickness only, it is possible to write:

$$\frac{D}{E_f b} = \frac{t^3}{6} + 0.5t(C+t)^2 \qquad (4.3)$$
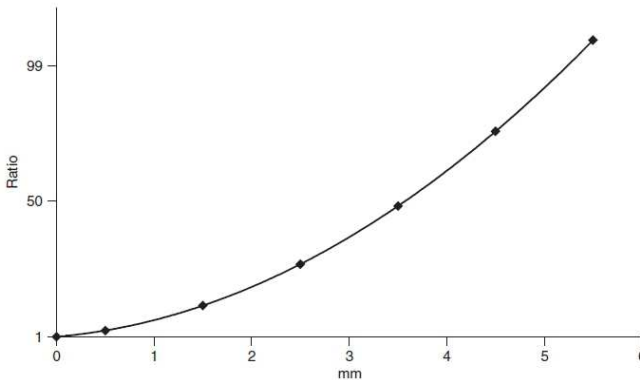
Figure 4.3: Example of panel rigidity/facing rigidity ratio *vs.* foam thickness

By application of this equation for a facing thickness of 0.5 (t = 0.5), Figure 4.3 shows the ratio of $D/(E_f b)$ for a sandwich panel to $D/(E_f b)$ for the facings without foam, as a function of the foam core thickness. To be noted that rigidity can be multiplied by 50 for a core thickness of 3.6, that is to say, a panel thickness of 4.6 and a practically unchanged weight.

Apart the high ratio of bending stiffness a sandwich construction has the following advantages:

- High resistance to mechanical and sonic fatigue.

- Good damping characteristic.

- Improved thermal insulation.

- No mechanical fasteners, hence, no crack initiation sites.

Several core types are available and they can be mainly divided in two groups: honeycombs and foams [81]. Honeycombs are categorised as 2-dimensional cellular materials since the arrangement of the cells varies only in two directions as shown in Figure 4.5a. Foam materials, (Figure 4.5b), are classed as 3-dimensional cellular materials, as the arrangement of the cells varies throughout the solid.

The type of core to be used should be carefully selected depending on their application requirements. In fact, among the load bearing capability, the selection of the core should consider the enhancement of the performance in terms of fire retardant, thermal conduction and sound transmission/absorption. Honeycomb cores have the greatest shear strength and stiffness-to-weight ratios but require special care to ensure adequate bonding of the face sheets to the core since honeycombs are hollow. Different topologies of cellular lattices configured as core materials are depicted in Figure 4.6. The hexagonal honeycomb is the basic and most common cellular honeycomb configuration and it is available in many metallic and non-metallic materials. Honeycombs have the highest modulus and are, therefore, preferred for stiffness dominated design (Figure 4.4). Indeed, foam cores have very low thermal conductivity, making them a prime choice for thermal insulation; very low dielectric loss, allowing transmission of microwaves without attenuation or scattering; good absorption capability, suiting them as materials for noise abatement. Furthermore, they are cheaper than the honeycomb cores and allows an easy manufacturing of sandwich panels [81, 82].
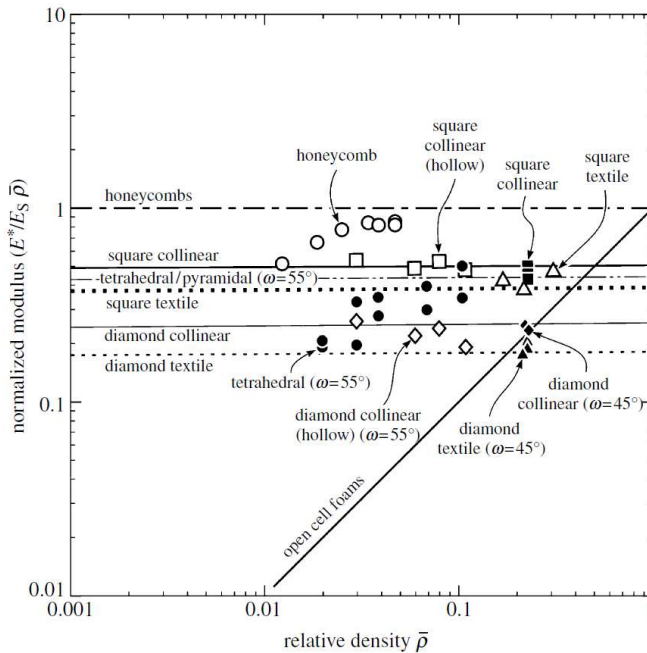
Figure 4.4: Normalized stiffness (modulus) variation with relative density for cellular metals [83]
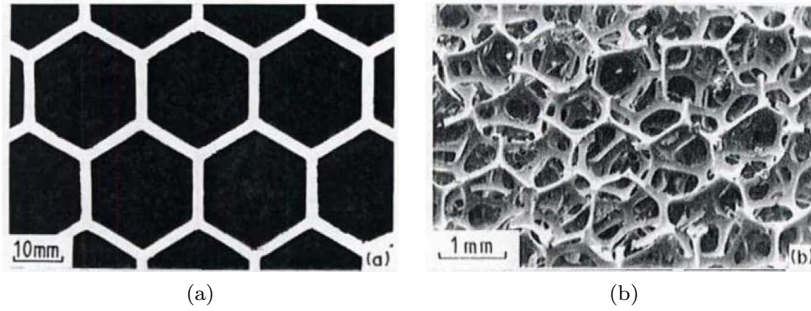
Figure 4.5: Core types: honeycomb (a) and foam (b) [81]
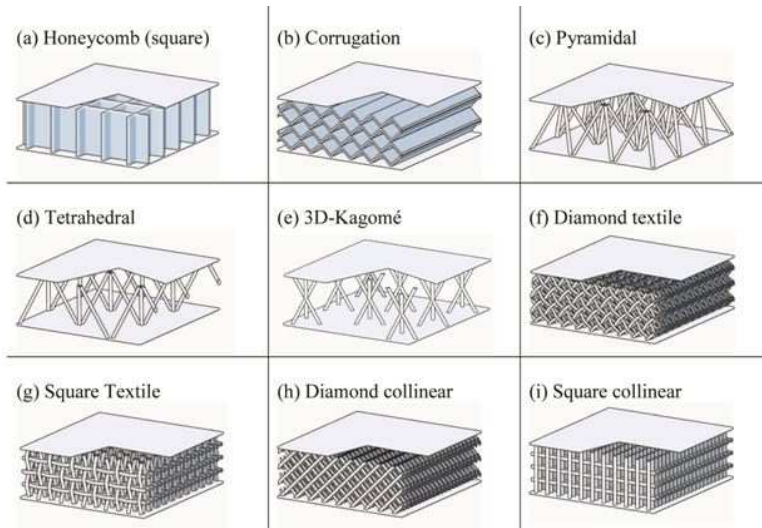
Figure 4.6: Different topologies of cellular lattices configured as the cores of sandwich panels

Among the good properties arising from their configuration honeycomb construction have some disadvantages, such as:

- In-service trapped moisture in the core material causes corrosion problems. Hence, degradation in the structural integrity of the parts.

- A good quality control is needed during the fabrication process to make sure that there is no disbonding in the adhesive layer.

- Disbonds may initiate and propagate in the adhesive layer during service and thereby reduce the load carrying capacity of structures.

4.2   Flax-PE as honeycomb core materials

Honeycomb materials are described as cellular solids [81], materials that make use of voids to decrease mass, whilst maintaining qualities of stiffness and energy

absorption. As a core material for composite sandwiches, engineers are able to produce low-mass components with high stiffness properties. This improvement, at relatively little expense, in terms of mass, is of great interest in aerospace, automotive and many other applications [84]. They are multifunctional in nature and have a wide range of applications in structural and non-structural areas. In structural applications, they are generally used as core material for sandwich construction, where they are bonded to thin rigid face sheets on either side of them, and in non structural applications they are used as acoustic panels, in air vents for changing the air direction and as thermal insulators/conductors. As the honeycomb cores are made up of a network of hollow cells, considerable amount of weight can be saved if they were to be used instead of a homogeneous core made of the same material.

From a design or application prospective, the properties of honeycomb can be simplified in such a way as to assume a simple block of homogeneous material with orthotropic properties. Hexagonal honeycomb materials have three axes of orthotropy and produce the stress-strain relationship shown in equation 4.4. The three principal directions, shown in Figure 4.7, are described relative to the pattern of the hexagonal geometry.

$$
\begin{Bmatrix} \epsilon_T \\ \epsilon_W \\ \epsilon_L \\ \gamma_{WL} \\ \gamma_{TL} \\ \gamma_{TW} \end{Bmatrix} = \begin{bmatrix} 1/E_T & -\nu_{WT}/E_W & -\nu_{LT}/E_L & 0 & 0 & 0 \\ -\nu_{TW}/E_T & 1/E_W & -\nu_{LW}/E_L & 0 & 0 & 0 \\ -\nu_{TL}/E_T & -\nu_{WL}/E_W & 1/E_L & 0 & 0 & 0 \\ 0 & 0 & 0 & 1/G_{WL} & 0 & 0 \\ 0 & 0 & 0 & 0 & 1/G_{TL} & 0 \\ 0 & 0 & 0 & 0 & 0 & 1/G_{TW} \end{bmatrix} \begin{Bmatrix} \sigma_T \\ \sigma_W \\ \sigma_L \\ \sigma_{WL} \\ \sigma_{TL} \\ \sigma_{TW} \end{Bmatrix}
$$
(4.4)
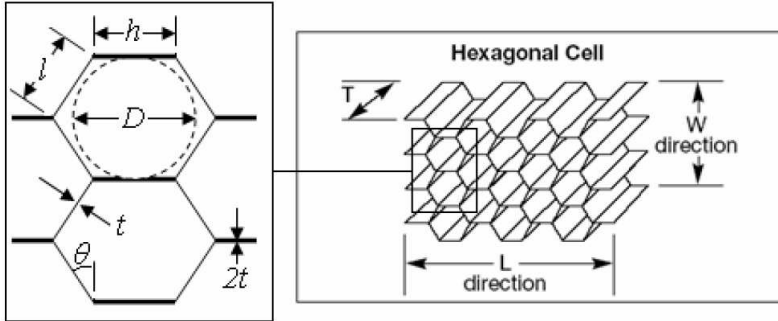
Figure 4.7: Principal directions of a honeycomb material and cell geometry

From a design or application prospective, the properties of honeycomb can be simplified in such a way as to assume a simple block of homogeneous material with orthotropic properties. Hexagonal honeycomb materials have three axes of orthotropy and produce the stress-strain relationship shown in equation 4.4. The three principal directions, shown in Figure 4.7, are described relative to the pattern of the hexagonal geometry.

The properties of these materials in published literature use these directions as a reference frame. The properties in the 'W' and 'L' directions are described as in-plane properties, whilst those in the 'T' direction are out-of-plane. Experimental studies have shown that traditionally the properties in the 'T' direction are higher
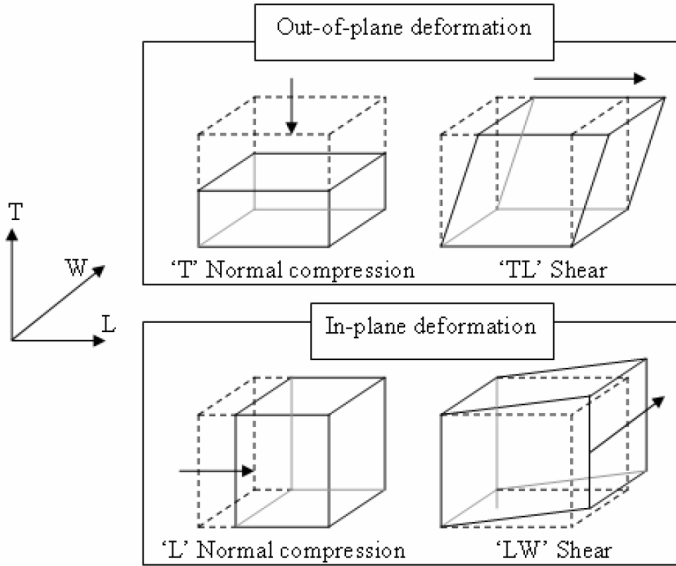
Figure 4.8: Definition of in-plane and out-of-plane loading

than those in the 'W' and 'L' directions [81]. The definitions of in-plane and out-of-plane normal and shear loading conditions are presented in Figure 4.8.

4.3 Energy absorption characteristic of flax-PE honeycomb core

Honeycomb cores have been used as efficient energy attenuators due to their hollow tube-like structure and their cellular arrangement. The Apollo 11 is a classic example, where crushable metal honeycombs have been used in all the four legs of the landing module to absorb impact energy during landing [80]. For effective energy absorption during impact loading it is desirable to have a system that exhibits large plastic deformation behaviour, with the effect to absorb all the impact kinetic energy. However, in order to achieve this, it is important to set tolerable limits on the magnitude of the force transmitted, which is often achieved through rigorous experimentation. Earliest work on the crushing behaviour of honeycomb cores was developed in 1960s by McFarland [85], which was then modified by Wierzbicki [86] who identified the collapse of the cell walls to be due to the folding of the element which is accomplished by the rolling type of mechanism and not due to shear type of deformation as described by McFarland. Zhang and Ashby [87] extended this approach to develop expressions for the failure loads of honeycombs under transverse compression and shear loading, which agree well with the experimental data for aramid paper honeycombs. Wu and Jiang [88] focussed on the investigation of the crushing phenomena of honeycomb structures under both quasi-static and dynamic loading conditions considering the effects of cell dimension, material strength and number of cells under loading. They found that the energy absorption is dependent on the cell

size and the core height and they recommend honeycombs with smaller cell size and core heights for higher energy absorption under quasi-static and impact loading conditions. Yamashita and Gotoh [89] investigated the effect of the cell shape and the cell wall thickness on crush behaviour under quasi-static conditions numerically. Their results showed cell wall buckling to be a predominant mode of failure during cyclic loading and the crush strength increased with decrease in cell wall angles and increase in cell wall thickness. Taken together, the energy absorption in a honeycomb core is dependent on the compressive behaviour of the core under different loading conditions, which in turn is dependent on the geometric parameters of the core. Three common modes of failure occurring during compression loading are fracture of the material, buckling of the cell walls and de-bonding at the double thickness cell walls interface. A generalised Stress vs. Strain curve depicting the regions of energy absorption is shown in Figure 4.9.
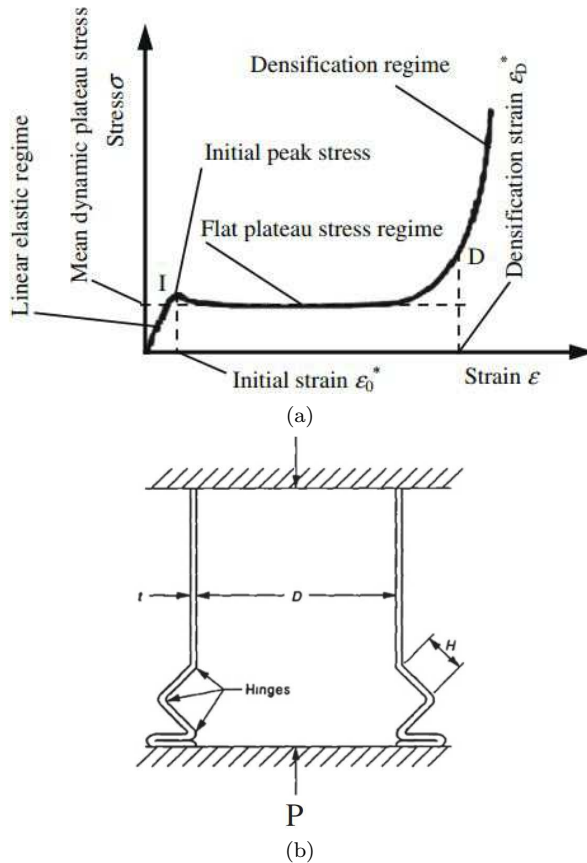
Figure 4.9: Generalised stress-strain curve used for calculating energy absorption (a) and buckling and fracture failure mechanism (b) [90]

In the linear-elastic region, most of the material deformation is recoverable. As the compressive load progresses, the cell walls shorten in the direction of the loading and elastic buckling occurs, during which the cell walls begin to bend and bulge. This buckling in the core is governed by the bending of the cell walls in essence proportional to the cell wall thickness-to-length ratio or to the relative

density of the core. After elastic buckling, if the cell wall material is brittle, they will typically fracture after this region and in case the material yields, the cell walls start to develop hinge lines and the material will begin to collapse along those lines in a similar fashion to that of a piano accordion. This region is referred to as the plateau region, and the cell wall material is plastically deformed. As the cell wall material proceeds to collapse it reaches a densification region after which no energy absorption can be expected (depicted as a vertical line in Figure 4.9).

For many packaging applications, it is desirable to have a long uniform plateau region [91] in order to absorb the impact energy before the packed material hits the ground. For honeycomb cores to enter into the plateau region and exhibit plastic deformation behaviour, the cell wall material must yield and not fracture immediately after the linear-elastic region, in effect consuming the impact energy to plastically deform the cell walls. Conventional honeycomb cores such as aluminium and Nomex offer energy absorption but this could be enhanced by the use of visco-elastic thermoplastic materials. Cores that are made from thermoplastics not only improve the energy absorption but also offer advantages such as reduced density and recyclability. However, the strength and stiffness of such cores are limited due to the inherent properties of the thermoplastic materials. Therefore, in view of improving the strength and stiffness of the thermoplastic materials without sacrificing other properties, natural fibres were used as reinforcements in the cell walls of the cores.
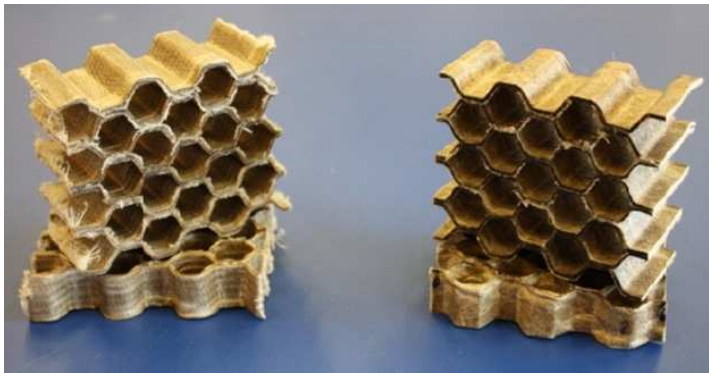
Figure 4.10: Flax-PE honeycomb cores for impact testing

4.3.1 Experimental investigation

Energy absorption in honeycomb cores is usually higher in the out-of-plane direction because of their higher load carrying capacities in that direction. As the absorption depends on the material properties, two different reinforcements, continuous unidirectional and not-continuous random fibres, were used as reinforcement in the cell walls with unidirectional continuous flax fibres orientated in the out of plane direction of the core. Additionally because the absorption is also influenced by the presence of face sheets, two cases, bare and stabilised, were considered. As the height of the core influences the buckling phenomenon, two core heights of 20 mm and 40 mm were considered. All specimens were tested
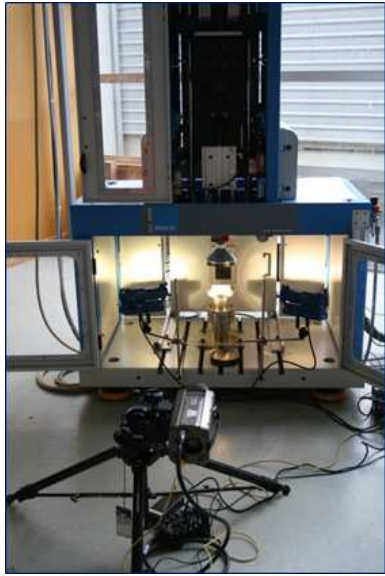
(a) *Impact test set-up*

(b) *Phantom high-speed camera*
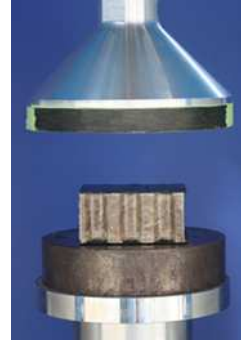
(c) *flat striker*

Figure 4.11: Experimental impact equipment

in an Imatek (model IM 10T-20ITS) drop weight impact tester equipped with a high-speed camera, Phantom, capable of capturing 250,000 fps. The displacement and the impact force were recorded using digital transducers. A 165 mm diameter flat striker with a mass of 16.46 kg was used as an impactor to test the samples, five for each configuration, that were placed on a flat platen anvil. The maximum allowable energy, set to 90 J, was determined after several trials such that all the specimens considered in this study were subjected to consistent energy. The experimental set-up equipment for the impact testing is shown in Figure 4.11a.

4.3.2 Results

The effect of low velocity impact on honeycombs investigated by [92] revealed that the materials used for their testing were not rate-dependent; hence strain rate sensitivity has been neglected in this study. A few images(from a slow motion videos) involving honeycomb cores with and without facings subjected to impact loading are shown in Figure 4.12 and Figure 4.14.

4.3.2.1 Deformation in honeycomb cores with thickness of 20 mm

Bare cores (without face sheets). It is clear from Figure 4.12 that the plastic deformation of continuous flax fibre reinforced cores is minimal compared to that of the not-continuous ones. At 1.5 ms after impact, the cell walls of the continuous fibre cores started to bend (indicated as green arrows) while hinge lines, indicated by white arrows in the Figure 4.12, already started developing in the not-continuous fibre reinforced cores. At 3 ms after impact, the not-

continuous random fibre reinforced cores reached the densification stage, where the cell walls started to collapse and fold, while their counterpart is still in the stage of elastic buckling where the cell walls are bending and bulging, entering into the plastic regime where the hinge lines are starting to develop (blue arrows). This is evident in the force *vs.* deflection trace shown in Figure 4.13 where the cores exhibit higher peak loads and prominent elastic region.

Stabilized core (with face sheets). In Figure 4.14, the deformation of the stabilized cores is less pronounced compared to that of the bare cores because a part of the energy is dissipated during the deformation (bending and stretching) by the face sheets. However, after 3 ms, the not-continuous fibre reinforced cores appear to have plastically deformed, exhibiting distinctive hinges along lines meaning that the cells begun to collapse while only shortening of the cell walls can be seen in their counterpart, indicating the deformation to be primarily elastic. This can be seen in Figure 4.15 where the core thickness is recovered immediately after the impact with negligible local deformation (indicated by white arrows).
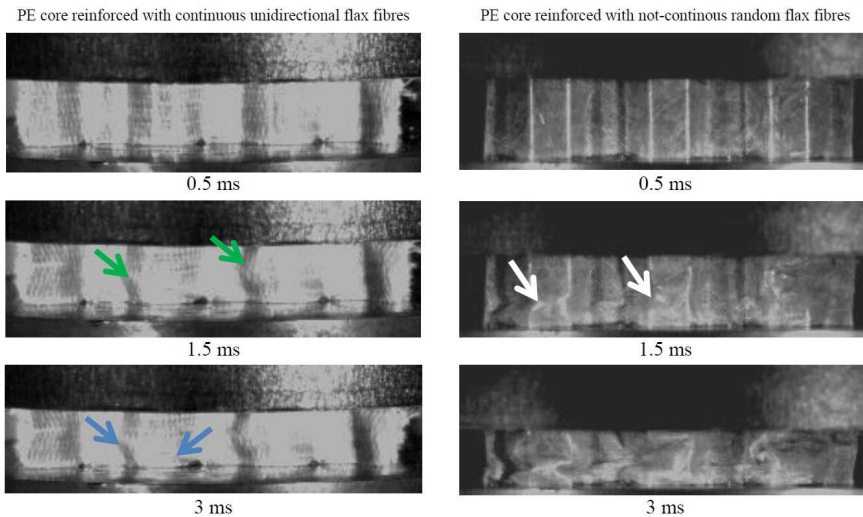
Figure 4.12: Video captures of 20 mm honeycomb cores subject to 90 J impact loading in out of plane direction

4.3.2.2 Deformation in honeycomb cores with thickness of 40 mm

Bare and stabilised cores. As the core thickness is increased, the energy absorption capability of the cores increases. All the 40 mm specimens were subjected to similar impact energy of 90 J and the deformation was similar in both types of cores. Also, the energies absorbed by the bare and stabilized cores were similar exhibiting an increase of ~ 0.4 J (0.5%) in the continuous fibre reinforced case. In all cases, bare or stabilized, the continuous fibre reinforced cores outperformed the not-continuous fibre reinforced cores which is mainly because of the alignment of the fibres (principal direction along the loading). Therefore from this test it is evident that the contribution of the face sheets towards energy absorption is minimum at higher core thicknesses, making it core dependent. These tests were
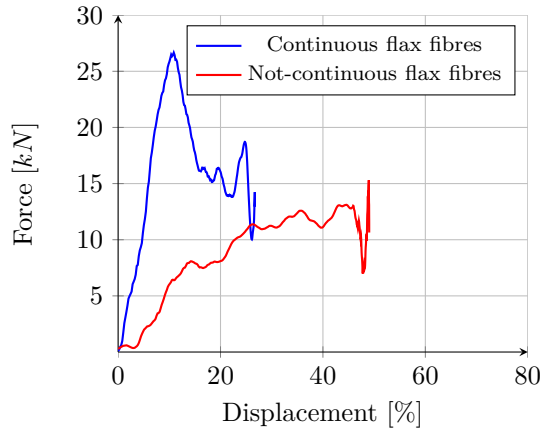
Figure 4.13: Force *vs.* displacement curve of 20 mm honeycomb cores
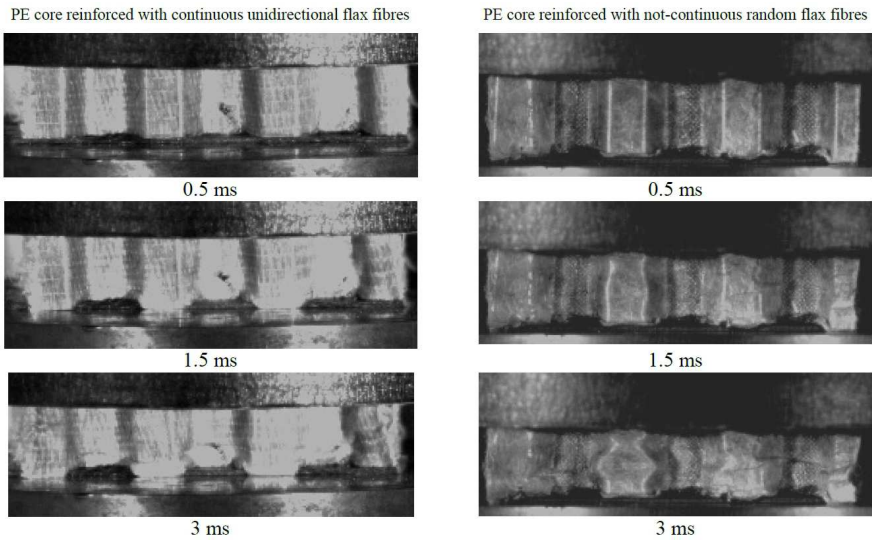
Figure 4.14: Video captures of 20 mm honeycomb cores with face sheets subject to 90 J impact loading in out of plane direction
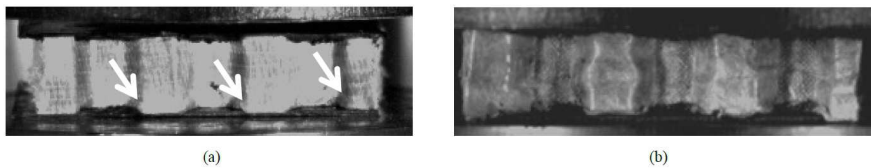
Figure 4.15: Elastic recovery immediately after impact (a) continuous unidirectional flax fibres (b) not-continuous random flax fibres reinforced cores

mainly performed to benchmark this type of problem as it is crucial to most of the finite element programs; in fact they rely on user-defined material behaviour,

and such behaviour at high strain rate has yet to be quantified for such honeycombs. The energy absorption in honeycomb cores is minimally dependent on the height of the cell walls but predominantly dependent on the geometrical parameters of the honeycombs, essentially the cell wall thickness-to-length ratio (t/l) or the relative density of the core, and in the case of compressive loads, the critical buckling load is dependent on the bending of the cell wall which is related (t/l^3). Hence, by increasing the relative density of the core, an increase in energy absorption in these cores can be expected.

4.3.2.3 Taguchi analysis

For all the set of tests a statistical approach was performed in order to identify the significant main/interaction effects that affect the energy absorption in the honeycomb core. The purpose of performing an experimental design analysis is to gather the maximum amount of robust system information from a limited number of carefully designed trials. This is achieved by selecting the factors and levels considered to have the most influence on the output value, and utilising a method of statistical analysis popularised in the fields of optimisation and quality control through the teachings of Taguchi [93, 94]. Experimental design analysis is performed by entering the test results into the correct columns of the design matrix and calculating the average effects for each factor at each level. Estimated effects are plotted for each factor and the larger the line connecting the high and low effect levels for any factor, the more significance it is likely to have on the output.

Two variations of these parameters/factors in this DoE (Table 4.2) are representative of their high and low levels respectively with the assumption that the factor effects are linear when the factor changes from one level to the other one. Three factors at two levels results in eight combinations and hence experimental trials as listed in Table 4.1. The objective of this analysis was to identify the significant main/interaction effects that affect the energy absorption in the honeycomb core. Graphical representation of the main factors and their interaction has been used to identify the contribution of the factors towards the absorption. Synergistic and antagonistic interactions were determined using Taguchi interaction plots. The energy absorbed during impact was estimated as the area under the force - displacement curve using the trapezium method.

Trial	Factors			Response (J)
	A	B	C	
1	0	0	0	86.50
2	0	0	1	89.05
3	0	1	0	86.96
4	0	1	1	87.40
5	1	0	0	85.05
6	1	0	1	85.28
7	1	1	0	85.03
8	1	1	1	85.40

Table 4.1: L_8 orthogonal array and factor response.

The Taguchi approach requires each factor to be varied between levels (low and high) in a systematic way, usually represented numerically as 0 and 1 respectively. The designation of high and low is arbitrary and does not necessarily imply that the low level has a numerically lower value than the high level. However, for the sake of convenience, low and high will be designated as numerical values 0 and 1 respectively.

The graphical representation of the Taguchi method of individual factor contribution towards the overall impact energy absorption is represented in Figure 4.16. In the Taguchi method, the contribution of each factor towards the overall energy absorption is calculated as the average of all the absorption values when the factor is set at its particular level (high or low). This gives an advantage in evaluating as to how much each factor contributes towards the overall property of the material. The main value is calculated using the following equation:

$$\bar{y}_{max} = \bar{y} + (A \quad contribution) + (B \quad contribution) + (C \quad contribution) \quad (4.5)$$

where $\bar{y}_{max}$ is the maximum attainable energy absorption value and $\bar{y}$ is the grand average and the others are as described in the Equation 4.5. The contribution of each factor is the amount it deviates from the overall average and is evident from Figure 4.16 that factor A contributes substantially towards the overall energy absorption followed by factor C.

Factor	Value	Levels
Material type (A)	0	Continuous-unidirectional
	1	Not-continuous-random
Core thickness (B)	0	20 mm
	1	40 mm
Fixity (C)	0	Bare (without face sheets)
	1	Stabilized (with face sheets)

Table 4.2: Factors and their levels
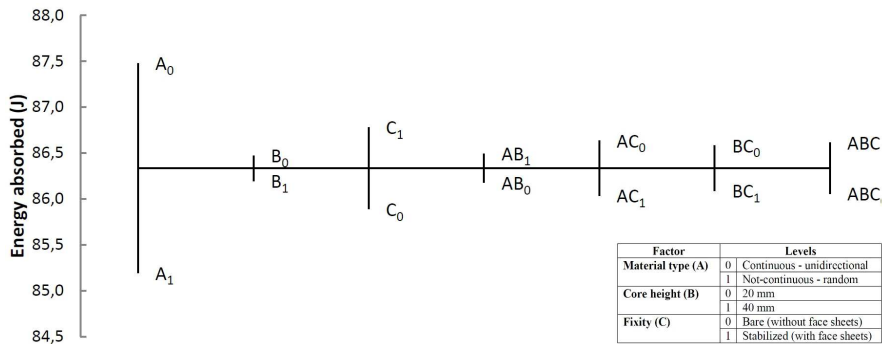
Figure 4.16: Taguchi representations of all contributing factors towards energy absorption of flax-PE honeycomb cores

The maximum attainable energy absorption when the factors A, B are at level

0, and C is at level 1 is 88.061 J. However, the factors at these levels in Table 2 correspond to 89.05 J which is about 1.0 J lesser, suggesting the presence of another parameter. As there are only three factors, the other factor influencing the energy absorption could be due to the interaction between these variables, and is termed the 'interaction factor'.

A	B	Observed trials	Observed averages	Average
0	0	y_1, y_2	86.50, 89.04	87.77
0	1	y_3, y_4	86.96, 87.40	87.18
1	0	y_5, y_6	85.05, 85.28	85.17
1	1	y_7, y_8	85.03, 85.39	85.21

Table 4.3: Observed averages of the factors at their respective levels.

This factor can be estimated by examining the variation of each factor with respect to their levels. For example, to examine the interaction effect of the factors A and B, the trials consisting of both these variables at both their levels are isolated, as shown in Table 4.3. As this method consists of two levels, the values of A and B will occur in two trials. Hence, the factors, A and B, when set at level 1, occur in trials y_1 and y_2. The average response of the two factors, when set at level 1, is the average of the response values in y_1 and y_2. Similarly, the averages of these factors at other levels are calculated, shown in Table 4.3. For a graphical representation, these obtained average values are then plotted against their respective levels, as shown in Figure 4.17. The line depicted as 'A_0' represents the factor A at level 0 and 'A_1' represents the factor A at level 1. If the factors do not interact, the line segments will appear almost parallel but if they interact with each other, the line segments will intersect.
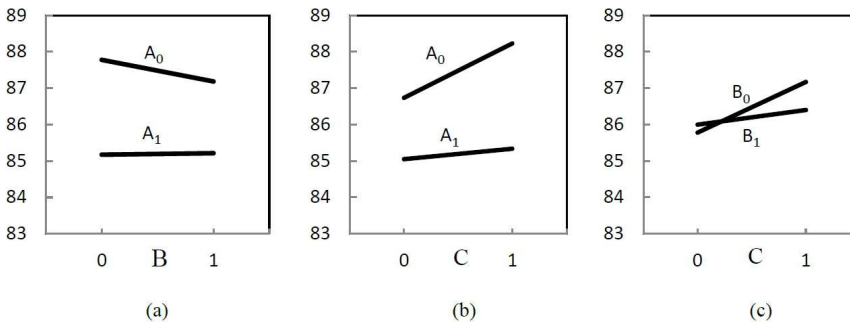
Figure 4.17: Factor interaction effects for energy absorbed: a) AB interaction, b) AC interaction, c) BC interaction

In Figure 4.17, they are all considered to be interacting since all the lines are non-parallel. Greater is the degree of departure from being parallel, stronger is the interaction effect. This is prominent in Figure 4.17 (c) where the lines cross each other and is termed an antagonistic interaction, indicating that the change in mean response for factor C at low level (represented by 0) is noticeably high compared to high level: the factor C is less sensitive to variation in mean response at high level of factor B. In Figure 4.17 (a), the graph indicates that the effect

of B is insensitive to mean yield at low level of A. However, maximum yield is obtained when material type is kept at high level and B at low level. Therefore, by considering all the interactions in addition to main factor effects, maximum energy absorption will yield to ~ 88.8 J (neglecting 3-way ABC interaction).

4.4 Acoustic performance of flax-PE honeycomb core

The acoustic performance of the sandwich panels can be categorised by, sound transmission loss (TL) and sound absorption. The former relates to the application of the panel as a sound barrier, preventing the sound to pass through it and the latter relates to the ability of the panel to absorb the sound which is incident on it. In many cases, a panel exhibiting good sound absorbance will also be a good sound barrier; however, the panels can be manufactured to cater to the acoustic requirements. The TL of a material is measured by mounting a sample of the material in an opening of a wall separating two reverberation test rooms. Broadband noise is played in the source room using a speaker assembly and the intensity of the sound signal is measured using a microphone in the receiver room. The difference between the sound levels in the source room and the receiving room is defined as Noise Reduction (NR). As the frequency and/or density increases the TL also increases. The density of the material is a key factor in determining the transmission loss; for example, an improvement in the TL of the panel may not be observed if the core type and height are changed keeping the cell wall thickness and density same. The TL of a sandwich panel may be due to spreading of the sound waves and/or absorption of the sound waves, where the sound energy is absorbed in the material. The sound absorption in the material can be due to direct mechanical damping in the material, viscous damping, thermo-elastic damping, and by vortex shedding at sharp corners. An intensive review on models and experiments of the vibro-acoustic of sandwich panels is reported in [95].

The absorption of the sound is represented by the sound absorption coefficient, which is the fraction of the plane sound wave which is absorbed when it is incident on the material, meaning that, a material having an absorption coefficient of 0.9 would absorb 90% of the incident sound wave and this corresponds to the change of sound level of 10 dB. The sound absorption coefficient of common building materials at indicated frequencies are shown in Table 4.4, and can be seen that the absorption coefficient increases with the increase in the porosity of the material, with glass wool exhibiting maximum absorption.

In this study, the sound absorption has been preferred to the TL because it is an acoustic property more linked to the material rather than to the structure and it indicates how much of the sound is absorbed in the material. It can be expresses as the ratio between the sound intensity absorbed and the incident sound intensity and it can be due to direct mechanical damping in the material, viscous damping and thermo-elastic damping. The sound absorption of the honeycomb core sandwich panels with glass-PP face sheets was determined using a standing plane wave impedance tube. The schematic of the impedance tube, shown in Figure 4.18 consists of a loud speaker that produces an acoustic wave which

Medium	500 Hz	1000 Hz	2000 Hz	4000 Hz
Glazed tiles	0.01	0.01	0.02	0.02
Roughened concrete surface	0.02	0.03	0.04	0.04
Timber floor	0.15	0.10	0.10	0.08
Cork tiles	0.20	0.5	0.60	0.55
Expanded polystyrene	0.55	0.20	0.10	0.15
Acoustic spray (12 mm on backing)	0.50	0.80	0.85	0.60
Glass wool (50 mm on backing)	0.50	0.90	0.98	0.99

Table 4.4: Sound-absorption coefficient of some building materials

travels down the pipe and reflects from the specimen. The phase interference between the waves in the pipe which are incident upon and reflected from the test sample will result in the formation of a standing wave pattern in the pipe. If all the sound waves are reflected (100%) then the amplitude of reflected wave pattern will be of the same of that of the incident wave, meaning that the nodes will have zero pressure and the antinodes will have double pressure. However, if the material absorbs sound, then the reflected wave will have different amplitude compared to that of the incident wave, this gives rise to a change in pressure at the nodes and the antinodes. In an impedance tube, the pressure is recorded using a microphone probe attached to a car which slides along a graduated ruler. The ratio of the maximum pressure at the antinode to the minimum pressure at the node is called the standing wave ratio (SWR) and is used to determine the specimen's reflection coefficient amplitude R, its absorption coefficient α, and its impedance Z.
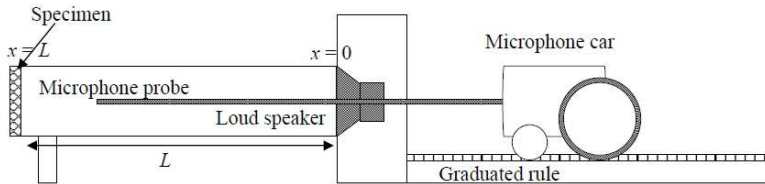
Figure 4.18: Schematic of an impedance tube

If the tube is of cross-sectional area S and length L, driven by a piston at x=0, the maximum distance the probe could travel is $x = L$ due to the presence of a mechanical impedance Z_{max}. The pressure wave in the tube due to harmonic vibration at a given frequency is given by

$$P = Ae^{i[\omega t+k(L-x)]} + Be^{i[\omega t-k(L-x)]} \tag{4.6}$$

where A and B are determined by the boundary conditions at $x = 0$ and $x = L$. The particle velocity in the tube may be expressed as

$$v = \frac{1}{\rho c}(Ae^{i[\omega t+k(L-x)]} + Be^{i[\omega t-k(L-x)]}) \tag{4.7}$$

where ρ is the density of air and c is the speed of sound in air, k is the wave number and i^2 = -1. Applying Euler's law, the impedance of the plane waves in the tube may be expressed as

$$Z_A(x) = \frac{\rho c}{S}\left[\frac{Ae^{ik(L-x)} + Be^{-ik(L-x)}}{Ae^{ik(L-x)} - Be^{-ik(L-x)}}\right]$$

(4.8)

The mechanical impedance at x = L, expressed in terms of acoustic impedance is given as

$$Z_L(x) = Z_A S^2 = \rho c S\left(\frac{A+B}{A-B}\right)$$

(4.9)

where $A= A$ and $B=B^{ei\theta}$

(a)

(b)
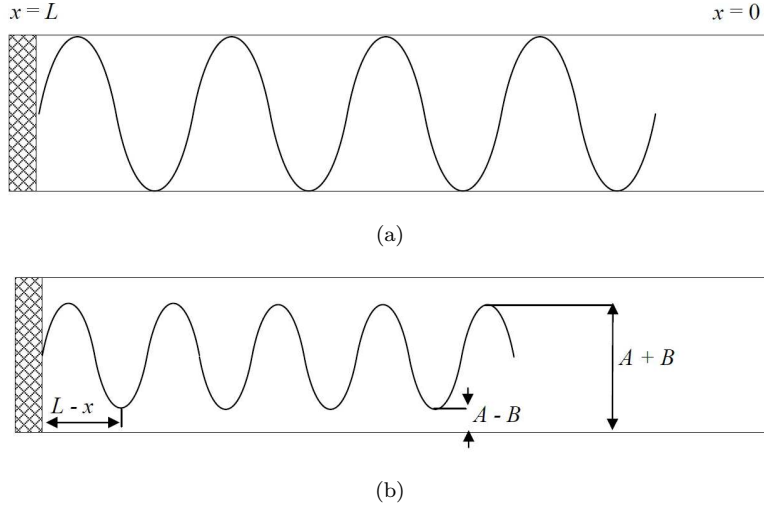
Figure 4.19: Pressure amplitude in the impedance tube in case of total reflectance (a) and partial reflectance (b)

Hence, if the ratio of the amplitude of incident wave to the reflected wave and the phase angle θ are given, the mechanical impedance can be calculated using Equation 4.10. The pressure amplitude is given by

$$P = \left\{(A+B)^2 cos^2\left[k(L-x) - \frac{\theta}{2}\right] + (A+B)^2 sin^2\left[k(L-x) - \frac{\theta}{2}\right]\right\}^{0.5}$$

(4.10)

The pressure amplitude is shown in Figure 4.19 where (a) represents the case of a case where 100% of the incident wave is reflected back, meaning that the amplitude will be the same and (b) represents the case where there is some absorption

by the specimen, which is indicated as the decrease in the amplitude of the reflected wave upon reflectance. The amplitude at the antinode is represented as *(A+B)*, and the amplitude at the node is represented as *(A-B)* which is picked up by the receiver probe as maximum pressure and minimum pressure, respectively. The ratio of the pressures is defined as the standing wave ratio *(SWR)* expressed as

$$SWR = \frac{A + B}{A - B} \tag{4.11}$$

The equation may be rearranged to provide the reflection coefficient

$$R = \frac{B}{A} = \frac{SWR - 1}{SWR + 1} \tag{4.12}$$

and the sound absorption coefficient at a given frequency is given by

$$\alpha = 1 - R^2 = 1 - \frac{(SWR - 1)^2}{(SWR + 1)^2} \tag{4.13}$$

4.4.1 Experimental investigation

To determine the absorption coefficient, the flax-PE honeycomb core sandwich panels were tested in a Bruel & Kjaer standing wave apparatus. An impedance tube of diameter 150 mm, a length of 2.0m and diameter 30mm, length 500mm were used to determine the absorption coefficient up to 200Hz - 1.6kHz and 1.6kHz - 4kHz respectively (Figure 4.20). The upper frequency is limited to those where only plane waves can propagate in the impedance tube (f<0.586 c/d, being c is the speed of sound and d the tube diameter). The influences of the reinforcement type (continuous-unidirectional and non-continuous-random) and of the core thickness (20 and 40 mm) on the acoustic absorption coefficient were investigated. It is well known that the sound absorption increases with the increase in the porosity of the material; hence by adding porous filler in the honeycomb cells the sound absorption can be enhanced. A common material having high porosity that is frequently used in construction industry is glass wool, they are laid as batts in between wall panels as sound absorbers. Though the material offers excellent sound absorbing properties, it is obtained from non sustainable resources, its incorporation in this study would nullify the primary objective of eco-friendly cores. Hence, in the view of maintaining the integrity of eco friendly cores, wool fibres was used insulating material in the cores. Furthermore, two variations of honeycomb cores were tried; hollow cores (air-filled) and wool fibres filled. For the wool fibre filled cores, the cells of the honeycomb cores were manually filled with medium density wool fibres. For each kind of test five nominal identical samples for different configurations were investigated (Figure 4.21).
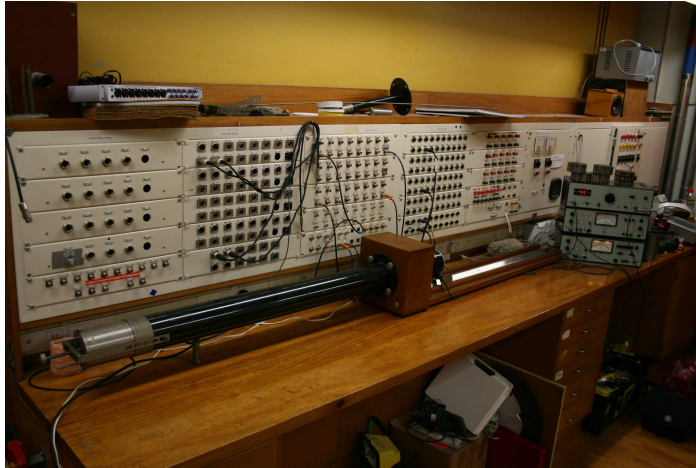
Figure 4.20: Impedance tube to measure absorption coefficient up to 1.6 kHz

Figure 4.21: Test specimen for acoustic test

4.4.2   Results

Sound absorption coefficients of eco-friendly sandwich panels is measured in the frequency range 200 Hz - 4 kHz, in one-third octave bands. All the specimens had face sheets made of glass-PP and a thickness of 1 mm. Since the influence of different parameters on sound absorption coefficient was investigated, the section of the results is presented in subsections.

4.4.2.1   Effect of reinforcement type on sound absorption

Sound absorption coefficients for honeycomb cores, 20 mm thick, reinforced with not-continuous random and continuous unidirectional fibres, at low, intermediate and high frequencies, are depicted in Figures 4.22 and 4.23. In the low frequency range (< 500 Hz), continuous fibre reinforced LLDPE cores exhibit high sound

absorption coefficient, peaking between 0.3-0.4, Figure 4.22, outperforming the not-continuous fibre reinforced cores whose maximum absorption is ~ 0.3. However, as the frequency approaches intermediate-high frequency, at 1.6 kHz, the absorption occurs irrespective of the type of fibre reinforcement within the cell wall and is dominated by the fibrous arrangement behind the faceplate. At higher frequencies (3 kHz-4 kHz) when the facings start to vibrate independently about their neutral axis, the absorption appears to occur irrespective of the fibrous arrangement behind the face plates or reinforcement type, which may be due to the presence of damped visco-elastic matrix behind stiff facings.
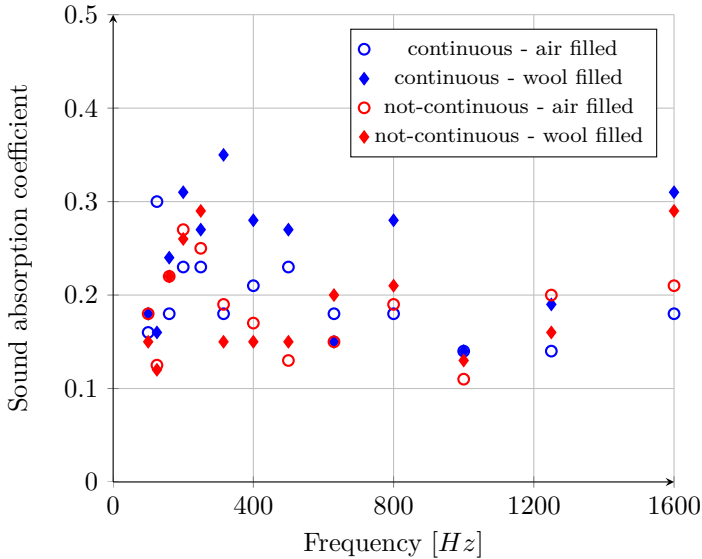
Figure 4.22: Sound absorption coefficient of specimen with core thickness of 20 mm at low frequency range

4.4.2.2 Effect of core thickness on sound absorption

Sound absorption coefficients for honeycomb cores with short random and continuous unidirectional fibre reinforcement, shown in Figure 4.24 and 4.25, gives the behaviour of the curves of two configurations of sandwich panels with core thickness of 40 mm. It is evident from Figure 4.24 that the absorption coefficient trend seem to be similar to those of the previous test of the specimens with thickness of 20 mm, meaning that the core thickness plays little role in sound absorption at low-intermediate frequencies, exhibiting similar absorptions. However, at higher frequencies (Figure 4.25), the sound absorption coefficients are higher than the ones obtained for the specimens with core thickness of 20 mm, peaking the maximum value of 0.5 at 2 kHz. Absorption coefficient of 0.5 compares to a reduction of about 3 dB in sound level. The sound absorption at lower frequencies appears to be due to the presence of fibrous wool arrangement behind the facings, similar to those of 20 mm thick. However, in Figure 4.25, the jump in absorption coefficient to 0.45 is irrespective of the fibrous loading behind the facings, which is again due to the presence of visco-elastic honeycomb core
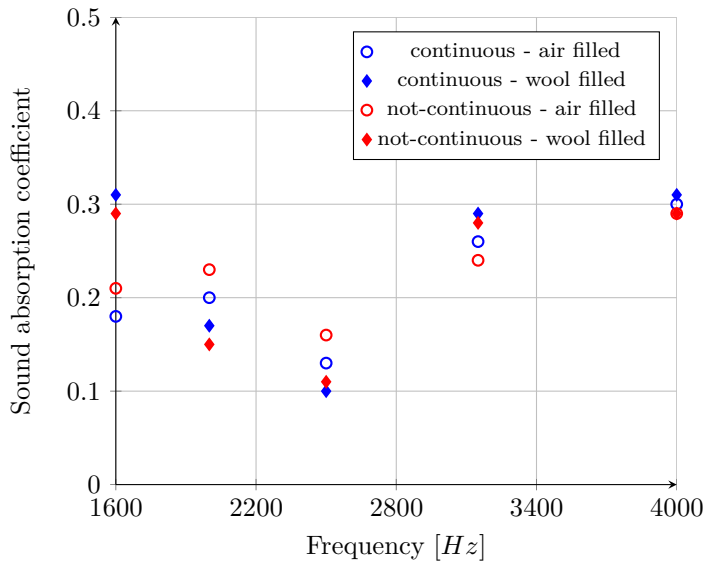
Figure 4.23: Sound absorption coefficient of specimen with $c_t = 20$ mm at high frequencies

behind the stiff facings. The increase in absorption coefficients from 0.2 to 0.4 when the core thick were changed might be due to the availability of larger cell wall height, which would in effect alter its damping effect.
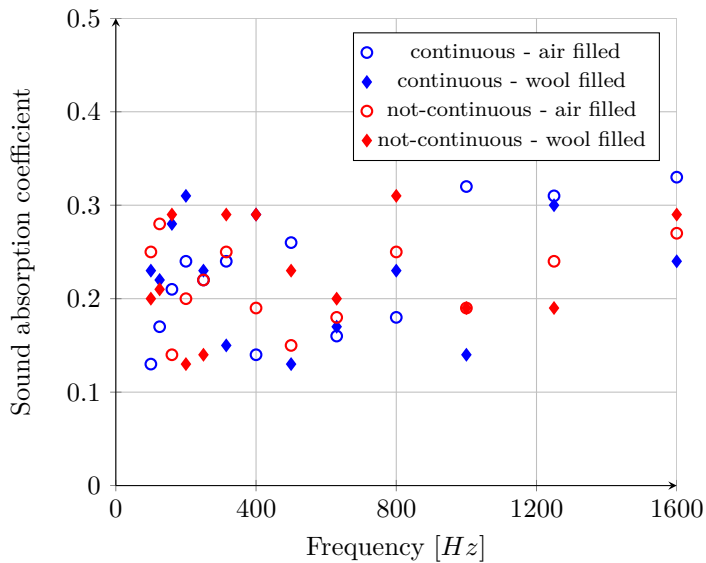
Figure 4.24: Sound absorption coefficient of specimen with $c_t = 40$ mm at low frequencies
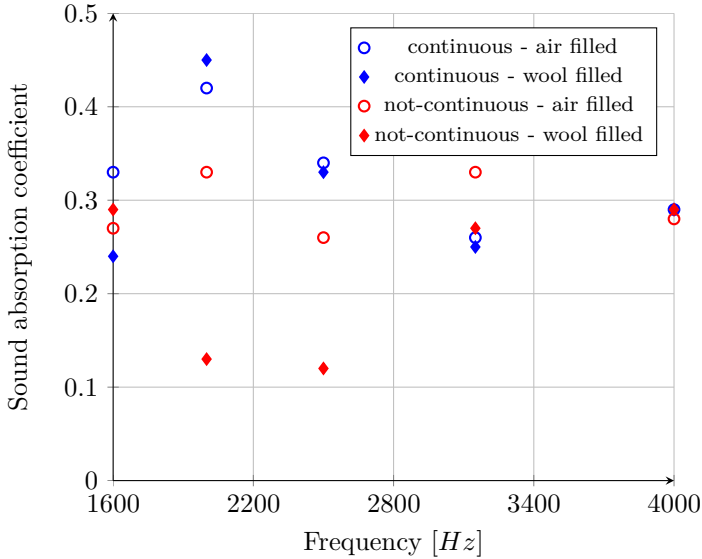
Figure 4.25: Sound absorption coefficient of specimen with $c_t = 40$ mm at high frequencies

4.5 Damping measurements: the influence of reinforcement

In this section an experimental modal campaign was performed on sandwich beams in order to evaluate the damping capability of these structures. Specimens in the form of beams, having dimensions 440 x 40 x 22 mm, were formed. Each was marked up into 23 grid points at which vibration response measurement were taken. The excitation was provided by a modal hammer while the response was measured by using a laser vibrometer. The sampling frequency was chosen between 0 to 4 kHz and the frequency response data was recorded using an HP analyzer and exported to a universal file to be processed in LMS Test.Lab 8B. The investigated sandwich beams, shown in Figure 4.26, have the same dimensions and face sheets materials and thickness, but different core materials:

- unreinforced PE core;

- PE core reinforced with continuous unidirectional fibres;

- PE core reinforced with not-continuous random fibres.

Experimental studies of the dynamic characteristics of laminated sandwich honeycomb beams with wool fibres inserted in the honeycomb cells were also performed. The fibres were inserted before the composite was cured and the amount of fibres in each cell is the same for every sample.

Figure 4.26: Sandwich beams with flax-PE honeycomb cores air and wool filled

4.5.1 Results

Damping ratio was estimated using the first modes and test results show that the beam with core reinforced with continuous fibres has natural frequencies lower than the one made with not-continuous fibres. This difference is due to the effect of orientation of fibres. In fact continuous fibres were oriented along the thickness of the honeycomb, resulting in a high reinforcement along that direction and low in the ribbon direction. This leads to a low flexural rigidity in the ribbon-transverse plane, where the mode shapes were investigated. Not-continuous fibres, instead, were oriented randomly inside the core, providing a homogeneous distribution of mechanical properties. The modal damping values carried out from the experiments are depicted in Figure 4.27. The unreinforced (PE) core panel has modal damping values higher than the fibre reinforced cores for all the modes, peaking 0.05 for the third mode. For the specimens with PE cores reinforced with continuous unidirectional and not-continuous random flax fibres, the maximum modal damping value occurs at the third mode and is equal to 0.031 and 0.026 respectively. The damping in composite is controlled by several parameters: matrix properties, fibre properties, interaction between fibres and matrix, laminar stacking sequence. The results carried out suggest that damping due to visco-elastic nature of the matrix material has more influence than interface between fibre and matrix. It is also seen that the continuous fibres reinforced core has somewhat higher damping than the not-continuous one.

Experimental measurements are also performed for the laminated sandwich honeycomb beams with wool fibres inserted in the cells. The fibres are inserted before the composite is cured and the amount of fibres in each cell is the same for every sample. The natural frequencies tend to be slightly smaller than those for hollow core cells beams, as a consequence of the additional mass of the wool fibres. Filling the core with fibres results in a small weight increase, relatively unchanged mechanical properties and improved acoustical absorption properties and damping. A comparison of modal damping values for the laminated sandwich beams, the one with hollow core cells and the one filled with wool fibres is finally shown in Figure 4.28. The wool filled cores have slightly higher damping value for the first two modes and significantly higher for the remaining modes, reaching a maximum value of about 0.065 for fourth mode of the beam reinforced with continuous fibres. This increase could be due to frictional slip damping between wool fibres inserted in the core.
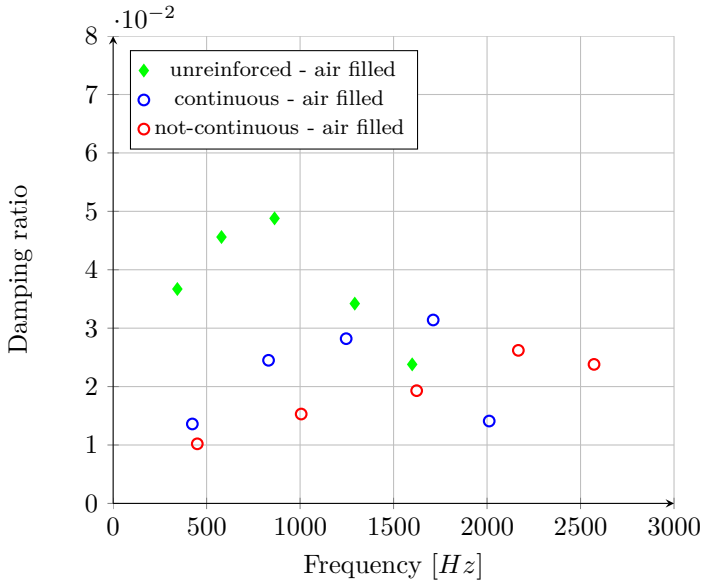
Figure 4.27: Damping ratio of sandwich beams air filled

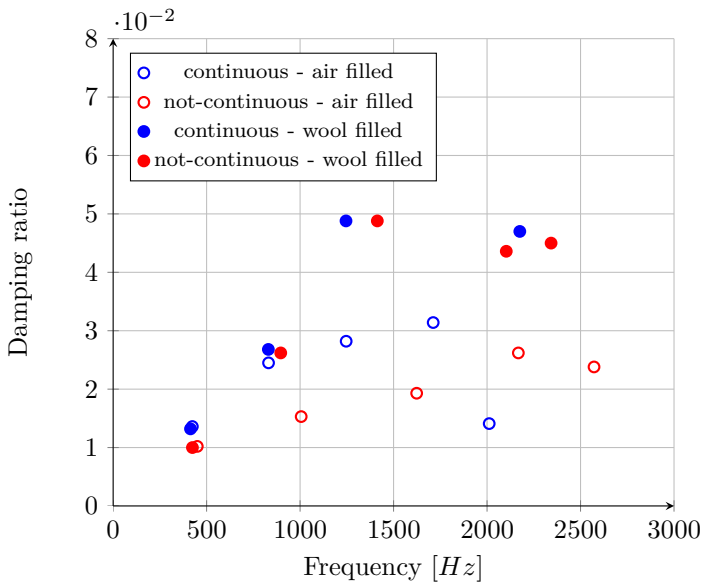Figure 4.28: Damping ratio of sandwich beams air and wool filled

4.6   Flax-PE as face sheets materials

In the previous section flax-PE honeycomb cores were manufactured and some of their characteristics were evaluated both numerically and experimentally. In this section flax-PE composites were produced for using as face sheets materials and their performance in terms of damping was evaluated.

	Young's modulus E [MPa]	Shear modulus G [MPa]	Poisson's ratio ν	Mass density ρ [kg/m^3]
Foam F90	59.0	9.0	0.35	90

Table 4.5: Core mechanical properties

	Longitudinal Young's modulus E$_1$ [GPa]	Transversal Young's modulus E$_2$ [GPa]	Shear modulus G$_{12}$ [GPa]	Poisson's ratio ν_{12}	Mass density ρ [kg/m^3]
flax-PE	12.3	1.1	0.85	0.10	1100
glass-PP	29.0	5.0	2.70	0.24	1550

Table 4.6: Face sheets mechanical properties

4.6.1 Experimental investigation

Two different kinds of sandwich panels were manufactured and investigated. In order to study the possibility of replacing glass fibres with flax ones, the two panels were manufactured by using the same core material and different face sheet materials. The used core is a recyclable, pre-preg compatible foam core (DIAB® Divinycell F90), offering excellent FST (Fire, Smoke and Toxicity) properties, good mechanical and processing characteristics. The material properties of the core are listed in Table 4.5 .

The first type of face sheets is made of five plies of Plytron, with a lay-up 0/90/0/90/0. Plytron is a commercially available pre-preg material consisting of 35 percent volume fraction of unidirectional glass fibres in a polypropylene (PP) matrix. The synthetic glass fibres typically exhibit high strength and stiffness and although it is not a Natural Fibres Composite (NFC), the use of a PP matrix still allows for mechanical recycling of the entire sandwich panel. The other type of face sheets is made of five plies of flax/PE, with a lay-up 0/90/0/90/0. Flax is a natural fibre that has become recently available in commercial grades for use in NFCs. Flax fibres were consolidated with polyethylene (PE) sheets to manufacture a face sheet laminate. The material properties of both the face sheets, indicating with the subscript 1 the longitudinal direction and the subscript 2 the transversal one, are listed in Table 4.6.

The sandwich panels were manufactured at CACM (Centre for Advanced Composite Material) of the University of Auckland, using a vacuum bag technique. No adhesive layers were used to bond face sheets and cores, in order to reduce the number of parameters affecting the damping of the panels. The bonding was obtained during curing, where the resin flows out from the uncured face sheets and creates the bonding between the face sheets and the core. Experimental tests on two different sandwich panels were performed. The two panels, shown in Figure 4.29, have the same in-plane dimensions (400 mm x 200 mm) but different thickness of the core. In particular the panel A has the core thickness of 26 mm, that is slightly higher than the panel A having the core thickness of 20 mm. Panel
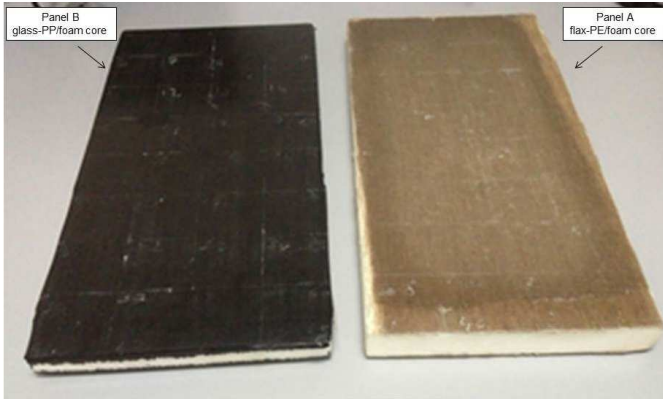
Figure 4.29: Tested sandwich panels

Class	Material	Core thickness [mm]	Dimensions [mm]	Weight [kg]
A	flax-PE/Foam core	26	400 x 200 x 28	0.314
B	glass-PP/Foam core	20	400 x 200 x 22	0.389

Table 4.7: Sandwich panels characteristics

dimensions are listed in Table 4.7.

The dynamic characteristics of the sandwich panels were determined through modal tests, adopting the so-called roving hammer technique. The experimental equipment is the same shown in Figure 3.1. An experimental mesh, 5 by 9 nodes, was drawn on the investigated panels and vibration measurements were taken in the frequency range 0-1.6 kHz.

For the damping measurements, the set-up is similar to the modal one with the panels hanged up using bungee cords, an instrumental hammer to provide the excitation and an accelerometer to measure the response. The Reverberation Time (RT_{60}) was measured by means of the software SAMURAI 2.0, that is a software package for noise and vibration measurements included in the Soundbook system [96].

4.6.2   Numerical Investigation

Finite Element models of the two types of sandwich panels were built [97]. The sandwich panels were modelled using 4-nodes quadrilateral elements (CQUAD4) for the face sheets and 8-nodes solid elements (CHEXA) for the core. The numerical mesh consisted of 41 by 21 nodes along the in-plane directions and 3 nodes along the thickness of the core. Measured values of damping were taken into account in the numerical models, since experimental tests highlighted a strong variation of damping ratio in the frequency range of interest. The modal analysis were carried out using the commercial finite element solver MSC/Nastran 2008 [98]. Moreover, in order to compare the experimental and numerical Frequency Response Function (FRFs), a unit force was applied on the node of one corner
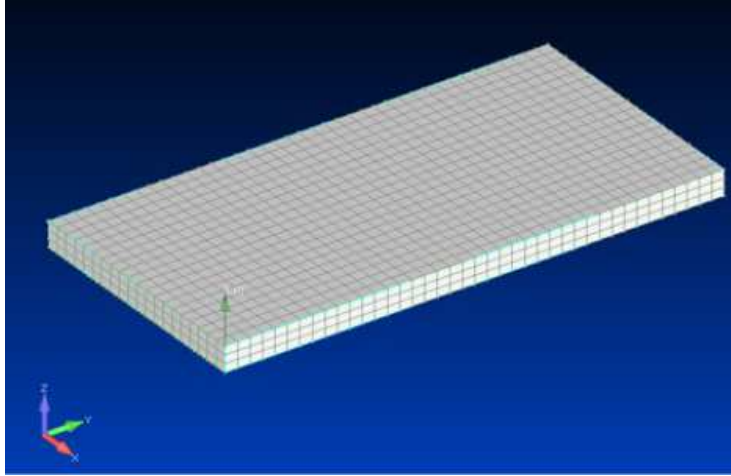
Figure 4.30: Isometric view of the numerical model of the sandwich panel

Mode	Panel A		Panel B	
number	Frequency [Hz]	Damping (%)	Frequency [Hz]	Damping (%)
1	313.1	1.85	359.7	2.09
2	510.6	1.59	502.8	0.90
3	712.9	1.62	689.2	1.32
4	792.6	2.66	873.2	1.16
5	915.2	2.28	905.8	1.11
6	1080.9	2.36	956.2	1.23
7	1163.9	2.40	1006.7	1.12
8	1392.0	2.33	1115.7	1.29

Table 4.8: Modal parameters of the sandwich panels A and B

of the upper face sheet, and prediction of the acceleration as a function of the frequency were carried out on the opposite corner. An isometric view of the numerical model is shown in Figure 4.30.

4.6.3 Results

4.6.3.1 Experimental results

Modal parameters in terms of natural frequency, modal shape and modal damping were extracted by the analysis of the FRFs. Table 4.8 shows the natural frequencies and the modal damping values of the original panels according to their modes.

The evaluated modal damping is the critical damping ratio (ζ), which is the ratio between the damping coefficient (c) and the critical damping value ($c_{cr} = 2\sqrt{km}$, $\zeta = c/c_{cr}$) [57]. The damping in composite materials is essentially due to the
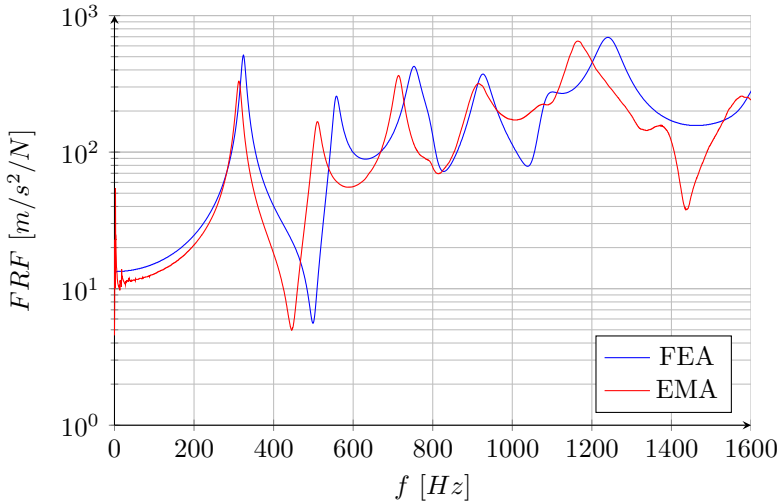
Figure 4.31: Comparison of numerical and experimental FRFs of the panel A

matrix viscoelasticity, to the fibre material and to the sliding of the fibre at the interface with the matrix. It can be concluded, from the results, that the panel A outperforms the panel B in damping value in overall frequency range. Comparing the natural frequencies of the two sandwich panels, it is evident that they are comparable although the panel A, i.e. the one with face sheets made of flax fibre-PE, has a total thickness higher and a mass lower than the panel B.

4.6.3.2 Experimental-Numerical correlation

The correlation between experimental measurements (indicated in the legend as EMA) and numerical predictions (indicated as FEA) is evaluated in Figures 4.31 and 4.32 for panels A and B, respectively. A good correlation between numerical and experimental curves is observed up to 1 kHz. However, some little differences in the amplitude of the two curves can be appreciated despite a variable value of damping in the whole frequency range was used in the numerical model. Furthermore, some discrepancies in the estimation of the natural frequencies for the panel A are evident, in particular for the flexural modes. These can be attributed to the inaccurate material properties used for the face sheets in flax fibre-PE.

The evaluation of the correlation between estimated and measured modal shapes is performed by calculating the Modal Assurance Criterion (MAC). The MAC matrix calculated between the numerical and experimental mode shapes of panels A and B is depicted in Figure 4.33. The comparison of the numerical and experimental results, in terms of natural frequencies is reported in Table 4.9, while Table 4.10 shows the comparison between the numerical and the experimental mode shapes obtained by using FEMtools solver. Table 4.10 shows a quantitatively and qualitatively analysis of two sets of results. It consists in overlapping the experimental (red grid mesh)and the numerical (blue grid mesh) models associating nodes of the first with those of the second; then the MAC is calculated according to eq. 3.5.
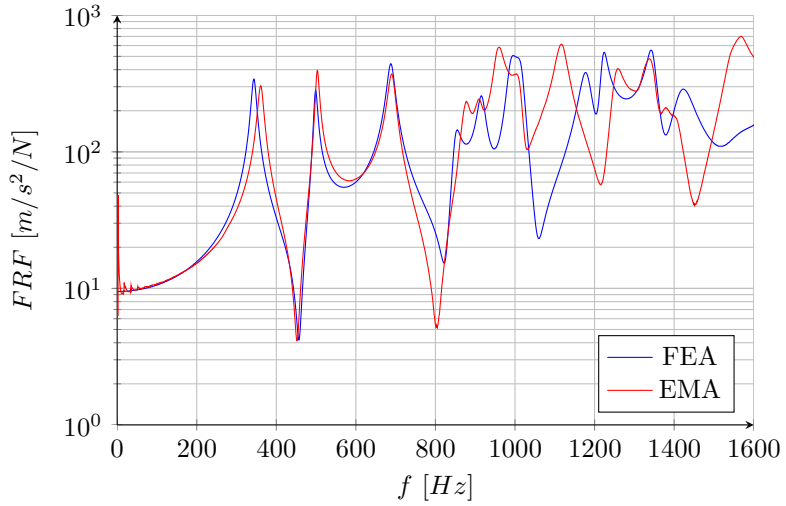
Figure 4.32: Comparison of numerical and experimental FRFs of the panel B

	Panel A				Panel B			
Mode number	FEA [Hz]	EMA [Hz]	Diff. (%)	MAC (%)	FEA [Hz]	EMA [Hz]	Diff. (%)	MAC (%)
1	324.2	313.1	3.54	98.9	343.7	359.7	-4.47	87.4
2	556.5	510.6	8.98	91.7	498.4	502.8	-0.85	95.0
3	752.7	712.9	5.58	92.3	688.1	689.2	-0.15	94.6
4	795.6	792.6	0.38	88.7	850.8	873.2	-2.57	83.4
5	925.4	915.2	1.11	50.3	915.9	905.8	1.12	91.3
6	-	-	-	-	989.7	956.2	3.50	89.5
7	-	-	-	-	1015.7	1006.7	0.90	81.8
8	-	-	-	-	1178.1	1115.7	5.59	84.7

Table 4.9: Numerical-Experimental correlation of the panels A and B
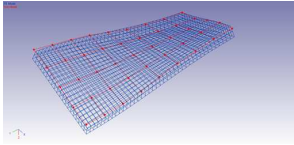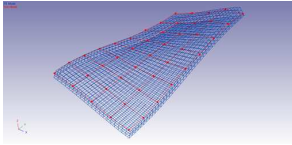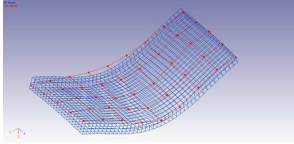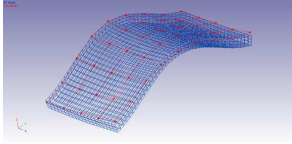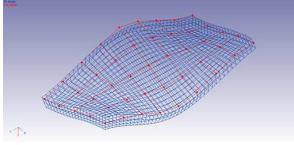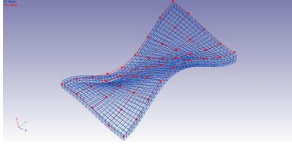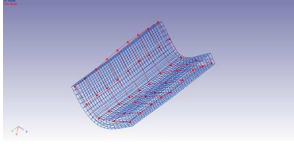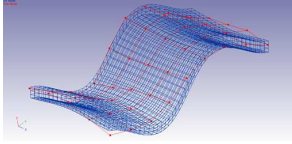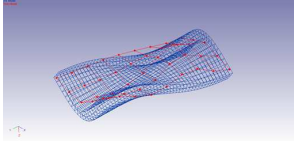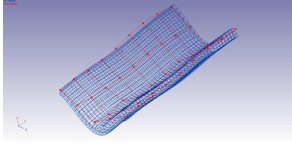
Mode number	Panel A	Panel B
1		
2		
3		
4		
5		

Table 4.10: Numerical-Experimental correlation of the first five modal shapes of the panels A and B

For both panels, the MAC matrix is diagonal and the non-zero values approach 100%: this means that the order of the eigenvectors is preserved and, furthermore, the numerical mode shapes are good estimates of the experimental ones.

4.6.3.3 Damping Measurements

Several techniques are available in literature for the estimation of the damping of a structure [57]. Most methods for damping measurements are based on the modal behaviour of the structure, i. e. valid for low frequencies, such as half-power bandwidth, mode picking and circle fitting [58]. In the high frequency range, other methods based on energy dissipation are employed, such as reverberation time [99], impulse response decay and similar [100]. In our case, since the modal damping (in terms of critical damping ratio ζ) is already known from the experimental modal analysis, the structural loss factor is also calculated by using the reverberation time RT_{60} measurements [101]. The relation between the

(a) (b)
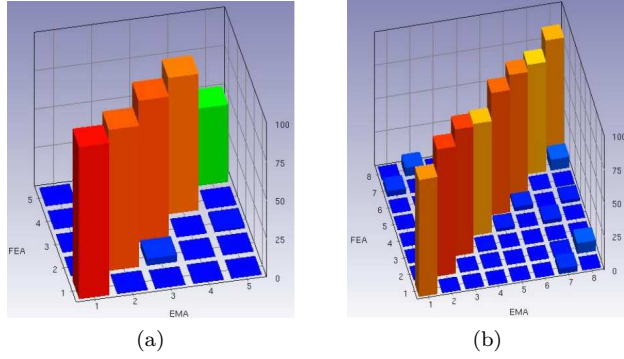
Figure 4.33: MAC of panels A (a) and B (b)

loss factor and the reverberation time is given by:

$$\eta(f) = \frac{2.2}{f \cdot RT_{60}} \qquad (4.14)$$

where f is the centre frequency in third octave band, RT_{60} is the corresponding measured reverberation time and η is the damping. The structural loss factor was calculated in third octave band and for different positions of the accelerometer on the panels. The structural loss factor of both the panels is presented in Figure 4.34, compared to the one calculated by doubling the critical damping ratio ($\eta = 2\zeta$). As shown from the Figure, it is possible to highlight that, for both panels, the values of the loss factor, calculated with two different methods, are almost the same, confirming the accuracy of the results. Furthermore, the loss factor of the panel A is higher than the one of the panel B in overall the frequency range, despite the trend of the two panels is quite similar.
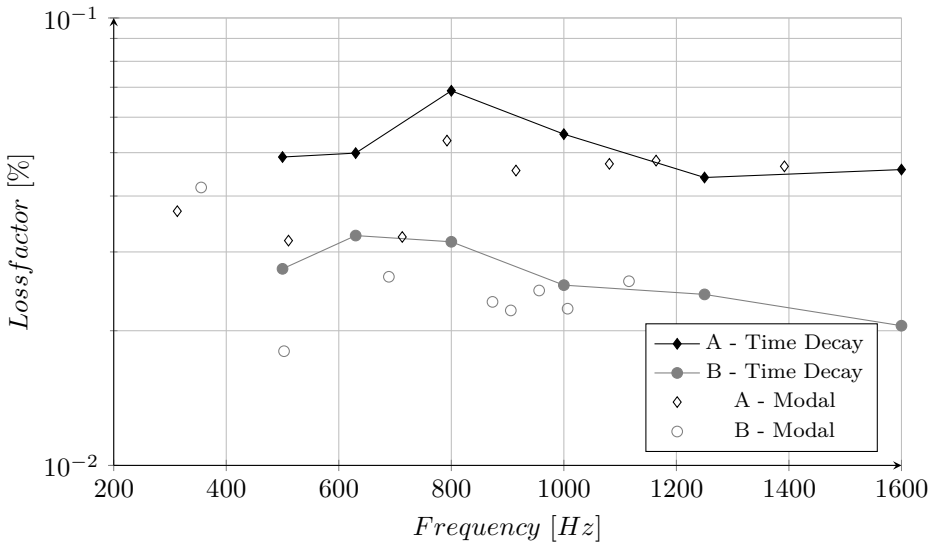
Figure 4.34: Structural loss factor of the panels A and B

Conclusions

 Current environmental awareness coupled with societal needs require the production of components made of materials that are less toxic and are recyclable. The concept of natural fibres is of key importance at present due to low cost involved in obtaining this renewable resource. The natural fibres are ideal substitute for synthetic ones, which are potentially toxic.

 Composites based on natural fibres can be recycled many times without significant loss of mechanical properties. This provides benefits in terms of cost reduction of these composites and in terms of preservation of the environment.

 Furthermore, in the engineering field, the reduction of the mass of a structure is an important issue since it leads to reduced emissions and operating costs. On the other hand, weight saving often leads to an increase of vibration and noise transmission and for this reason the dynamic design of lightweight structures and the use of "green materials" has received more emphasis with the intention to satisfy both weight and comfort requirements.

 The primary aim of this research was to evaluate the performance of innovative structures in order to replace the conventional ones in engineering applications. Eco-friendly structures using natural fibres reinforced thermoplastics were manufactured and investigated in this thesis. Natural Fibre Composites (NFC) have already found widely used in different applications: sport, musical instrumentation, infrastructure, marine and automotive. The least, the automotive field, is the predominant field in NFC applications: incorporating these structures into car components. Among all the natural fibres, flax fibres were chosen because of their specific stiffness very close to the one of the glass fibres, and for their high damping properties. Flax fibres combined with polyethylene resin were used to manufacture both flat and sandwich panels. Before to investigate the functional performance of these structures the mechanical properties were carried out by means of the static tests. These properties were, than, validated by using ultrasonic wave propagation techniques. In particular dispersion curves of a unidirectional panel were calculated, experimentally, by using Lamb waves. A numerical model was hence, built in a FE code using the mechanical properties measured by static test. Good correlation was found between the numerical and experimental results, confirming the trustworthiness of the mechanical properties. These results are further validated by a WFEM code, who estimated the group velocity of the unidirectional flax/PE panel along 0° and 90° directions. WFEM results show a potential use of this method to reduce the computational cost in FEM, since only the element matrix from the basis cell is needed, instead of assembling all elements in the model. Again analysis in the low frequency range,

modal analysis and frequency response function, were performed numerically and experimentally and good correlation of the results was found. These analysis give also informations about modal parameters: natural frequency, mode shape and damping ratio.

Once ensured the mechanical properties of flax-PE materials, due to the low values, flax-PE composites were studied for using as sandwich structures. Honeycomb cores and face sheets were manufactured separately and the influence of many parameters on structural and functional capability was investigated. Vibration and acoustic tests were performed on honeycomb cores reinforced with flax fibres and the influence of reinforcement material type, presence of face sheets and arrangements filling cores were investigated. Vibration test results reveal that fibre reinforced cores lead to an improvement of greater than 100% in mechanical properties and a reduction of about 40% in damping. In particular the cores made from continuous fibre reinforced composites show better response in damping value compared to that of not-continuous one, though this value is lesser than the one obtained from unreinforced core. In view to reduce this gap a solution is found filling the cores with wool fibres resulting in minimal weight increase and unchanged mechanical properties, plus improved acoustic absorption properties and higher damping. This possibility makes these materials very attractive since it is possible to obtain an increase in mechanical and damping values, and other functional values, by varying the several parameters involved. Acoustic test results show that the specimens exhibit different energy absorption coefficients at different frequency ranges. At the lower frequencies the sound absorption coefficient is influenced by the type of reinforcements with continuous fibre outperforming the not-continuous one. In the mid-high frequency range the absorption is dominated by the fibrous arrangement behind the faceplate while at higher frequencies it is mainly influenced by the presence of the damped visco-elastic matrix behind stiff face sheets. Additionally, since one of the main requirement of the honeycomb is to be stiff enough along the normal to the faces to keep constant the distance between them the energy absorption capabilities of these specimens was evaluated. Again the influence of different parameters, reinforcement material type, presence or not of face sheets and core thickness, were investigated. The first set of tests were conducted on specimens with thickness of 20 mm and without face sheets. Results show a better response to impact loading of the specimens with continuous fibre reinforced cores compared to the ones reinforced with not-continuous one exhibiting a large elastic region, higher peak loads and minimum plastic deformation. This is mainly due to the alignment of the fibres in the principal direction along the loading. Subsequently the influence of the presence of the face sheets on energy absorption was investigated and an improvement of the energy absorption in the panel was observed. This increase could be due to the energy dissipation encountered in bending and stretching the face sheets. Finally, similar configurations but with the core thickness of 40 mm were tested and as the core thickness increases the energy absorption capability of the specimens increases. Furthermore it seems that the contribution of the face sheets towards energy absorption is minimum at higher core thickness, making it core dependent.

In order to have a global understanding of sandwich panels made of eco-friendly materials, experimental modal analysis was performed on sandwich structures with same foam core but different face sheets materials: flax fibres combined

with polyethylene for one panel and glass fibres combined with polypropylene for the second panel. The influence of different material face sheets in a sandwich structure on damping was evaluated. From the results, it is evident that the sandwich panel made of natural fibres outperforms, in terms of damping values, the panel made of glass fibre, with an average value of 2.29. However, it is also evident that the natural frequencies of the two panels are comparable although one of the panel has a total thickness slightly higher and a weight lower than the other one. Panel made of glass fibres shifts the natural frequencies to higher values, i.e. the effective stiffness of the panel increases. The experimental results are also used to validate the numerical model. The numerical-experimental correlation is quite good, highlighting that a FE model with a homogeneous core is enough able to describe the global dynamic behaviour of a structure. The damping estimation by means of the reverberation time measurements confirm the results carried out from the modal analysis, showing the panel having the face sheets material in natural fibres outperforms the panel with face sheets made of glass fibres.

The possibility to change fibre materials for the face sheets in order to get a more (or less) damped structure and/or filling the cores with wool fibres resulting in minimal weight increase and unchanged mechanical properties, plus improved acoustic absorption properties and higher damping gives to the designer an additional degree of freedom to design the laminate. This possibility makes once more these materials very attractive since it makes possible to obtain the desired natural frequencies and/or damping factors without changing geometry. Furthermore from these analysis it is possible to highlight the high functional capability, in terms of damping, of the panel made in natural fibres and, at same time, from the analysis of the natural frequencies, the moderate values of the mechanical properties and the low weight, that makes this panel suitable for applications, such as interiors, where low load are expected and high functional values are desired in order to increase the comfort of the passengers.

Future work

Some recommendations and suggestions are presented below to provide some insight about future research work in this area.

- Further experiments should be done using different material configurations to investigate the influence on properties.

- All the honeycomb cores were of similar geometry in this study. It may become essential to test cores with different cell wall thicknesses and lengths to estimate the difference in the property with the incorporated changes.

- Further studies on the flammability of natural fibres are required and the using of some fire retardant that reduce the flammability of natural fibre composites to acceptable levels and that contains non-harmful ingredients so to keep the final structures "green".

- Investigation of the dynamic behaviour on a fully eco-friendly sandwich panel made of flax fibres combined with Polythylene both as core and face sheets materials.

Bibliography

[1] J. M. Barthelot. *Composite Materials. Mechanical Behavior and Structural Analysis.* Springer, 1999, 641 p.

[2] R. M. Jones. *Mechanics of Composite Materials.* Taylor & Francis Group, 1999, 519 p.

[3] M.F. Vaz, H. Canhao, and J.E. Fonseca. "Bone: A composite Natural Material". *Advances in Composite Materials - Analysis of Natural and Man-Made Materials.* Ed. by Dr. Pavla Tesinova. 2011. Chap. 8.

[4] B. D. Agarwal and L. J. Broutman. *Analysis and performance of fiber composites.* John Wiley e Sons, Inc., 1980.

[5] C. T. Herakovich. *Mechanics of Fibrous Composites.* John Wiley & Sons, 1998, 410 p.

[6] D. Hull. "An introduction to composite materials: the Press Syndicate of the University of Cambridge" (1981).

[7] L. E. Nielsen. *Mechanical properties of Polymers and composites.* Vol. 1. Marcel Dekker, 1974.

[8] A. K. Mohanty, M. Misra, and L. T. Drzal. "Sustainable Bio-Composites from Renewable Resources: Opportunities and Challanges in the Green Materials World". *Journal of Polymers and the Environment* **10** (2002), pp. 19 –26.

[9] A. K. Mohanty, M. Misra, and L. T. Drzal. *Natural fibers, biopolymers, and biocomposites.* Taylor & Francis, 2005, 896 p.

[10] B. English, P. Chow, and D.S. Bajwa. *Paper and Composites from Agro-Based Resources.* CRC Press, 1996, 464 p.

[11] R. Rowell, J.S. Han, and S.S. Bisen. "Changes in Fiber Properties During the Growing Season". *Paper and Composites from Agro-Based Resources.* Ed. by R. Rowell and J. Rowell. 1996. Chap. 2, pp. 23–36.

[12] R. Rowell. "The state of the art and future development of bio-based composite science and technology towards the 21st century". *Proceedings of the 4th Pacific Rim Bio-based Composite Symposium.* (Bagor, Indonesia). 1998.

[13] R.T. Cullen et al. "Toxicity of Cellulose Fibres". *The Annals of Occupational Hygiene* **46** (2002), pp. 81 –84.

[14] R. M. Rowell. "The state of the art and future development of bio-based composite science and technology towards the 21st century". *Proceedings of the 4th Pacific Rim Bio-Based Composite Symposium, 1998. Bagor, Indonesia.* 1998.

[15] K.G. Kaveline, N.S. Ermolaeva, and P.V. Kandachar. "Investigation of stochastic properties of the natural fiber mats". *Composites Science and Technology* **66** (2006), pp. 160 –165.

[16] A.R. Sanadi, D.F. Caulfield, and R.E. Jacobson. "Agro-Fiber/Thermoplastic Composites". *Paper and Composites from Agro-Baed Resources.* Ed. by CRC Press. 1996.

[17] M. Kazayawoko, J.J. Balatinecz, and L.M. Matuana. "Surface Modification and Adhesion Mechanisms in Wood Fiber-Polypropylene Composites". *Journal of Materials Science* **34** (1999), pp. 6189 –6199.

[18] R. Rowell. "Penetration and Reactivity of Cell Wall Components". *The Chemistry of Solid Wood.* Ed. by R. Rowell. Vol. 207. American chemical Society, 1984. Chap. 4, pp. 175–210.

[19] L.H. Carvalho. "Chemical Modification of Fibers for Plastics Reinforcement in Composites". *Lignocellulosic-Plastcs Composites.* Ed. by A.L. Leao, F.X. Carvalho, and E. Frollini. 1997.

[20] A.N. Netravali and S. Chabba. "Composites get greener". *Materials Today* **6** (4 2003), pp. 22 –29.

[21] C. Baillie. "Eco-Composites". *Composites Science and Technology* **63** (2003), pp. 1223 –1224.

[22] R.A. Auras et al. *Poly (lactic acid): synthesis, structures, properties, processing and application.* John Wiley & Sons, 2010, 528 p. ISBN: 978-0-470-29366-9.

[23] P. Wambua, J. Ivens, and I. Verpoest. "Natural fibres: can they replace glass in fibre reinforced plastics?" *Composites Science and Technologies* **63** (2003), pp. 1259 –1264.

[24] "S. V. Joshi et al. "Are natural fiber composites environmentally superior to glass fiber reinforced composites?" *Composites Part A: Applied Science and Manufacturing* **35** (2004), pp. 371 –376. ISSN: 1359-835X. DOI: http://dx.doi.org/10.1016/j.compositesa.2003.09.016.

[25] A.K. Bledzki, O. Faruk, and V.E. Sperber. "Cars from Bio-Fibres". *Macromolecular Materials and Engineering* **291** (5 2006), pp. 449 –457.

[26] P.N. Prasad et al. *Science and technology of polymers and advanced materials.* Plenum Press, 1998.

[27] B. Dahlke et al. "Natural fiber reinforced foams based on renewable resources for automotive interior applications". *Journal of Cellular Plastics* **34** (1998), pp. 361 –379.

[28] Ford Motor Company. *From Bangladesh to a Mondeo, Kenaf Adds to Ford's Use of Ecological-friendly Materials.* Available at www.media.ford.com. Accessed on 24 July 2013. 2005.

[29] M. Karus, M. Kaup, and D. Lohmeyer. *Study on Markets and Prices for Natural Fibres (Germany and EU).* Report FNR-FKZ:99NR163. nova Institute.

[30] L. A. Utracki. *Polymer blends handbook*. Kluwer Academic Publishers, 2002, 896 p.

[31] G. Carotenuto, M. Giordano, and L. Nicolais. "Advanced Thermoplastics Composites". *Handbook of Thermoplastics*. Ed. by Olagoke Olabisi. 1997. Chap. 42, pp. 1017–1020.

[32] T. A. Osswald and M. Menges. *Materials Science of polymers for engineers*. Hanser Publishers, 1995.

[33] S. Advani and M. Sozer. *Process Modeling in Composite Manufacturing*. Mercel-Dekker, 2003.

[34] S.J. Mander et al. "Roll Forming of Sheet Materials". *Composite Sheet Forming*. Ed. by Olagoke Olabisi. Vol. 11. Amsterdam: Elsevier, 1997. Chap. 12, pp. 473–516.

[35] R. Brooks. "Forming technology for thermoplastic composites". *Composites forming technologies*. Ed. by A.C. Long. Woodhead PublishingLimited and CRC Press LLC, 2007. Chap. 11.

[36] R. J. Crawford. *Plastics Engineering*. Butterworth-Heinemann, 1998, pp. 323–326.

[37] M.E. Bowis. "Thermoforming Woodfibre-Polypropylene Composite sheets". PhD thesis. University of Auckland, 1997.

[38] B. Dewilde. "20 Eeuwen Vlas in Vlaanderen" (1983). Lannoo pvba, Tielt, Belgium.

[39] R. R. Frank. "The history and present position of linen". H. S. S. Sharma and C. F. van Sumere. *The Biology and Processing of Flax*. Ed. by M. Publications. Belfast, 1992.

[40] S. Kalia, B.S. Kaith, and I. Kaur. *Cellulose Fibers: Bio and Nano Polymer Composites*. Springer, 2011.

[41] J. Mussig and C. Stevens. *Industrial Applications of Natural Fibres: Structures, properties and technical Applications*. John Wiley & Sons, 2010.

[42] C. Baley. "Analysis of the flax fibres tensile behaviour and analysis of the tensile stiffness increase". *Composites Part A - Applied Science and Manufacturing* **33** (2002), pp. 939 –948.

[43] H. Bos, M. Van Den Oever, and O. Peters. "Tensile and compressive properties of flax fibres for natural fibre reinforced composites". *Journal of Materials Science* **37** (2002), pp. 1983 –1992.

[44] K. Charlet et al. "Characteristics of Hermes flax fibres as a function of their location in the stem and properties of the derived unidirectional composites". *Composites Part A - Applied Science and Manufacturing* **38** (2002), pp. 1912 –1921.

[45] D.V. Rosato, D.V. Rosato, and M.G. Rosato. *Injection Molding Handbook*. Ed. by Kluwer Academic Publishers. Norwell, USA, 2000.

[46] K. Van de Velde and P. Kiekens. "Influence of fiber surface characteristics on the flax/polypropylene interface". *Journal of Thermoplastc Composite Materials* **14** (2001), pp. 244 –260.

[47] A.C.N. Singleton et al. "On the mechanical properties, deformation and fracture of natural fibre/recycled polymer composites". *Composites Part B* **34** (2003), pp. 519 –526.

[48] J.Z. Lu, Q. Wu, and I.I. Negulescu. "Wood fibre/High density polyethylene composites: Coupling agent performance". *Journal of Applied Polymer Science* **96** (2005), pp. 93 –102.

[49] M. Brahmakumar, C. Pavithran, and R.M. Pillai. "Coconut fibre reinforced polyethylene composites: effect of natural waxy surface layer of the fiber on fiber/matrix interfacial bonding and strength of composites". *Composites Science and Technology* **65** (2005), pp. 563 –569.

[50] J. George, S.S. Bhagawan, and S. Thomas. "Improved interactions in chemically modified pineapple leaf fiber reinforced polyethylene composites". *Composites Interfaces* **5** (1998), pp. 201 –224.

[51] S. Rao, K. Jayaraman, and D. Bhattacharyya. "Short fibre reinforced cores and their sandwich panels: processing and evaluation". *Composites Part A* **42** (2011), pp. 1236 –1246.

[52] W. Weibull. "A statistical distribution function of wide applicability". *Journal of Applied Mechanics* **18** (1951), pp. 293 –299.

[53] ASTM D3039. *Standard test method for tensile properties of polymeric matrix composite materials*. Report.

[54] ASTM D4255. *Standard test method for in-plane shear properties of polymeric matrix composite materials by the rail shear method*. Report.

[55] J. M. M. Silva, N. M. M. Maia, and A. M. R. Ribeiro. "Cancellation of Mass-Loading Effects of Transducers and Evaluation of Unmeasured Frequency Response Functions". *Journal of Sound and Vibration* **236** (2000), pp. 761 –779.

[56] M. R. Ashory. "Correction of Mass-Loading Effects of Transducers and Suspension Effects in Modal Testing". *Proceedings of the XVIth IMAC*. CA, USA. 1998, pp. 815 –828.

[57] I. L. Vér and L. L. Beranek. *Noise and vibration control engineering: principles and applications*. Hoboken, New Jersey: John Wiley & Sons, 2006.

[58] W. Heylen, S. Lammens, and P. Sas. *Modal Analysis Theory and Testing*. Katholieke Universiteit Leuven, Faculty of Engineering, Department of Mechanical Engineering, Division of Production Engineering, Machine Design and Automation, 1997. ISBN: 907380261X.

[59] D. Aggelis and T. Makitas. "Effect of plate wave dispersion on the acoustic emission parameters in metals". *Computers & Structures* **98** (2012), pp. 17 –22.

[60] S. Banerjee et al. "A wave propagation and vibration-based approach for damage identification in structural components". *Journal of Sound and Vibration* **322** (2009), pp. 167 –183.

[61] S. Banerjee et al. "A wave propagation and vibration-based approach for damage identification in structural components". *Journal of Sound and Vibration* **322** (2009), pp. 167 –183.

[62] L. Yam et al. "Numerical analysis of multi-layer composite plates with internal delamination". *Computers & Structures* **82** (2004), pp. 627 –637.

[63] Z. Su, L. Ye, and Y. lu. "Guided Lamb waves for identification of damage in composite structures: a review". *Journal of Sound and Vibration* **295** (2006), pp. 753 –780.

[64] M. Sale, P. Rizzo, and A. Marzani. "Semi-analytical formulation for the guided waves-based reconstruction of elastic moduli". *Mechanical system signal processing* **25** (2011), pp. 2241 –2256.

[65] I.A. Viktorov. *Rayleigh and Lamb waves: Physical Theory and Applications.* Plenum Press, 1967.

[66] J. R. Rose. *Ultrasonic waves in solid media.* Vol. 1. Cambridge University Press, 1999.

[67] V. Giurgiutiu. *Structural Health Monitoring with piezoelectric wafer active sensors.* Academic Press, 2008.

[68] D. Guo, A. K. Mal, and K. Ono. "Wave Theory of Acoustic Emission in Composite Laminates". *Journal of Acoustic Emission* **14** (1996), pp. 19 –46.

[69] S. S. Lih and A. K. Mal. "Response of a Multilayered Composite Laminates to Dynamic Surface Loads". *Composites Part B* **55** (1996), pp. 663 –641.

[70] A. K. Mal and S. S. Lih. "Elastodynamic Response of a Unidirectional Composite Laminate to Concentrated Surface Loads, Parts I & II". *ASME Journal of Applied Mechanics* **55** (1992), pp. 878 –892.

[71] X. M. Zhang and J. G. Yu. "Effect of initial stresses on guided waves in unidirectional plates". *Archives of Mechanics* **65** (2013), pp. 3–26.

[72] B. R. Mace et al. "Finite element prediction of wave motion in structural waveguides". *Journal of Acoustical Society of America* **117**.5 (2005), pp. 2835–2843.

[73] D. Duhamel, B. R. Mace, and M. J. Brennan. "Finite element analysis of the vibrations of waveguides and periodic structures". *Journal of Sound and Vibration* **294**.1–2 (2006), pp. 205–220. ISSN: 0022–460X.

[74] M. N. Ichchou, S. Akrout, and J. M. Mencik. "Guided waves group and energy velocities via finite elements". *Journal of Sound and Vibration* **305** (2007), pp. 931–944. ISSN: 0022–460X.

[75] J. M. Renno and B. R. Mace. "On the forced response of waveguides using the wave and finite element method". *Journal of Sound and Vibration* **329**.26 (2010), pp. 5474–5488. ISSN: 0022–460X.

[76] J. M. Mencik. "On the low- and mid-frequency forced response of elastic structures using wave finite elements with one-dimensional propagation". *Computers & Structures* **88** (2010), pp. 674–689. ISSN: 0045–7949.

[77] B. R. Mace and E. Manconi. "Modelling wave propagation in two dimensional structures using finite element analysis". *Journal of Sound and Vibration* **318** (2008), pp. 884–902. ISSN: 0022–460X.

[78] E. Manconi. "Modelling wave propagation in two-dimensional structures using a wave/finite element technique". PhD thesis. Parma, Italy: Department of Industrial Engineering, University of Parma, 2008, ix, 172 pp.

[79] V. D'Alessandro. "Investigation and Assessment of the Wave and Finite Element Method for structural waveguides". PhD thesis. Napoli, Italy: Department of Industrial Engineering, University of Napoli Federico II, 2014, pp. xx, 122.

[80] T. Bitzer. *Honetcomb Technology. Materials, Design, Manufacturing Applications and Testing*. Hoboken, New Jersey: Chapman & Hall, 1997.

[81] L. J. Gibson and M. F. Ashby. *Cellular solids: structure & properties*. Pergamon Press, 1988.

[82] D. Zenkert. *An introduction to sandwich construction*. Cradley Heath, 1995.

[83] N. Haydn and G. Wadley. "Multifunctional periodic cellular metals". *Philosophical Transactions of the Royal Society A* **364** (2006), pp. 31 –68.

[84] S. Wilson. "A new face of Aerospace Honeycomb". *Materials & Design* **11** (1990). Technical Report, pp. 323 –326.

[85] R.C. McFarland. "Hexagonal cell structures under post-buckling axial load". *AIAA Journal* **1** (1963), pp. 1380 –1385.

[86] T. Wierzbicki. "Crushing analysis of metal honeycombs". *International Journal of Impact Engineering* **1** (1983), pp. 157 –174.

[87] J. Zhang and M.F. Ashby. "Buckling of honeycombs under in-plane biaxial stresses". *International Journal of Mechanical Sciences* **34** (6 1992), pp. 491 –509.

[88] E. Wu and W.S. Jiang. "Axial crush of metallic honeycombs". *International Journal of Impact Engineering* **19** (1997), pp. 439 –456.

[89] M. Yamashita and M. Gotoh. "Impact behaviour oh honeycomb structures with various cell specifications - numerical simulation and experiment". *International Journal of Impact Engineering* **32** (1-4 2005), pp. 618 –630.

[90] W. Goldsmith and J.L. Sackman. "An Experimental Study of Energy Absorption in Impact on Sandwich Plates". *International Journal of Impact Engineering* **12** (1992), pp. 241 –262.

[91] M.F. Ashby et al. *Metal foams: A design Guide*. 150-170. Butterworth-Heinemann, 2000.

[92] M.A. Hazizan and W.J. Cantwell. "The low velocity impact response of an aluminium honeycomb sandwich structure". *Composites Part B* **34** (2003), pp. 679 –687.

[93] R. H. Lochner and J. E. Matar. *Design for quality: An introduction in the best of Taguchi and western methods of statistical experimental design*. Quality Resources, 1990.

[94] P. J. Ross. *Taguchi techniques for quality engineering*. Mc-Graw-Hill, 1988.

[95] V. D'Alessandro et al. "A review of the vibroacoustics of sandwich panels: Models and experiments". *Journal of Sandwich Structures and Materials* **15** (2013), pp. 541 –582.

[96] *Soundbook – Samurai Technical manual*. Available at www.spectra.it. Spectra.

[97]   George Laird. *Modeling Composites with Femap 10.1.1 - An Introduction to The How's and Why's.* Available at www.predictiveengineering.com. 2010.

[98]   *MSC Nastran 2008 - Quick Reference Guide.* MSC Software Corporation. 2008.

[99]   L. Cremer, M. Heckl, and B. A. T. Petersson. *Structure-borne Sound: Structural Vibrations And Sound Radiation At Audio Frequencies.* 3rd. Springer-Verlag, 2005, 607 p.

[100]   J. E. Cooper. *Parameter estimation methods for flutter testing.* AGARD, SMP Meeting, Rotterdam, May 1995. 1995.

[101]   Christer Heed. *Reverberation Time and structure loss factor.* KTH Acoustical Measurements Course SD2165, Stockholm. 2008.

List of Publications

Peer reviewed papers

1. Petrone Giuseppe, Rao Sanjeev, Mace Brian, De Rosa Sergio, Franco Francesco, Bhattacharyya Debes. *Behaviour Of Fibre-Reinforced Honeycomb Core Under Low Velocity Impact Loading.* Composite Structures, June 2013, Volume 100, pp. 356-362. DOI: 10.1016/j.compstruct.2013.01.004.

2. Petrone Giuseppe, Rao Sanjeev, De Rosa Sergio, Mace Brian, Franco Francesco, Bhattacharyya Debes. *Initial experimental investigations on natural fibre reinforced honeycomb core panels.* Composites: Part B, 2013, Volume 55, pp. 400-406. DOI: 10.1016/j.compositesb.2013.06.047.

3. D'Alessandro Vincenzo, Petrone Giuseppe, Franco Francesco, De Rosa Sergio. *A review of the vibroacoustics of sandwich panels: Models and experiments.* Journal of Sandwich Structures and Materials, September 2013, Volume 15(5), pp. 541-582. DOI: 10.1177/1099636213490588.

4. Petrone Giuseppe, D'Alessandro Vincenzo, Franco Francesco, De Rosa Sergio. *Damping evaluation on eco-friendly sandwich panels through reverberation time (RT60) measurements.* Accepted for publication in Journal of Vibration and Control. Available online on February 14, 2014, doi: 10.1177/1077546314522507.

5. D'Alessandro Vincenzo, Petrone Giuseppe, De Rosa Sergio, Franco Francesco. *Modelling of aluminium foam sandwich panels.* Accepted for publication in Smart Structures and Systems.

6. Petrone Giuseppe, D'Alessandro Vincenzo, Franco Francesco, Mace Brian R., De Rosa Sergio. *Modal characterization of recyclable foam sandwich panels.* Accepted for publication in Composite Structures - in Press. Available online on March 28, 2014. doi: 10.1016/j.compstruct.2014.03.026

7. D'Alessandro Vincenzo, Petrone Giuseppe, Franco Francesco, De Rosa Sergio. *Numerical and experimental investigations on the acoustic power radiated by aluminium foam sandwich panels.* Submitted to Applied Acoustics - Under review.

Conference proceedings

1. Petrone Giuseppe, Rao Sanjeev, Mace Brian, De Rosa Sergio, Bhattacharyya Debes. *Behaviour Of Fibre-Reinforced Honeycomb Core Under Low Velocity Impact Loading.* In Proceedings of the International Conference on Mechanics of Nano, Micro and Macro Composite Structures (ICMNMMCS). Editori: Antonio Ferreira e Erasmo Carrera, June 18-20 2012, Turin (Italy). Paper # 260.

2. Petrone Giuseppe, Rao Sanjeev, Mace Brian, De Rosa Sergio, Bhattacharyya Debes. *The effect of core height on the vibro-acoustic behavior of fibre reinforced cores.* In Proceedings of the 15th European Conference on Composite Materials (ECCM15), June 24-28 2012, Venice (Italy). Paper # 1799.

3. Petrone Giuseppe, Rao Sanjeev, Mace Brian, De Rosa Sergio, Bhattacharyya Debes. *Vibration characteristics of fiber reinforced honeycomb panels: experimental study.* In Proceedings of the 25th International Conference on Noise and Vibration Engineering (ISMA2012), September 17-19 2012, Leuven (Belgium). Paper # 643.

4. D'Alessandro Vincenzo, Petrone Giuseppe, Franco Francesco, De Rosa Sergio. *The acoustic power radiated from aluminium foam sandwich panels.* In Proceedings of the International Conference on Acoustics AIA-DAGA 2013. ISBN: 978-3-939296-05-8, Publisher: German Acoustical Society (DEGA), March 18-21 2013, Merano (Italy). pp. 354-357.

5. Petrone Giuseppe, D'Alessandro Vincenzo, Franco Francesco, Brain R. Mace, De Rosa Sergio. *Modal characterization on recyclable foam sandwich panels.* In Proceedings of the 9th International Conference on Composite Science and Technology (ICCST/9). ISBN 13: 9781605951133. Editore: Michele Meo. April 24-26 2013, Sorrento (Italy). pp. 665-676.

Curriculum Vitae

Giuseppe Petrone got the Bachelor Degree in Aerospace Engineering in 2008 at the Second University of Napoli (SUN) and the Master Degree in Aerospace and Astronautic Engineering in 2010 at the University of Napoli Federico II. He submitted this dissertation in partial fulfillment of the requirements for the Degree of Doctor of Phylosophy in Aerospace, Naval and Quality Engineering, attended at the University of Napoli Federico II. During the Ph.D. course, funded by European SUPERPANELS project (PEOPLE MARIE CURIE ACTIONS, International Research Staff Exchange Scheme FP7-PEOPLE-2009-IRSES) in which he was involved, he spent 8 months as Graduate Trainee at CACM (Centre for Advanced in Composite Materials), research centre at the University of Auckland in New Zealand. During this time, he improved his knowledge on composite materials working on the manufacturing, mechanical characterization and vibro-acoustic testing of sandwich panels and beams made of natural fibres combined with thermoplastic resin. These activities led to publish several works on this topic. His research interests lie in the area of vibrations, dynamic and control of composite materials and sandwich structures. He is a member of AIDAA (Italian Association of Aeronautics and Astronautics) and of AIAN (Aerospace and Aeronautical Engineering Association of University of Naples Federico II). Away from work, his interests include walking, travelling and playing volley.